MODULATING AMYLOID PEPTIDE SELF-ASSEMBLY WITH NUCLEOBASE INCORPORATION

By

Peng Liu
B.S. Tsinghua University, 2001

Advisor: David G. Lynn, Ph. D.

An Abstract of
A dissertation or thesis submitted to the Faculty of the Graduate School of Emory University in partial fulfillment
of the requirements for the degree of
Doctor of Philosophy

Department of Chemistry
2007

The folding of proteins into a compact three-dimensional structure with precision and fidelity is one of the most significant examples of biological self-assembly. Failure of folding properly is the origin of many pathological conditions. Amyloid beta peptide is associated with one of the well-known misfolding disease, Alzheimer's disease. Elucidation of the structure, the assembly pathway and the regulatory factors of amyloid fibrils would be crucial for both the disease therapy and bionanotechnology application. In this dissertation, self-assembly of several short peptides originating from amyloid-β peptide was investigated and was specifically probed with nucleobases incorporation.

The Synthesis of β-(cytosine-1-yl)alanine is successful, and for the first time, nucleobases are successfully incorporated into amyloid beta peptide side chain. The synthesis route of nucleobase modified Aβ peptide under Fmoc protocol is successfully developed by our group. I have designed and synthesized a series of nucleobase modified Aβ peptide based on the method described above.

My analysis suggested that nucleobase modified amyloid peptide, Aβ(10-21)CyCy-NH_2, is sufficient to form homogeneous amyloid fibrils. Cytosine nucleobase incorporation in Aβ(10-21) reduced the nucleation phase and initiation of sheet-sheet contacts is crucial for the formation of nucleus. In order to simplify possible geometric constraints on assembly, Aβ(13-21)CyCy was designed to exposure of the CyCy dyad at peptide N-terminus. The results established that Aβ(13-21)CyCy forms homogenous nanotubes around the pKa of cytosine. The fibrils formed by Aβ(10-21)CyCy and nanotubes formed by Aβ(13-21)CyCy possess remarkably similar structural elements to those of the normal assembled amyloid fibrils, such as cross-β diffraction pattern and β-

sheet secondary structures. Formation of homogenous stable nanotubes by Aβ(13-21)CyCy was clearly pH-dependent.

Isotope edited FTIR result of Aβ(13-21)CyCy established a parallel β sheet arrangement of Aβ(13-21)K16A amyloid fibrils. SSNMR suggests two peptide arrangement patterns, a parallel β–sheet organization and an anti-parallel β–sheet organization, which probably results from the two clear morphologies. SSNMR results are consistent with isotope edited FTIR spectroscopy result so far. Combination of structural analysis and linear dichroism results, argues that the cytosine base interaction is along the β–sheet lamination, inducing significant lamination growth and stabilizing the morphology of nanotubes.

These nucleobase modified amyloid peptides now have potential applications in the design of synthetic materials. Peptide self-assembly can be controlled by varying the the length of the peptide, and functional groups exposed on the surfaces can be tailored with different nucleobases. Moreover, the self-assembly could be controlled by pH, temperature and solvent condition, and result in different structural isomers. These studies have set the good base for more extensive development of peptide self-assembly for novel material development.

ACKNOWLEDGEMENTS

I would like to thank my advisor Professor David G. Lynn for his education all these years. I am one of the luckiest people to meet such an inspirational advisor in graduate school and develop the skills of critical thinking and independent research, and gains the confidence to presenting all under his direction. Dave is not only a great scientist, but also a great mentor. He cheers me up whenever I meet difficulties in research. He reminds me to think further whenever I obtain good data. He gives me the freedom to find my interests and strengths. Without his support, I could not be where I am today. From him, I have learned the meaning of passion, commitment and dedication in science, and these will impact me for the rest of my life. I am highly appreciated for the insightful and critical suggestion from my committee members, Professor Vincent Conticello and Professor Dale Edmondson.

It was a great experience to work with Dr. Pappannan Thiyagarajan and Dr. Venkatesh Pingali at Argonne National Laboratory. I would like to thank Dr. Thiyagarajan for supporting the research proposal at Advanced Photon Source and Intense Pulsed Neutron Source. I would like to thank Dr. Venky for instrument setting up and data fitting.

I would like to thank Dr. Hong Yi at Department of Neurology for teaching me to operate the TEM instrument and to process the images. I would like to thank Jeannette Taylor and Steven Dublin for running the cryo-HRSEM samples at the department of chemistry.

Dr. Anil Metha and Seth Childers are the best colleagues I have ever met. I would like to thank them for running the solid state NMR sample and many others. Anil

walked me through understanding the principle of SSNMR and interpreting the spectra, besides, he helped me build the models. His optimistic attitude and great patience makes everyday work in the lab cheerful. Seth is so considerate and willing to help at anytime. He gave me a lot of constructive suggestions that I really appreciate. I would like to thank Dr. Ami for the molecular dynamic modeling work. I would like to thank Dr. Ken Walsh and Dr. Xiaoyu Li for teaching me the skills to do organic synthesis. I would like to thank Dr. Kun Lu and Dr. Jijun Dong for their insight on our Amyloid projects. It is my great pleasure to have Kun as my alumni of both Emory University and Tsinghua University. I would like to thank the support and help from all members of Lynn group in the past and present. Each member of the Lynn group is so unique.

Finally, I would like to thank my father Tieniu Liu and my mother Chunying Zhang for their love over the years. I would like thank my husband Wei Liao, especially the encouragement and support given at my lowest point. I enjoy every minute we spend together.

TABLE OF CONTENTS

LIST OF FIGURES

LIST OF ABBREVIATIONS

^{1}H	proton
Å	Angstrom
aa	amino acids*
Aβ	Amyloid β peptide
AD	Alzheimer's Disease
APP	Amyloid Precursor Protein
AFM	Atomic Force Microscopy
CD	Circular Dichroism
LD	Linear Dichroism
Fmoc	Flourenylmethoxycarbonyl
FT-IR	Fourier Transform Infrared Raman spectroscopy
HPLC	High-Performance Liquid Chromatograph
Hz	Hertz
kcal/mol	Kilocalories per mole
MALDI-TOF	Matrix Assisted Laser Desorption Ionization - Time Of Flight mass spectrometry
MAS	Magic Angle Spinning
MES	2-Morpholino Ethane Sulfonic acid
MeCN	Acetonitrile
MD	Molecular Dynamics
min	minute

ml	mili-liter
mM	milli-Molar
NMM	4-methylmorpholine
NMR	Nuclear Magnetic Resonance
REDOR	Rotational Echo DOuble-Resonance
RP-HPLC	Reversed-Phase HPLC
SANS	Small Angle Neutron Scattering
SAXS	Small Angle X-ray Scattering
SSNMR	solid state NMR
TEM	transmission electron microscopy
TFA	trifluoroacid
UV	ultra-violet
WAXS	Wide Angle X-ray Scattering

* All amino acids were abbreviated according to the standard three-letter or one-letter codes.

CHAPTER 1

INTRODUCTION

The Amyloid-β (Aβ) Peptide Self-Assembly System

Amyloid fibrils are found to be associated with a variety of disorders including Alzheimer's disease, Parkinson's disease, Huntington's disease, prion diseases and type II diabetes (Husby, Stenstad et al. 1994; Kelly 1996; Sunde, Serpell et al. 1997). In spite of the significant difference of the protein primary structure, amyloid fibrils share some common features. All amyloid fibrils stain with Congo Red and give a green birefringence under polarized light. Electron microscopy revealed that amyloid fibrils are straight, unbranching fibrils with diameters around 10nm (Shiraham.T and Cohen 1967). X-ray diffraction data indicating a β-sheet type structure for the fibrils (Sunde, Serpell et al. 1997). It is of great interest to understand how so many different protein sequences can adopt similar structure and control disease-related amyloid formation. Specifically, knowledge of the three-dimensional structure of amyloid fibrils and factors that affected

self-assembly process is critical for understanding the pathology of the amyloidoses and for finding possible way to inhibit or reverse amyloid formation.

With more than 20 million cases world wide, Alzhemier's disease (AD) is currently the most common neurodegenerative disease. The characteristic pathology of AD patient is associated with extracelluar neuritic plaque deposits as well as intracellular neurofibrillary tangles in brain tissues (Selkoe 1991). Amyloid β, a peptide with 39-43 amino acids in length generated by proteolytic cleavage of amyloid precursor protein (APP), is identified as the major plaque component. The overall sequence is amphiphilic with three notable regions: a hydrophilic N-terminus (aa 1-16), a central hydrophobic stretch (aa 17-21), and a long hydrophobic C-terminus (aa 29-42) (Figure1-1).

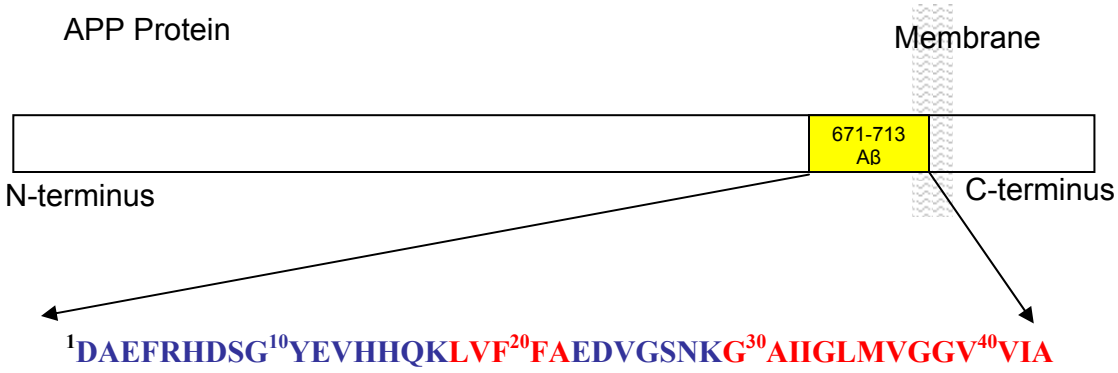

Figure 1.1. The primary sequence of Amyloid β peptide and its location within amyloid precursor protein (APP). Blue / red represent the hydrophilic / hydrophobic regions, respectively.

Structure Characterization of Amyloid Fibril in Vitro

Characterization of synthetic full length as well as truncated Aβ peptides *in vitro*, has been performed extensively and proved to be an effective approach to investigate the structure and kinetics of amyloid formation. The shorter peptide cassettes, e.g., Aβ(10-

35) and Aβ(10-21), constituting the central core and retaining the amphiphilic pattern, are reported to form similar fibril structures compared with full length amyloid beta peptide (Lee, Stimson et al. 1995; Benzinger, Gregory et al. 1998; Morgan, Dong et al. 2002). The truncation versions allow for great synthetic flexibility and homogeneous preparation of the intermediate states that are critical for successful analysis. Much of the high-resolution, detailed structural data has been obtained from these truncated peptide assembled under physiological or nonphysiological condition. Studies of these Aβ peptide model systems *in vitro* have provide detailed understanding of the interactions that govern amyloid fibril formation (Sorimachi and Craik 1994; Talafous, Marcinowski et al. 1994; Sticht, Bayer et al. 1995).

A wide variety of techniques has been used to build structural models of amyloid fibrils, including circular dichroism (CD), Fourier transform infrared spectroscopy (FTIR), atomic force microscopy (AFM), X-ray diffraction, electron microscopy, solid state NMR, small angle neutron scattering (SAXS) and small angle X-ray scattering (SAXS).

Secondary structure of soluble Aβ has been characterized by using circular dichroism (CD) and Fourier transform infrared (FTIR) spectroscopy, and both of them support a high β-sheet content for amyloid fibrils (Hilbich, Kisterswoike et al. 1991; Fraser, Nguyen et al. 1992; Wood, Maleeff et al. 1996). Isotopic-edited IR spectroscopy is a sensitive technique to probe amide backbone structure of amyloid protein(Halverson, Sucholeiki et al. 1991; Silva, Nguyen et al. 2002). Atomic force microscopy (AFM) and transmission electron microscopy (TEM) have proved a valuable tool to investigate the nature of the intermediates in the amyloid pathway. TEM observations show amyloid

fibrils to be straight, unbranching, 70-120 Å in diameter and of intermediate length (Shiraham.T and Cohen 1967).

Small angle neutron scattering (SANS) and small angle X-ray scattering (SAXS) were powerful tools for obtaining structural information of marcromolecules in solution (Trewhella 1997). In particular, SANS and SAXS are used to monitor the conformational change of proteins during folding and provide information of protein aggregation ((Lattman 1994; Semisotnov, Kihara et al. 1996; Doniach 2001). For instance, kinetics of Aβ(10-21) self-assembly has been followed by SANS (Morgan, Dong et al. 2002); Structures of Aβ(16-22) formed at pH2 in 40% acetelnitrile has been studied by SAXS (Lu, Jacob et al. 2003).

X-ray diffraction of amyloid fibrils revealed reflections at 4.7 Å and 10.6 Å corresponds to the distance between peptide strands in the H-bonding direction within the sheet and between laminated sheets (Kirschner, Abraham et al. 1986; Inouye, Fraser et al. 1993; Serpell, Berriman et al. 2000). Such a "cross-beta" pattern has been observed in amyloid fibrils formed by many proteins with different sequence and therefore implying a common structure feature.

Determination of high-resolution molecular structures of amyloid fibrils remains a highly challenging task due to their noncrystalline and insoluble nature. Therefore limited structural information could be obtained by solution NMR and X-ray crystallography. Solid state NMR spectroscopy has emerged as a principal methodology for structural studies of amyloid fibrils in the past decade. This techique has provided answers to central questions concerning the supramolecular organization of amyloid fibrils, peptide conformations within amyloid fibrils, and the diversity of amyloid

structures. The first solid state NMR studies was performed on Aβ(34-42) fibrils through dipolar recoupling techniques (Spencer, Halverson et al. 1991; Griffiths, Ashburn et al. 1995; Lansbury, Costa et al. 1995). Based on that, an antiparellel β-sheet with an alternating hydrogen bond registry model was proposed. Subsequently, extensive investigations of Aβ(10-35) fibrils were performed by our group (Benzinger, Gregory et al. 1998; Burkoth, Benzinger et al. 2000). For the first time, a parallel, in-register β-sheet arrangement in amyloid fibrils was found and now widely believed to be the most common β-sheet organization in amyloid fibrils, especially for fibrils formed by relatively long peptide chains (Figure 1-2).

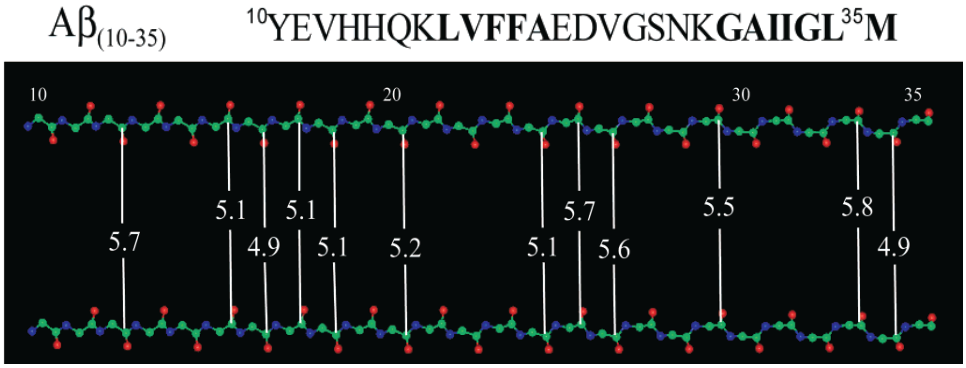

Figure 1.2. (A) Amino acid sequence of Aβ(10-35). (B) Summary of the inter peptide 13C carbonyl contacts observed for Aβ(10-35) by solid-state NMR. Inter-peptide distances were measured using DRAWS at positions V12, Q15-V18, F20, V24-G26, G29, G33, and L34. Peptide strands run parallel, in-register within each β-sheet.

More recently, full length amyloid β peptide Aβ(1-40) and Aβ(1-42), as well as the fragments Aβ(16-22) and Aβ(11-25) have been studied thoroughly by Tycko's group (Balbach, Ishii et al. 2000; Tycko and Ishii 2003; Petkova, Buntkowsky et al. 2004).

They proposed a Aβ(1-40) model composing of two β-strands segments each forming parallel in register β-sheets with a loop (Figure 1-3).

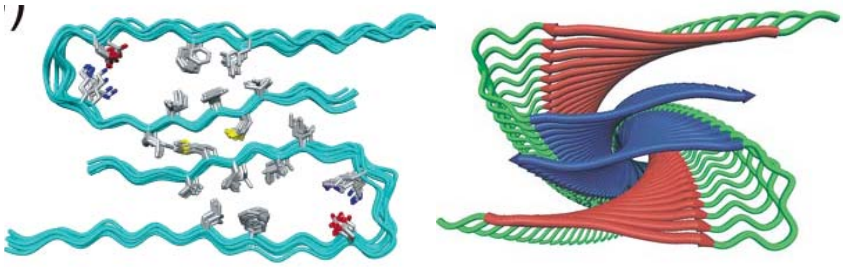

Figure 1.3. Structural model for Aβ1-40 fibrils based on solid-state NMR measurements. (A) Bundles of central pairs of molecules in energy-minimized structures. Side chains of L17, F19, D23, K28, I31, I32, L34, M35, and V36 are shown. (B) A cartoon representation of a full fibril, viewed from the top of the fibril. Residues 12-21 in red and residues 30-40 in blue.

Kinetics of Amyloid Fibril Formation

Spontaneous formation of amyloid fibrils from disordered peptides is often described as a nucleation-dependent polymerization pathway (Harper and Lansbury 1997). In this mechanism, the overall rate of amyloid formation is limited by the nucleation phase, and followed by a rapid elongation phase. Fibrillogenesis usually includes three steps: (1) a slow nucleation step, in which the protein undergoes a series of unfavorable associations to form an ordered oligomeric nucleus; (2) a rapid growth step, in which the nucleus grows to form larger polymers by monomer addition to the fibril ends; (3) a final step, in which the ordered aggregate and the monomer appear to be at equillibium (Fig. 1-4). The characteristic features of a simple nucleation-dependent polymerization are as follows: (*a*) No aggregation occurs at a protein concentration below

the critical concentration. (*b*) At protein concentrations that exceed the critical concentration by a small amount, there is a lag time before polymerization occurs. (*c*) During the lag time, addition of a seed results in immediate polymerization (Andreu and Timasheff 1986; Jarrett and Lansbury 1993; Eaton and Hofrichter 1995).

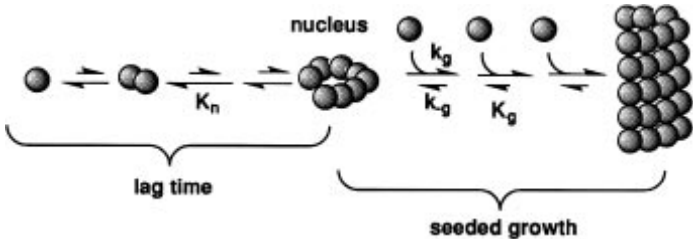

Figure 1.4. The nucleation-dependent polymerization pathway. Nucleus are formed through a series of unfavorable protein-protein association equilibria (Kn). Then a series of favorable equilibria (Kg) leads to fibril formation.

Metals and Amyloid-β in Alzheimer's Disease

Metals are suggested to play a role in the pathogenesis of Alzhemier's disease (AD). The aggregation of Amyloid-β is mediated by interaction with metals ions, in particular zinc (Zn^{2+}), copper (Cu^{2+}) and iron (Fe^{3+}). These metals are reported to be concentrated in and around amyloid plaques in AD brains. Zn^{2+} induces rapid and extensive aggregation of both synthetic and endogenous Aβ in canine cerebrospinal fluid (Bush, Pettingell et al. 1994; Brown, Tummolo et al. 1997; Huang, Atwood et al. 1997; Lovell, Robertson et al. 1998; Suh, Jensen et al. 2000). Trace amount of Cu^{2+} in the diet has been shown to induce β-amyloid plaques and learning deficits in rabbit model of AD (Sparks and Schreurs 2003). Zn^{2+} and Cu^{2+}-bounded senile plaque cores were identified by Ramman microscopy in the brain of AD patients (Dong, Atwood et al. 2003). Aβ catalyzes the reduction of Cu^{2+} and Fe^{3+}. In the absence of sufficient antioxidant

mechanisms, this could lead to the production of toxic reactive oxygen species (ROS) that may contribute to the pathogenesis of AD. In turn, the oxidative stress could contribute to Aβ accumulation by generating modified Aβ species that are easily to aggregate and resistant to clearance.

Since metal ions such as Cu^{2+} and Zn^{2+} bind Aβ strongly and specifically, it is possible to use metal ions as both structural and kinetic probes for Aβ self-assembly. The pH dependence and mutagenesis studies of Zn^{2+} on Aβ aggregation reveal that histidine 13 is crucial for Zn^{2+} binding (Atwood, Moir et al. 1998; Liu, Howlett et al. 1999; Miura, Suzuki et al. 2000; Yang, McLaurin et al. 2000; Curtain, Ali et al. 2001). Zn^{2+} addition to Aβ(10-21), a fragment of full length amyloid beta peptide, revealed conditions that radically alter the relative rates of nucleation and propagation in amyloid formation and implicated that Zn^{2+} may coordinate to histidine through lamination dimension (Morgan, Dong et al. 2002).

Exploring Amyloid Growth in Lamination Dimension

Although full length Aβ peptide and truncated variants of form similar fibrils with approximately 10 nm in diameter, they may contain different laminates. Fibrils formed by the longer Aβ(1-40) may contain 2-4 laminates while those by the shorter Aβ(18-28) peptides contain as many as 24 laminates (Kirschner, Inouye et al. 1987; Garzon-Rodriguez, Sepulveda-Becerra et al. 1997; Petkova, Ishii et al. 2002). Thus lamination energetics becomes a critical issue in our understanding of fibril structure and stability. Consistent with these observations, the structural model for Aβ(10-35) suggests that the common fibril diameter could be attained by variation in the degree of lamination

(Lakdawala, Morgan et al. 2002). For Aβ(10-35), the lamination of six in-register parallel β-sheets define a 6 × 8 nm fibril.

Severely truncated variant Aβ(16-22) forms homogeneous nanotubes with 50 nm internal diameters under appropriate pH and solvent condition. Helical ribbons were observed as intermediates of the nanotubes, and could be composed of as many as 130 laminates (Lu, Jacob et al. 2003) (Figure1-5A). Similar ribbons and nanotubes were observed in Aβ(13-21)K16A with Zn^{2+} incorporation. Based on FTIR, solid-state NMR and XAS data, Zn^{2+} was implied to chelate between two β−sheets and stabilize the β−sheet lamination, inducing significant lamination growth (Dong, Shokes et al. 2006) (Figure1-5B). The control of conditions modulating β−sheet growth and sheet/sheet packing opens the possibility of better constraining amyloid structure and the mechanism of amyloid self-assembly (Dong, Lu et al. 2006) (Figure1-5C). The variety of self-assembled architectures raises the possibility of adapting such scaffolds for novel materials applications.

Molecular Recognition Motifs and Self-Assembled Peptide Nanostructure

As the formation of amyloid fibrils is associated with major human disease, great effort has been spent to search for the recognition elements that mediate the processes of molecular recognition and self-assembly that lead to the formation of the fibrils. Exploring these recognition elements not only helps to understand the self- assembly mechanism that governs amyloid formation, but also enables the identification of novel motifs to control this process.

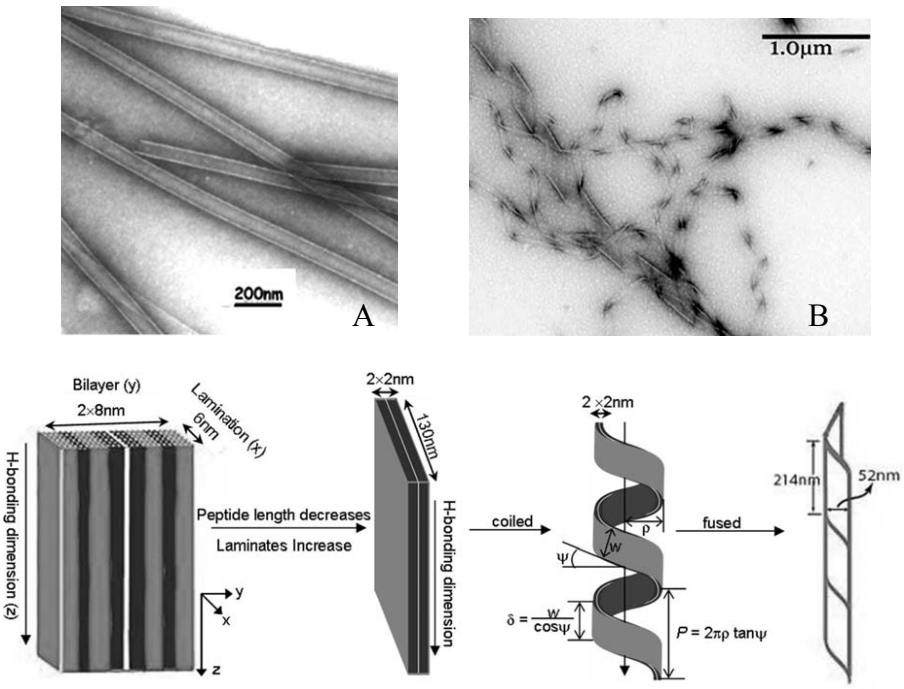

Figure 1.5. (A) TEM images of Aβ(16-22). (B) TEM images of Aβ(13–21)K16A in the presence of one equivalent of Zn^{2+}. (C) Model for Amyloid growth in lamination dimension of Aβ(16–22). (a) A bilayer model for Aβ(10–35) fibril. Lamination of six β-sheets is perpendicular to the long axis, defining the width of the bilayer. (b) Aβ(16–22), the lamination increases from 6 to 130 nm. (c) Laminated β-sheet bilayer coils up to form a helical ribbon. (r, radius; o, pitch angle; P, pitch; w, width; d, width along the z-axis.) (d) Helical ribbon fuses into tubular structure (Dong, Lu et al. 2006).

Short fragments of islet amyloid polypeptide (IAPP), a 37-amino acid residue peptide hormone that is associated with type II diabetes, have been found to form amyloid fibrils (Tenidis, Waldner et al. 2000; Mazor, Gilead et al. 2002; Reches, Porat et al. 2002). Comparison of the primary sequences of these peptide fragments revealed the

aromatic residues in common. A hypothesis was proposed that aromatic residues play a key role in the formation of amyloid fibrils through π-stacking interactions (Gazit 2002).

Besides π-stacking interactions, pH and metal may also plays an important role in determination of amyloid peptide morphology. Aβ(16-22) with sequence of KLVFFAE, forms homogeneous nanotubes with 50 nm internal diameters when pH is decreased to 2 (Lu, Jacob et al. 2003). Similar ribbons and nanotubes were observed in Aβ(13-21)K16A with Zn^{2+} incorporation (Dong, Shokes et al. 2006).

One of the most common and robust molecular recognition motifs is nucleobase of DNA or RNA. Recognition between nuleic acids is essential for storing and transferring of genetic information during DNA replication and transcription. A synthetic biomolecule, peptide nucleic acid (PNA), has emerged in recent years mimic the molecular recognition process occurred in natural DNA or RNA. PNAs are pseudopeptides in which the nucleobases are attached via a linker to a neutral and achiral backbone consisting of N-(2-aminoethyl)glycine units (Nielsen, Egholm et al. 1991). PNA is capable of hybridizing to complementary DNA, RNA or PNA following the Watson-Crick base pairing rules, and the restultant duplexes show higher thermal stability than the corresponding DNA-DNA or DNA-RNA duplexes (Egholm, Buchardt et al. 1993; Jensen, Orum et al. 1997). Carrying genetic information, PNAs are considered to be of great importance as antisense and antigene agents (Hanvey, Peffer et al. 1992; Nielsen 1999). PNA is used as probes for gene cloning, mutation detection, and in homologous recombination studies (Demers, Curry et al. 1995; Perry-OKeefe, Yao et al. 1996; Veselkov, Demidov et al. 1996).

Alanyl-PNA is designed and synthesized based on a regular peptide backbone with alternating configuration of the amino acids. The nucleobases are covalently linked at β position of the side chains (Diederichsen 1996). The backbone of the alanyl PNA is in extended β–sheet conformation, which allows the nucleobases in the peptide side chain to accommodate the favored base-pairing distance. Therefore, alanyl PNA oligomers are able to form self-pairing linear double strands (Diederichsen 1997; Diederichsen and Weicherding 1999) (Figure 1-5A). More interestingly, the linear double-strand topology does not restrict the base-pair size and orientation as in DNA double helix. The favored base pairs are formed mostly dependent on recognition by H-bonding. Examples of 2,6-diaminopurine-xanthine and guanine-isoguanine base pairs with high stabilities support this hypothesis (Hoffmann, Bruckner et al. 2000) (Figure 1-5B). These unique features of alanyl-PNA inspire us the possibility to incorporate alanyl-PNA molecules into Aβ peptide and control the self-assembly of Aβ peptide through nucleobase recognition.

Peptide-base nanostructures have raised great interest as a bio-materials or delivery systems due to their advantage in tailored molecular design, availability of a variety of functional groups, low toxicity, biodegradability and ability of self assembly into desired structure scaffold. Various peptide-based nano-materials have been prepared using different building blocks, including cyclic peptides with alternating D- and L-amino acids, peptide amphiphiles, peptide bolaamphiphiles, aromatic dipeptides and hydrophobic dipeptides (Ghadiri, Granja et al. 1993; Hartgerink, Granja et al. 1996; Hartgerink, Beniash et al. 2001; Gorbitz 2003; Reches and Gazit 2003). Peptide assemblies have been used for tissue engineering (Holmes, de Lacalle et al. 2000; Silva,

Czeisler et al. 2004) and biosensor applications (Yemini, Reches et al. 2005; Zhao, Banerjee et al. 2005).

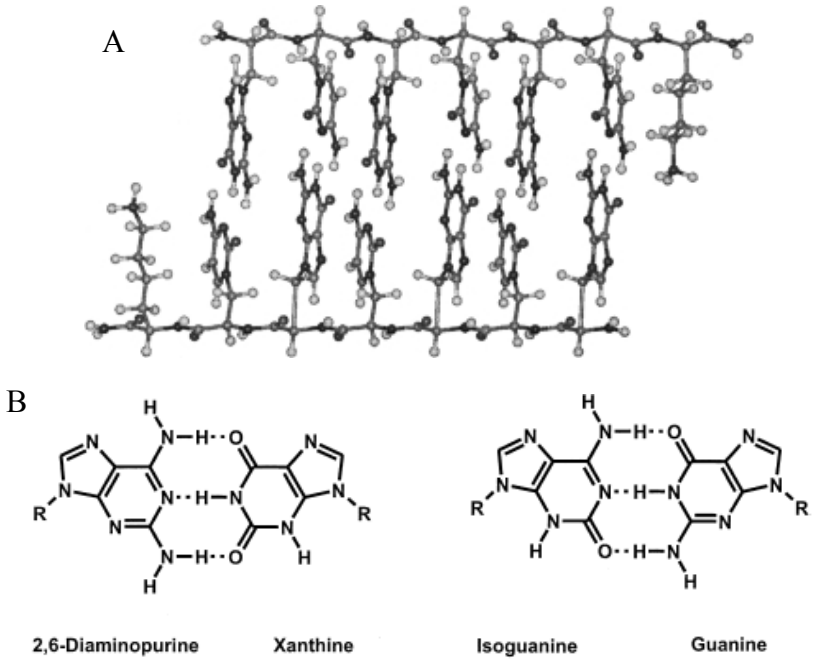

Figure 1.6. A. Model of a linear alanyl-PNA double strand. B. 2,6-diaminopurine-xanthine and guanine-isoguanine base pairs (Hoffmann, Bruckner et al. 2000).

Amyloid fibril formation is associated with many types of human diseases (Dobson 2002), however, a large number of non-pathogenic peptides have been shown to form ordered fibrils under particular solvent, temperature and pH conditions (Jarrett and Lansbury 1992; Konno, Murata et al. 1999). The diphenylalanine recognition motif of the Aβ peptides self-assembles into nanotubes which can serve as a mold for the fabrication of nanoscale inorganic materials (Reches and Gazit 2003; Song, Challa et al. 2004). Self-assembled nanotubes of Aβ(16-22) have been shown to template colloidal metal nanoparticles (Lu 2004).

Summary

The controlled self-assembly of proteins into well defined hierarchical structures is becoming increasingly important for the fabrication of nanodevices. The rational and controlled fabrication of new nano building blocks are tightly tied to a better understood of protein self-assembly, both the protein organization inside the assemblies and the assembly pathways.

In this thesis, nucleobases, one of the most robust molecular recognition motif in nature, are incorporated into amyloid beta peptide self-assembly model system. Based on the simulation results, nucleobase modified Aβ peptides are investigated. The introduction of nucleobases at the side chain of these Aβ peptides has greatly changed self-assembly process kinetically and morphologically. This is the first time that homogeneous nano-fibrils and nano-tubes assembled by the peptide with nucleobases incorporation. Detailed structural characterizations are developed and the nucleobases functions are discussed in this thesis. Novel nucleobases modified nanostructure will provide extensive applications in biomedical fields in the future.

CHAPTER 2

MODELING AND SYNTHESIS OF NUCLEOBASE MODIFIED AMYLOID PEPTIDE

INTRODUCTION

As discussed in chapter one, knowledge of the three-dimensional structure of amyloid fibrils and of the factors that affected self-assembly process are critical for understanding the mechanism of fibrillogenesis. Previous investigations have shown that amyloid peptide self-assembly can be modulated by metal ions such as Zn^{2+}. Zn^{2+} incorporation not only increased the self-assembly rate but also dramatically modulated amyloid mophorlogy (Morgan, Dong et al. 2002; Dong, Shokes et al. 2006). The results suggest that when appropriate agents are inserted between the histidines H13 and H14 along the face of one sheet or between the different sheets, it is possible to regulate peptide aggregation.

In the model of Aβ (10-35) fibril (Figure 2.1A), the strands are H-bonded and held roughly 5 Å apart within the β-sheet. The H-bonds are oriented along the fibril axis.

The packing of amino acid side chains, oriented perpendicular to the fibril axis, are separated 10 Å apart between the laminated sheets (Burkoth, Benzinger et al. 2000). On the other hand, in the DNA double-helix, the glycosidic bonds that are attached to a bonded pair of bases are 10-11 Å apart, so the distance between the laminated sheets of amyloid fibrils may accommodate a pair of DNA double-helix nucleoside units. As a result, the possibility for modifying histidine imidazole rings to base pair purine and pyrimidine rings was explored.

Previous studies suggested that the His 13 and His 14 residues from different sheets would be proximal and provide Zn^{2+} binding site between the sheets (Figure 2.1B, C). If the nucleobase pair could fit in the space between the laminated sheets, proximal to each other as in the His-His dyad and coplanar, hydrogen bonding and base stacking could be manipulated to regulate peptide aggregation.

Aβ (10-21) was first chosen for the investigation of nucleobases incorporation on the amyloid peptide self-assembly since Aβ (10-21) includes the core segment of full length amyloid peptide with emphasis on the metal impact of the His13 and 14 dyads. Moreover, this central cassette of Aβ maintains an amphiphilic pattern that is critical for fibril formation. Replacement of this His13 and 14 dyads with a nucleobase will probe the side chain properties on sheet lamination during self-assembly. More importantly, successful incorporation of nucleobases in the rigid and geometrically well defined amyloid fibrils would provide a unique model system to study peptide and nucleobase interactions.

Complementary base pairs display affinity, inherently arranging to maximize base stacking and hydrogen bonding. Because of the steric restrictions imposed by the regular

Figure 2.1

Metal binding sites predicted by the model of the Aβ(10-35) fibril.

A. Model of the $A\beta_{(10-35)}$ fibril. Schematic demonstration of the microstructure within one fibril. Single red-blue line represents the backbone of one Aβ(10-35) molecule. Parallel in-register β-strands orient perpendicular to and twist into β sheet structure along the fibril long axis. Six such sheets laminate by sidechain-sidechain interactions (not shown). The distance between two β-strands along the fibril axis is 5 Å, corresponding to hydrogen bounding, while the sheets are proximately 10 Å apart.

B. Zinc-binding site between two strands of different sheets, viewed down the axis of fibril propagation. Red, oxygen; Blue, nitrogen; Magenta, metal ion.

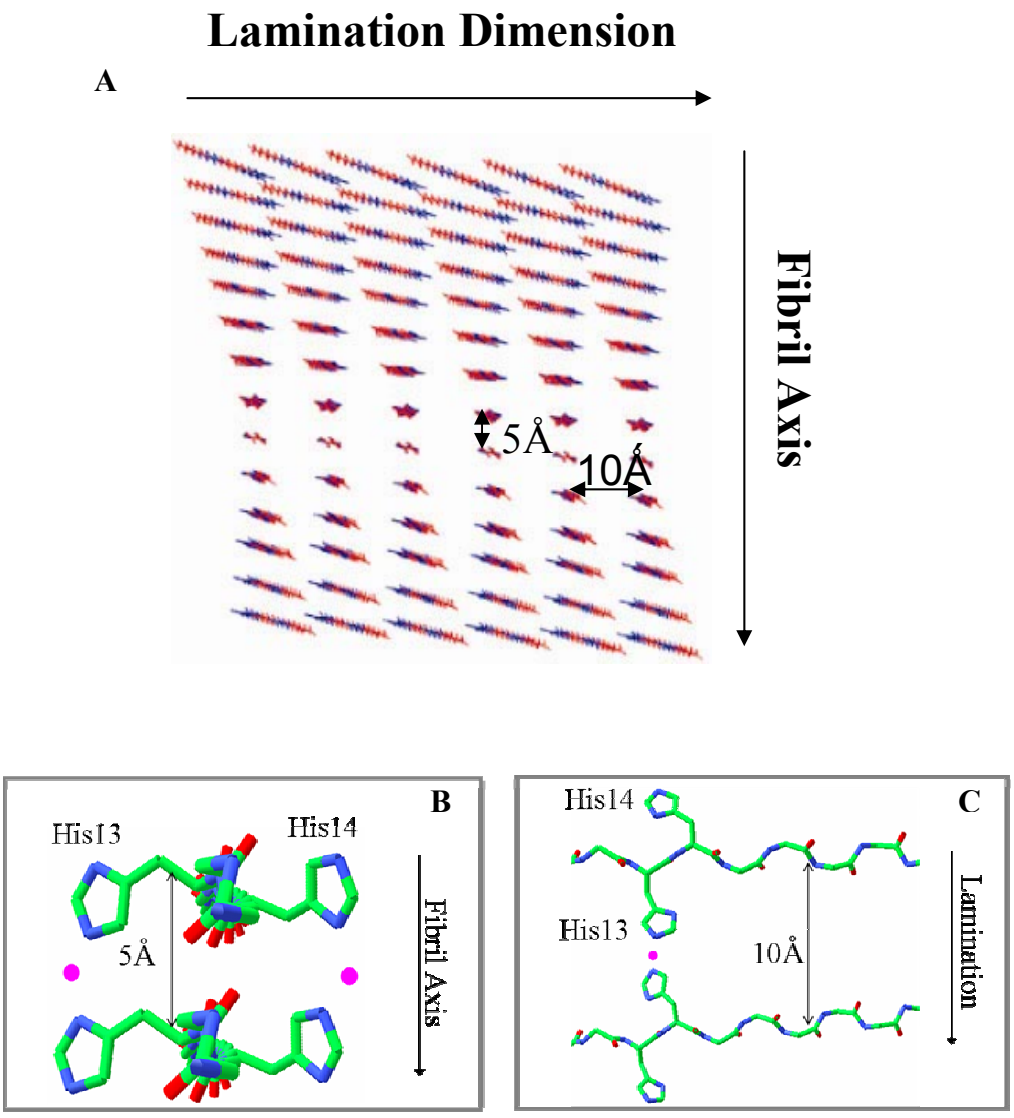
Lamination Dimension
A
Fibril Axis
5Å
10Å
B
His13
His14
5Å
Fibril Axis
C
His14
His13
10Å
Lamination

helical nature of the sugar-phosphate backbone and by hydrogen-bonding factors, the nucleobase pairings in DNA following Watson-Crick rule that adenine with thymine and guanine with cytosine. By contrast, the linear double-strand topology of alanyl PNA does not restrict the base-pair size and orientation as in the DNA double helix. The favored base pairs are formed mostly dependent on recognition by H-bonding (Diederichsen 1996; Diederichsen 1997). Examples of 2,6-diaminopurine-xanthine and guanine-isoguanine base pairs with high stabilities support this hypothesis (Hoffmann, Bruckner et al. 2000). These unique features of Alanyl PNA inspired the possibility of incorporating alanyl PNA molecules into Aβ peptide to control the self-assembly of Aβ peptide through nucleobase recognition.

Molecular Dynamics (MD) simulations of Aβ (10-21) were conducted for the normal purine-pyrimidine and the purine-purine base pairs as well as pyrimidine-pyrimidine base-pairs. These results suggested that a nucleobase modified Aβ (10-21) containing cytosine moieties at the amino acid side chain of H13 and H14 position could maintain a 10 Å separation between the laminate sheets. Based on the modeling results, β-(cytosine-1-yl)-alanine was synthesized and substituted for H13 and H14 in Aβ(10-21), resulting in Aβ (10-21)CyCy, where Cy represents the alanyl cytosinyl-amino acid. Synthesis of optically pure α-amino acid via ring-opening of N-protected β-lactones has proved practical and efficient (Arnold, Kalantar et al. 1985; Arnold, May et al. 1988). The first stereoselective synthesis of alanyl nucleo-amino acids was described for the adeninyl and thyminyl derivatives via nucleophilic ring opening of Boc-L-serinelactone by Eschenmoser and Lohse (Lohse 1992; Lohse 1996). Following that procedure, N-

Boc-thyminylalanine and N-Boc-adeninylalanine were used for oligomerization of alanyl PNA by Diederichsen. Alanyl peptide nucleic acids with alternating configuration of amino acids formed pairing complexes, and the formation of unnatural base pairs such as A-A is possible due to the linearity and the uncharged peptide backbone (Diederichsen 1996). In this chapter, the β-(cytosine-1-yl)-alanine is prepared and the modeling and synthetic route to peptide Aβ (10-21) CyCy is described. The non-native amino acids are successfully constructed into amyloid fibrils.

RESULTS

Molecular Dynamic Simulation of Nucleobases Modified Aβ(10-21)

A model for nucleobase modified Aβ(10-21) was constructed to predict the optimum modification of H13 and H14 by focusing on the β-sheets packing and the backbone distances between β-strands. Computational analysis and Molecular Dynamics (MD) simulations of Aβ(10-21) was conducted for purine-pyrimidine, the purine-purine, and pyrimidine-pyrimidine base-pairs. As DNA effectively accommodates the pyrimidine—purine combination at a 10 Å separation, the inclusion of two additional C—C bonds causes the amyloid sheets to spread. As a result, possible modifications of the di-pyrimidine nucleotide units were examined. Consistent with amyloid, the resulting Cy-Cy-modified structure maintains a 10 Å separation between laminate sheets. Unlike DNA which is not able to stabilize interactions between pyrimidine rings, Aβ(10-21) can preserve two hydrogen bonds between the cytidine NH_2 and C=O along the length of the

fibril segment (Figure 2.2). High level calculation (MP2/6-31G*//HF/6-31G**) predict pyrimidine—pyrimidine pairing of two cytosines to be stabilized by -17.5 kcal/mol (gas phase), and such interactions can also form a third H-bond at pH values around the pKa of the the amide (~4.2).

Synthesis of Nucleobase Modified Amino Acids and Their Oligomerization

According to MD simulation, β-(cytosine-1-yl)-alanine and β-(thymine-1-yl)-alanine was synthesized and substituted for H13 and H14 in Aβ(10-21). β-(cytosine-1-yl)-alanine was prepared starting from nucleophilic ring opening of N-Boc-L-serine-β-lactone **1** with the base benzyl-cytosine **5**, followed by Boc-deprotection, and reprotection with Fmoc (Scheme 2-1). The overall yield of Fmoc β-(cytosine-1-yl)-alanine was 15.6%. In a similar manner, β-(thymine-1-yl)-alanine was prepared starting from Boc-serinelactone **1** and thymine, followed by Boc-deprotection, and reprotection with Fmoc (Scheme 2-2). The overall yield of Fmoc β-(thymine-1-yl)-alanine was 14.4%.

Oligomerization of the nucleo-amino acids and natural amino acids was performed by solid –phase peptide synthesis on Fmoc Rink-amide polystyrene resin and HBTU/NMM was used as the coupling reagents. After deprotection and cleavage from the solid support with trifluoroacetic acid (TFA)/thiolanisole/EDT/anisole, 90%/5%/3%/2%, the crude peptide was isolated by trituration with diethyl ether and purified by HPLC on a RP-C18 column. The product was confirmed by MALDI-TOF mass spectral analysis.

Figure 2.2

Peptide Sequence of Aβ(10-21)CyCy and model predicted by SYBYL

A. Peptide Sequence of Aβ(10-21)CyCy.

B. Proposed hydrogen bonds *(dashed lines)* between modified Cy13 and Cy14 side chains residing in two extended β-sheets (model predicted by SYBYL in Aβ(10-21)CyCy). The carbon atoms are colored green, the oxygens red and the nitrogens blue.

A

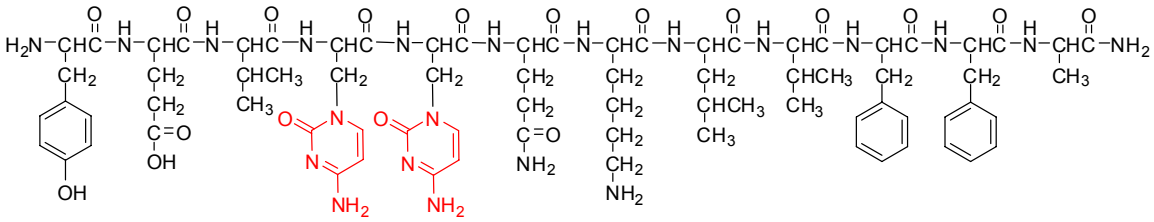

B

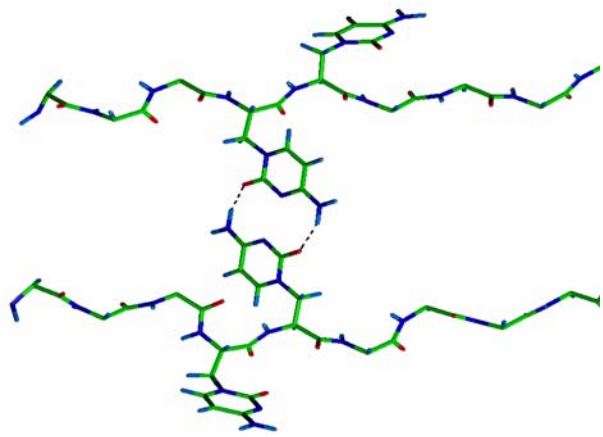

Scheme 2-1 Synthesis of β-(cytosine-1-yl) alanine

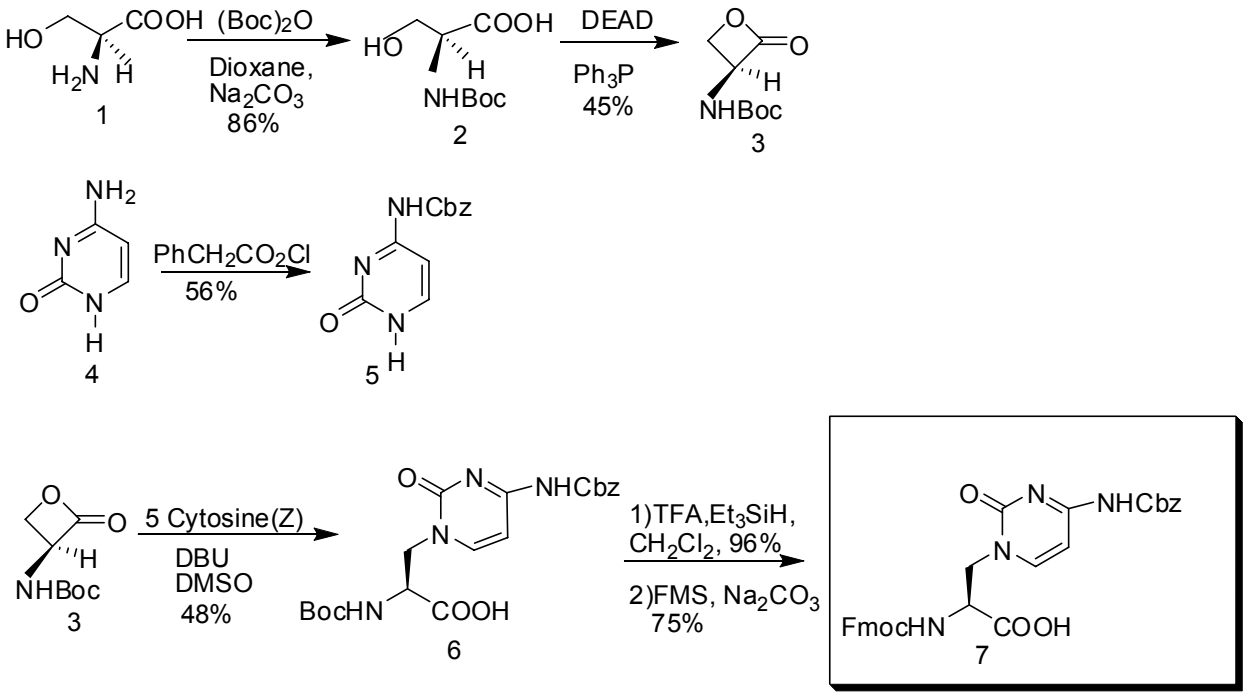

FMS: Fmoc N-hydroxysuccinimide Ester

Scheme 2-2 Synthesis of β-(thymine-1-yl) alanine

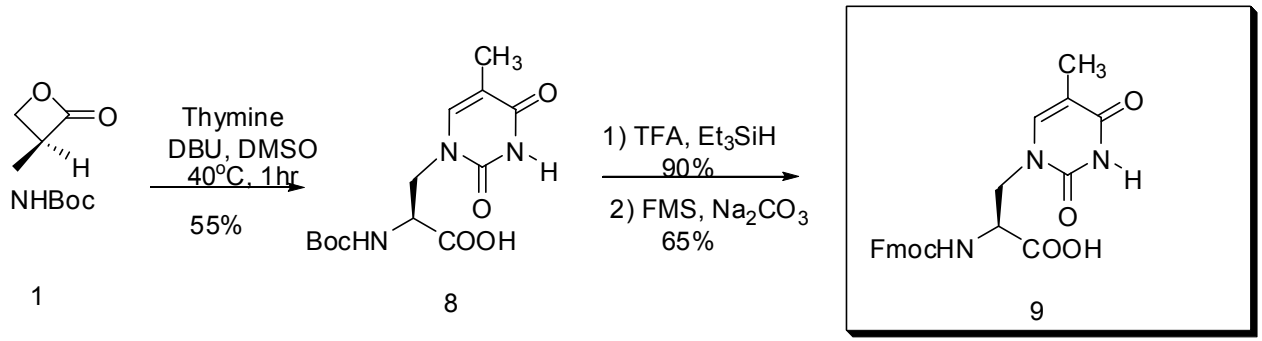

DISCUSSION

The synthesis of N-Boc-L-serine β-lactone through Mitsunobu dehydration readily cyclizes Boc-L-serine to the β-lactone without detectable epimerization. Dimethyl azodicarboxylate was found to be equally effective as diethyl ester. Boc-deprotection was more efficient in the presence of triethylsilane as a carbocation scavenger. Once the protecting group is deblocked, the functional group that is attached to the protecting group forms a hydrogen substituted product with triethylsilane acting as hydride donors, and the reaction is irreversible so that the efficiency of deblocking of protecting group is assured. Further advantage of using triethylsilanes as scavenger is that it is a volatile compound (boiling point 108 °C) (Pearson, Blanchette et al. 1989). Several Fmoc protection agents including 9-Fluorenylmethyl chloroformate and 9-Fluorenylmethyl N-succinimidyl carbonate were tested, and 9-Fluorenylmethyl N-succinimidyl carbonate was chosen due to high efficiency and easy work up procedure. During the solid phase peptide synthesis, N-(9-Fluorenylmethoxycarbonyl)- β -(cytosine-1-yl)alanine was manually loaded into the reaction vessel. Double coupling and longer reaction time is required for these unnatural amino acids. Incorporation of other nucleobases including thymine, adenine and guanine into Aβ peptide could be performed in a similar manner.

Nucleobases including cytosine and thymine were incorporated into amyloid peptide successfully. A suitable synthetic route to be applicable to all the four bases including A and G are under investigation. With the availability of all four bases incorporation, we would be able to use this nucleobase modified amyloid peptide to template DNA with any sequences.

MATERIALS AND METHODS

Materials

All commercially available chemicals and solvents were purchased from Aldrich, Lancaster and Nova Biochem. Anhydrous solvents were dried over molecular sieve (4 Å) that had been pre-treated overnight at 300 ºC. TLC plates were purchased from EMD (silica gel 60 F_{254}). Flash chromatography employed EMD silica gel (40-63μm). Fmoc-amino acids, resins and solid phase peptide synthesizer reagents were purchased from Anaspec. Distilled deionized water for sample preparation was obtained from EMD chemicals Inc. DMF, HPLC grade acetonitrile and methanol, morpholinoethanesulfonic acid monohydrate (MES, ≥ 99.5%) and all other reagents were obtained from Aldrich Chemical Co.

Methods

Synthesis of β -(cytosine-1-yl)alanine

N-(tert-Butoxycarbonyl)-L-serine β-lactone 1

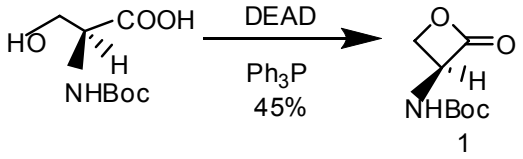

1

N-(tert-Butoxycarbonyl)-L-serine (6.2 g, 30 mmol) and triphenylphosphine (7.9 g, 30 mmol) was dissolved in 200 ml anhydrous tetrahydrofuran under nitrogen and cooled to -78 ºC. Diethyl azodicarboxylate (6.3 g, 36 mmol) was added dropwise over 10 min. The reaction was allowed to proceed overnight. The solvent was removed and and reaction mixture was purified by flash column packed in hexane. The solvent is changed

to hexane/ethyl acetate (65/35) gradually. The β-lactone was readily visualized by TLC (hexane/ethyl acetate (65/35) as solvent system, R_f ~0.44) by staining in iodine or potassium permanganate. **1** was isolated as a white solid (45%). mp 119.5-120.5°C; ^{1}H NMR ($CDCl_3$, 400MHz) δ: 1.45 (s, 9H, $C(CH_3)_3$), 4.4-4.45 (m, 2H, CH_2), 5.05-5.15 (m,1H NH-C<u>H</u>), 5.15-5.25 (br s, 1H, NH); ^{13}C-NMR ($CDCl_3$, 400MHz) 28.0 ($C(\underline{C}H_3)_3$), 59.8 (NH-CH), 66.9 (CH2), 81.9($\underline{C}(CH_3)_3$), 154.8 (NH-CO), 169.7(O-CO). IR (cm^{-1}) 3358, 1836, 1678, 1533, 1290, 1104. MS (CI) m/z $(M+H)^+$ 188.1 Calculated: 188.0923.

N_4-(Benzyloxycarbonyl)cytosine(5)

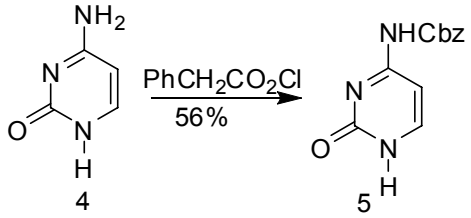

Benzyloxycarbonyl chloride (26 mL, 0.18 mol) was added dropwise over a period of ca. 1 h to a suspension of cytosine (10.0 g, 0.09 mol) in dry pyridine (500 mL) at 0 ºC under N_2. The mixture was stirred overnight and, the pyridine suspension was evaporated to dryness in vacuo. Water (100 mL) was added and the pH was adjusted to 1 with 4 M HC1 (aqueous). The resulting white precipitate was removed by vacuum, washed with water, and partially dried. The wet precipitate was boiled with absolute EtOH (250 mL) for 10 min, cooled to 10 ºC, filtered, washed thoroughly with ether and dried, in vacuum: yield 12.4 g (56%); mp > 250 ºC. ^{1}H NMR (DMSO-d_6, 400MHz) δ: 5.41(s, 2H, $CH_2(C_6H_5)$), 6.89 (d, 1H, HC(5)), 7.36 (m, 5H, (C_6H_5)), 7.76 (d, 1H, HC(6)).

N-(tert-Butoxycarbonyl)- β -(cytosine-1-yl)alanine 2

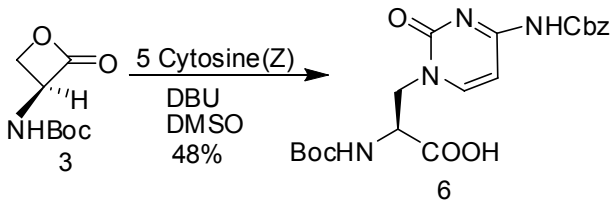

DBU (1.8 g, 12 mmol) was added to a suspension of N^4-(Benzyloxycarbonyl) cytosine (2.5 g, 10 mmol) in DMSO (10 ml). Within 15 min, a solution of N-(tert-Butoxycarbonyl)-L-serine β-lactone (2.2 g, 12 mmol) in DMSO (10 ml) was added. The mixture was stirred for 1h before the reaction was terminated with AcOH (686 μl, 12 mmol). The solvent was removed and reaction mixture was purified by flash column packed in methylene choloride. The solvent is changed to methylene choloride/methanol (2/1) gradually. **2** was readily visualized by UV on TLC plate (methylene choloride/methanol (2/1) as solvent system, R_f ~0.49). **2** was isolated as a white solid (48%). ^{1}H NMR (DMSO-d_6, 400MHz) δ: 1.29 (s, 9H, $C(CH_3)_3$), 3.48/4.15 (2H, $H_2C(\beta)$), 4.45 (ddd, 1H, HC(α)), 5.13(s, 2H, $CH_2(C_6H_5)$), 6.35 (d, 1H, HN(BOC)), 6.86 (d, 1H, HC(5)), 7.32 (m, 5H, (C_6H_5)), 7.86 (d, 1H, HC(6)), 10.6 (br s, 1H, HN(4)); MS (FAB) m/z $(M-H)^+$ 431.6 Calculated: 432.43.

N-(9-Fluorenylmethoxycarbonyl)- β -(cytosine-1-yl)alanine 3

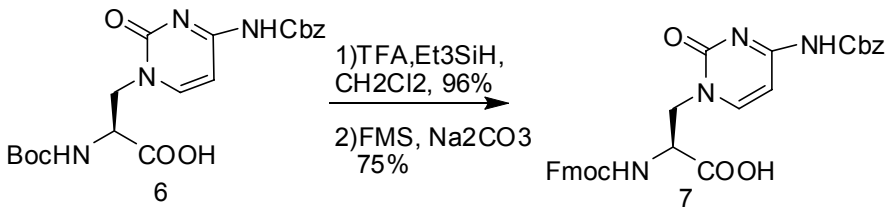

N-(tert-Butoxycarbonyl)-β-(cytosine-1-yl)alanine (2.1g, 4.8 mmol) was acidified by stirring in trifluoroacetic acid (4.8 ml, 62.4 mmol) and dichloromethane (9.8 ml, 154mmol) in the presence of triethylsilane (1.9 ml, 12.0 mmol) at room temperature with

the exclusion of moisture. After 2 hr the reaction was complete and the solvent was removed. Boc-depretection product was readily visualized by TLC (methylene choloride/methanol (2/1) as solvent system, R_f ~0.25) by staining in ninhydrin. The residue was triturated with diethyl ether and the precipitated product isolated by filtration (96%) ^{1}H NMR (DMSO-d_6, 400MHz) δ: 3.88 (2H, $H_2C(\beta)$), 4.29 (ddd, 1H, HC(α)), 5.16(s, 2H, $CH_2(C_6H_5)$), 6.95 (d, 1H, HC(5)), 7.32 (m, 5H, (C_6H_5)), 7.89 (d, 1H, HC(6)).

β-(cytosine-1-yl)alanine (1.4 g, 4.2 mmol) was suspended in 9% sodium carbonate solution (10 ml, 8.4 mmol) and cooled in an ice bath. A solution of 9-Fluorenylmethyl N-succinimidyl carbonate (11.8 g, 3.5 mmol) in dioxane was added in one portion at 0ºC and mixing continued at room temperature for 20 min. The mixture was diluted with water, extracted with ether and ethyl acetate. The remaining aqueous phase was cooled and acidified to pH 2 with concentrated hydrochloric acid. The aqueous phase and the precipitate product was extracted with ethyl acetate, the extract was washed with saturated sodium chloride solution, water, dried with sodium sulphate, and evaporated to a small volume under reduced pressure. On addition of petroleum ether a crystalline product **3** was obtained (75%). **7** was readily visualized by UV on TLC plates (methylene choloride/methanol (4/1) as solvent system, R_f ~0.33). ^{1}H NMR (DMSO-d_6, 400MHz) δ: 3.85/4.16 (2H, $H_2C(\beta)$), 4.22 (d, 2H), 4.37 (ddd, 1H, HC(α)), 4.4 (t, 1H), 5.15(s, 2H, $CH_2(C_6H_5)$), 6.91 (d, 1H, HC(5)), 7.28 (t, 2H), 7.32 (m, 5H, (C_6H_5)), 7.36 (t, 2H), 7.60 (d, 2H), 7.80 (d, 1H, HC(6)), 7.84 (d, 2H), 10.6 (br s, 1H, HN(4)); MS (ESI) m/z $(M+H)^+$ 555.1868 Calculated: 555.1874.

N-(tert-Butoxycarbonyl)- β -(thyminyl-1-yl)alanine 8

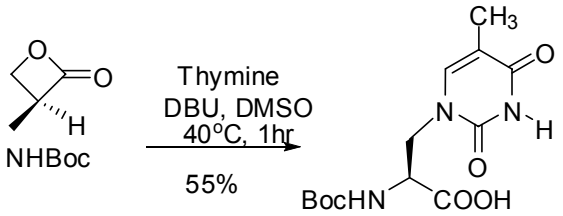

1 8

DBU (1.6 g, 15.0 mmol) was added to a suspension of thymine (2.6 g, 20.0 mmol) in DMSO (10 ml). Within 30 min, a solution of N-(tert-Butoxycarbonyl)-L-serine β-lactone (1.9 g, 10.0 mmol) in DMSO (10 ml) was added. The temperature was raised to 40°C and the reaction mixture was stirred for 1h before the reaction was terminated with AcOH (858 µl, 15.0 mmol). The solvent was removed at 45°C under high vacuum. Reaction mixture was washed with water, and the white precipitate was filtered. The remaining aqueous phase is cooled and acidified to pH 2 with concentrated hydrochloric acid. The mixture was extracted with ethyl acetate for three times, and the organic phase was dried with sodium sulfate. White powder was collected after removing the solvent. Product was visualized by UV on TLC plate (methylene choloride/methanol (2/1) as solvent system, R_f ~0.43). **8** was isolated as a white solid (55%). ^{1}H NMR (DMSO-d_6, 400MHz) δ: 1.31 (s, 9H, $C(CH_3)_3$), 1.72 (d, 3H, $H_3CC(5)$), 3.53/4.21 (dd, 2H, $H_2C(\beta)$), 4.35 (m, 1H, HC(α)), 6.71 (d, 0.15H, HN(BOC)), 7.12 (d, 0.85H, HN(BOC)), 7.35 (s, 1H, HC(6)), 11.26 (s, 1H, HN(3)); MS (FAB) m/z $(M+H)^+$ 314.1 Calculated: 313.31.

N-(9-Fluorenylmethoxycarbonyl)- β -(thymine-1-yl)alanine 9

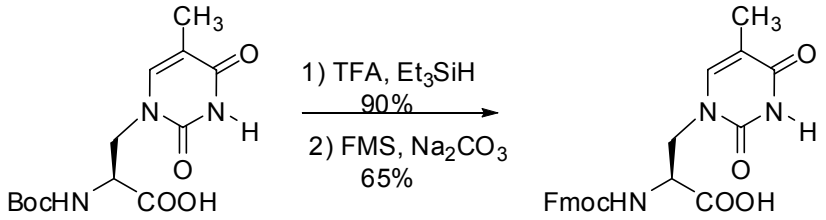

8 9

N-(tert-Butoxycarbonyl)-β-(thymine-1-yl)alanine (1.5 g, 4.8 mmol) was acidified by stirring in trifluoroacetic acid (4.8 ml, 62.4 mmol) and dichloromethane (9.8 ml, 154 mmol) in the presence of triethylsilane (1.9 ml, 12.0 mmol) at room temperature with the exclusion of moisture. After 2 hr the reaction was complete and solvent was removed. Boc-deprotection product was readily visualized by TLC (methylene choloride/methanol (2/1) as solvent system, R_f~0.3) by staining in ninhydrin. The residue was triturated with diethyl ether and the precipitated product isolated by filtration (96%) ^{1}H NMR (DMSO-d_6, 400MHz) δ: 1.74 (d, 3H, $H_3CC(5)$), 3.78 (2H, $H_2C(\beta)$), 4.21 (dd, 1H, HC(α)), 7.36 (s, 1H, HC(6)).

β-(thymine-1-yl)alanine (0.9 g, 4.2 mmol) was suspended in 9% sodium carbonate solution (10 ml, 8.4 mmol) and cooled in an ice bath. A solution of 9-Fluorenylmethyl N-succinimidyl carbonate (11.8 g, 3.5 mmol) in dioxane was added in one portion at 0 ºC and mixing is continued at room temperature for 20 min. The mixture is diluted with water, extracted with ether and ethyl acetate. The remaining aqueous phase is cooled and acidified to pH 2 with concentrated hydrochloric acid. The aqueous phase and the precipitate product was extracted with ethyl acetate, the extract was washed with saturated sodium chloride solution, water, dried with sodium sulphate, and evaporated to a small volume under reduced pressure. White powder product **9** was obtained (65%). **9**

was readily visualized by UV on TLC plate (methylene choloride/methanol (4/1) as solvent system, R_f ~0.35). ^{1}H NMR (DMSO-d_6, 400MHz) δ: 1.79 (d, 3H, H_3CC(5)), 3.62 (2H, H_2C(β)), 4.22 (d, 2H), 4.37 (dd, 1H, HC(α)), 7.28 (t, 2H), 7.36 (s, 1H, HC(6)), 7.38 (t, 2H), 7.60 (d, 2H), 7.84 (d, 2H).

Synthesis and Purification of Aβ(10-21)CyCy and Aβ(10-21)ThTh

Aβ(10-21)CyCy was synthesized on a Rainin Symphony Quartet peptide synthesizer using standard FMOC chemistry on FMOC Rink-amide polystyrene resin (AnaSpec, Inc., usually with substitution 0.4-0.7meq/g) and HBTU/NMM as the coupling reagents. Each amino acid was coupled for 2 hours, unless specified otherwise. Val12, Cy13, Cy14, Leu17, Val18 and Phe19 were double coupled. A capping step with acetylation was performed after every coupling reaction to prevent the formation of deletion peptides. After cleavage and deprotection by 90% trifluoroacetic acid (TFA) with scavengers (thiolanisole/EDT/anisole, 5%/3%/2%), the crude peptide was isolated by trituration with diethyl ether (repeated 4-5 times) and dried under vacuum. The peptide was then purified using a Waters Delta 600 HPLC with Zorbax 300SB-C18 preparative HPLC column (21.2 mm x 25 cm) and eluted at 10 mL/min, room temperature with a linear gradient from H_2O/MeCN (9:1) with 0.1% TFA to H_2O/MeCN (3:2) with 0.1% TFA over 30 min. The product was confirmed by MALDI-TOF mass spectral analysis: Aβ(10-21)CyCy (MALDI: [M+H^+] 1604.3, cal: [M+H^+] 1603.8). Aβ(10-21)ThTh was synthesized and purified in a similar way. Val12, Th13, Th14, Leu17, Val18 and Phe19 were double coupled. The product was confirmed by MALDI-TOF mass spectral analysis: Aβ(10-21)ThTh (MALDI: [M+H^+] 1631.8, cal: [M+H^+]

1630.1). The peptide fractions were collected, rotary evaporated to remove MeCN/TFA, then frozen and lyophilized. Lyophilized peptide was stored at 4°C until required.

CHAPTER 3

INVESTIGATION OF NUCLEOBASE EFFECT ON Aβ (10-21)

INTRODUCTION

Laminated β-sheets have been found to be the fundamental elements in the amyloid fibrils. One of the crucial questions in understanding amyloid self-assembly is how the β sheets laminate, especially the driving force for β-sheets lamination, and relative orientation of sheets. Insight into factors that govern amyloid stabilization will ultimately lead to a better understanding of the pathways for amyloid formation and to methods able to destabilize and/or block this event.

As β sheet lamination is primarily driven by side chain interactions of different amino acids from adjacent sheets, we are particularly interested in how the side chain interacts through basic forces such as electric interactions, hydrophobic interactions, hydrogen bonding and van der Waals interactions to stabilize sheet-sheet lamination.

As an example, Zn^{2+} ion has been identified to be corordinated with his13/his14 dyad in amyloid beta peptide, and investigations of β sheet lamination have been preformed by probing side chain properties of histidine with Zn^{2+} ion incorporation. HPLC spin down and small angle neutron scattering experiments show that the nucleation time for Aβ(10-21) is greatly reduced by zinc-binding to His13 and His14 (Morgan, Dong et al. 2002). This effect of Zn^{2+} coordination on the rate of amyloid formation can be used to differentiate between nucleation and propagation rates.

Based on understanding the role of Zn^{2+} ion incorporation in the process of amyloid self-assembly, we try to explore new recognition elements that manipulate electric interactions, hydrophobic interactions, hydrogen bonding and van der Waals interactions to stabilize sheet-sheet lamination. This study will not only help to understand the self-assembly mechanism that governs amyloid formation, but also enables the identification of novel motifs to control self-assembly process.

Molecular Dynamics (MD) simulations of Aβ (10-21) suggested that a nucleobase modified Aβ (10-21) containing cytosine moieties at the amino acid side chain of H13 and H14 position could maintain a 10 Å separation between the laminate sheets. Guided by the extended β-sheet model, Aβ(10-21)CyCy and Aβ(10-21)ThTh was synthesized for study. In this chapter, nucleobases are used as structural and kinetic probes for Aβ self-assembly, and trying to address the following questions:

1) How does nucleobase incorporation modulate the morphology and structure of amyloid assembly?
2) How does nucleobase incorporation modulate the kinetics of amyloid assembly?

3) What are the driving forces for β–sheets lamination?

4) Where does the nucleobase locate on the amyloid assembly?

RESULTS

Aβ(10-21)CyCy Forms Amyloid Fibrils

At pH 4.3, which is around the pKa of cytosine, it forms very homogeneous amyloid fibrils with an average width 8 ± 0.5nm by TEM and height 8.1 ± 1nm by AFM (Figure 3. 1). After assembly, the peptide solution becomes very viscous and gel-like, but remains transparent. Particles with height smaller than 2 nm were observed coexisting with the amyloid fibrils even after 30 days incubation (Figure 3.1B), which probably resulted from that the peptide self-assembly right after dissolved and reached equilibrium in solution. As was found with the full length Aβ peptide and other longer variants, fibrils formed with Aβ(10-21)CyCy exhibited the green birefringence characteristic of amyloid stained with Congo Red when viewed with polarized light, and the red shift in the absorption spectrum of Congo Red from 495 nm to 540 nm, indicating that Aβ(10-21) indeed forms amyloid.

Aβ(10-21)CyCy Self-Assembly Under Different pH

MD simulation predicted the incorporation of cytosine moieties at specific side chain positions of Aβ(10-21) would facilitate self-assembly. To test this hypothesis,

Figure 3.1

TEM (A) and AFM (B) images and measurements of Aβ (10-21)CyCy fibrils.

Aβ(10-21)CyCy 1.5 mM in 25 mM MES buffer with pH adjusted to 4.3.

A

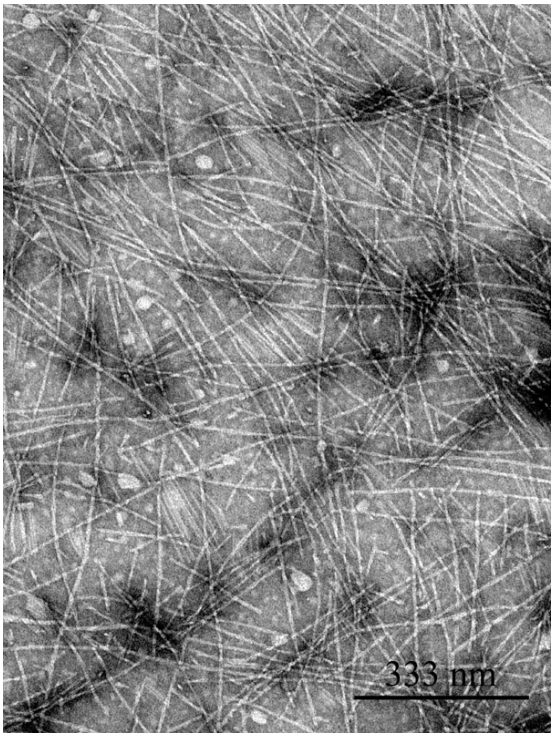

B

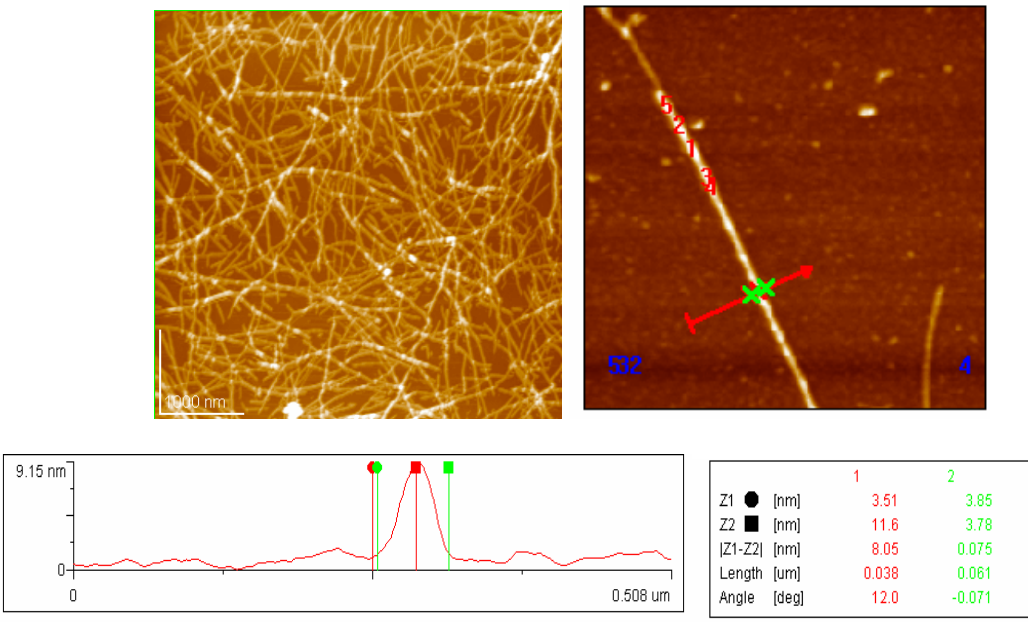

Aβ(10-21) and Aβ(10-21)CyCy were incubated in 25 mM MES buffer under different pH ranging from 3 to 6 at room temperature. To be comparable with Aβ(10-21), Aβ(10-21)CyCy was also dissolved in 25 mM MES buffers at pH 3.3, 4.3, and 5.5 respectively. AFM revealed Aβ(10-21)CyCy self-assembled into fibril like structure under these pH conditions. In contrast, Aβ(10-21) remains particles at pH 3.3 and 4.3, and self-assembles into fibrils only at pH 5.5 (Figure 3.2). Therefore, the nucleobase incorporation broadens the pH range of fibril formation in Aβ(10-21).

Small-angle X-ray scattering (SAXS) was used to delineate the solution structure of the supermolecular assembly of Aβ(10-21)CyCy. TEM images of SAXS samples were shown in Figure 3.3. The X-ray scattering cross section I(Q) for Aβ(10-21)CyCy samples in 25 mM MES buffer at different pH was shown in Figure 3.3A, and the data were interpreted using a modified Guinier analysis which involves plotting ln[Q·I(Q)] versus Q^2 (Figure 3.3B). Rod-like particles give rise to a linear region in the modified Guinier plot in the low Q region ($Q \cdot Rc < 1.1$) where the cross-sectional radius of gyration, Rc, can be derived from the slop of the straight line by the relation $R_c^2 = -2 \cdot \text{slope}$, and the average cross-sectional radius of the rod R is given by $R = R_c \cdot \sqrt{2}$ (Porod 1982; Burkoth, Benzinger et al. 1999; Thiyagarajan, Burkoth et al. 2000). Table 1 presents the cross-sectional radius at different pH value. Clearly, the radius of the rods increases rapidly with increasing pH (Table 3.1). At pH 7.2, the radius of the rod-like particles increased enormously, reaching a value of 117.8 ± 0.6Å. The fibrils are large and polydispersed, and the large radius indicates that at this pH fibril-fibril association was dominant leading to complex network of structures. This is consistent with the observation of TEM (Figure

Figure 3.2

AFM of Aβ(10-21) and Aβ(10-21)CyCy self-assembly under different pH

A, B, C AFM image of 1.5 mM Aβ(10-21) in 25 mM MES buffer with pH adjusted to 3.3, 4.3, 5.5.

D, E, F AFM image of 1.5 mM Aβ(10-21)CyCy in 25 mM MES buffer with pH adjusted to 3.3, 4.3, 5.5.

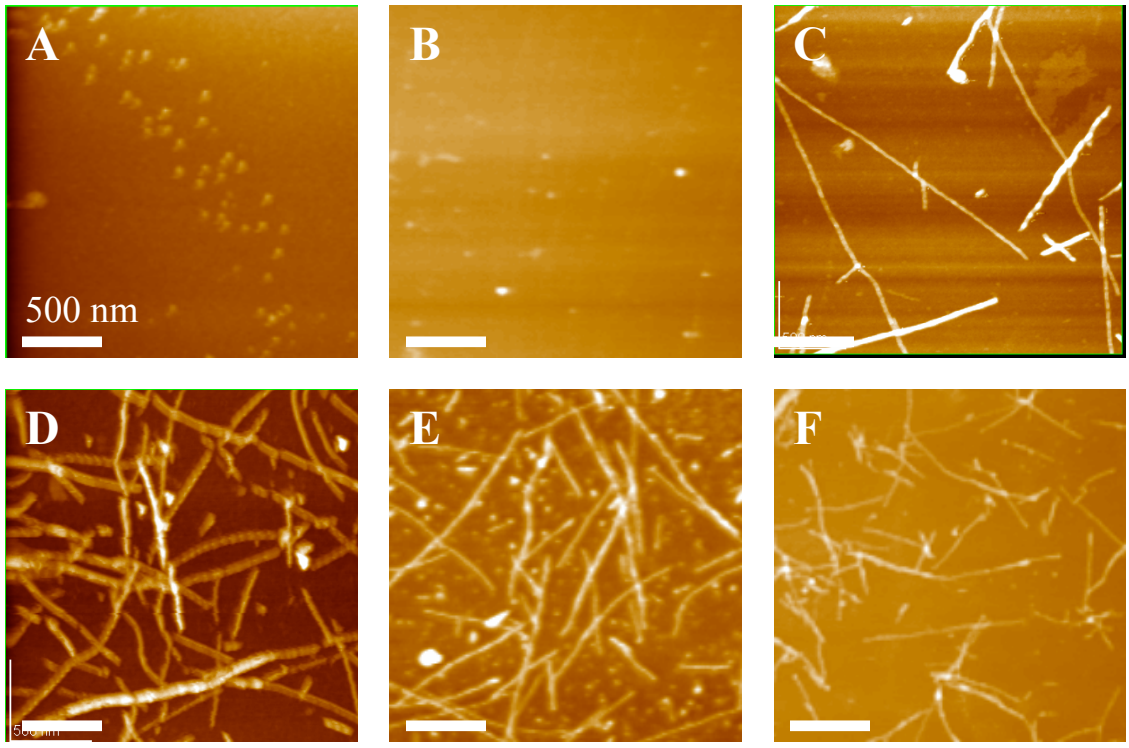

Figure 3.3

Small Angle X-ray Scattering (SAXS) of Aβ(10-21)CyCy.

A. Small angle X-ray scattering intensity I(Q) as a function of momentum transfer (Q= 4πsinθ/λ) of 1.5 mM Aβ(10-21)CyCy in 25 mM MES at pH 3.3, 4.3, 5.5, 7.2.

B. Modified Guinier Analyses for scattering profile of Aβ(10-21) CyCy shown in Figure 3.3A.

A

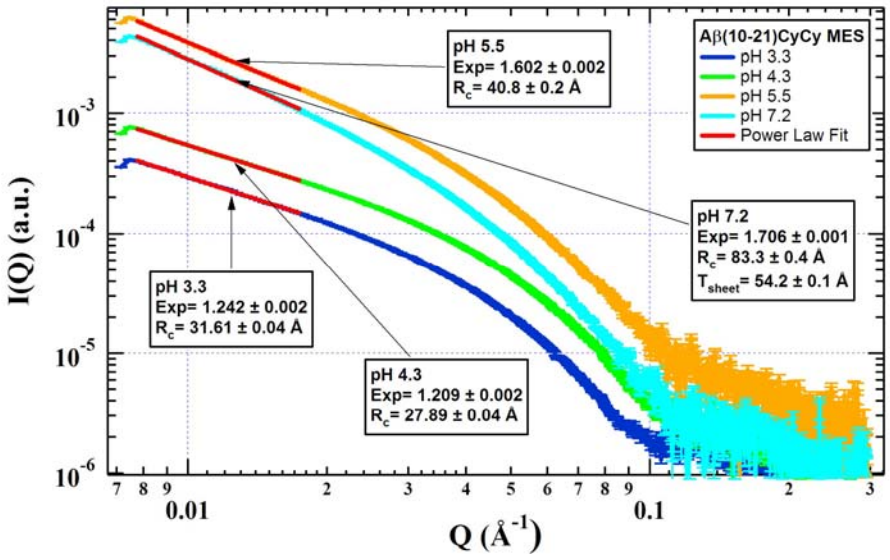

B

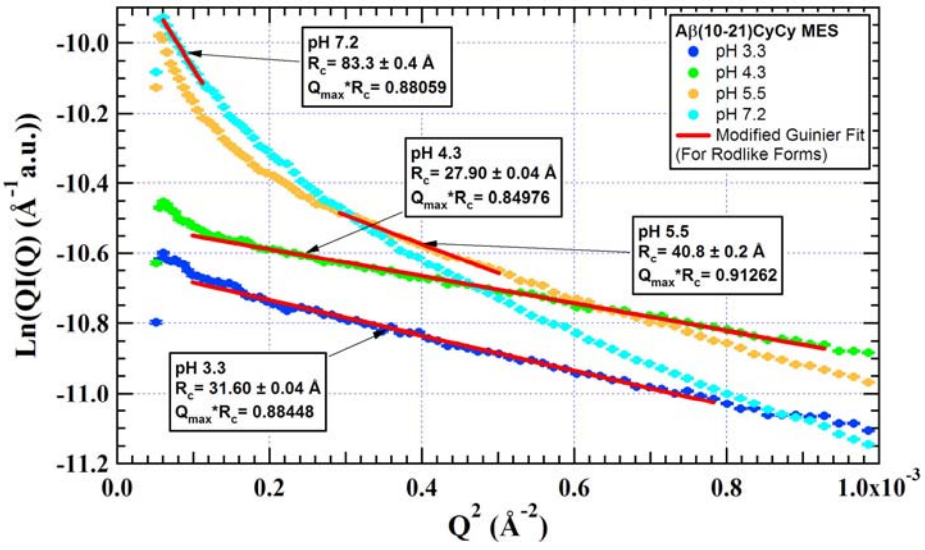

3.4D). The sample at pH 7.2 was also unstable and formed small precipitates over time. Similar observations were reported for Aβ(10-35) fibrils (Thiyagarajan, Burkoth et al. 2000).

Table 3.1 radius of the rods of Aβ(10-21)CyCy as function of pH.

pH	3.3	4.3	5.5	7.2
Rc (Å)	31.60±0.04	27.90±0.04	40.8±0.2	83.3±0.4
R (Å)	44.68±0.06	39.46±0.06	57.7±0.3	117.8±0.6

Aβ(10-21)CyCy Secondary Structure

The conformational changes coincident with amyloid fibril formation were followed by CD (Figure 3.5). At 0 hr, Aβ(10-21)CyCy showed negative molar ellipticity at 208 nm. Over time the intensity of the negative peak increased along with a small negative shoulder at 216 nm, but the spectra was inconsistent with CD spectra of any typical secondary structure. Significant light scattering by large particles, such as assembled fibrils and the viscosity of the assembled solution, may contribute to the observed elipticity. The cytosine was assigned to a maximum at 275 nm and a minimum at 235 nm. The elipticity at 275 nm might suggest the base pairing between cytosine moieties. Previous temperature-dependent studies of alanyl PNA self-pairing correlated the decrease of molar elipticity at 275 nm with the UV melting curve (Diederichsen and Schmitt 1996). However, the melting temperature of Aβ(10-21)CyCy fibrils is above 100 ºC, and there is no change in the CD spectra under 100 ºC.

Figure 3.4

TEM images of Aβ(10-21)CyCy

TEM images of 1.5mM peptide assembled in 25mM MES buffer at pH: A, pH=3.3; B, pH=4.3; C, pH=5.5; D, pH=7.2.

A

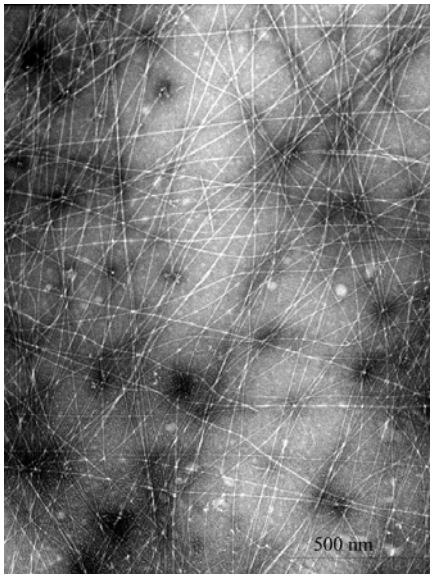

B

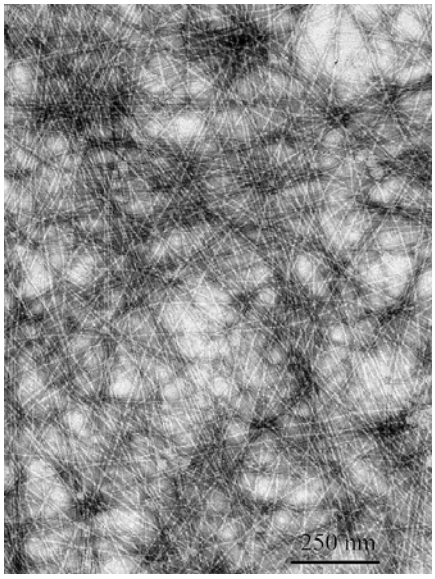

C

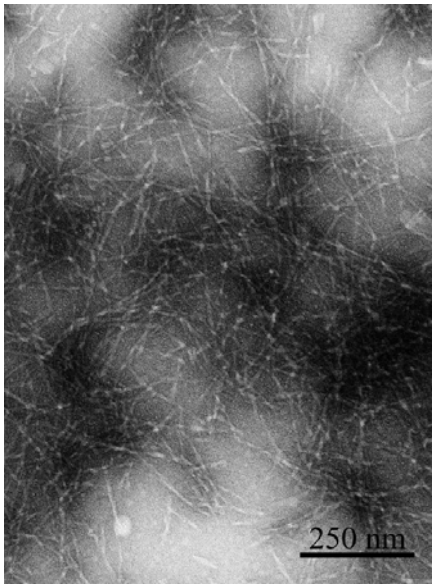

D

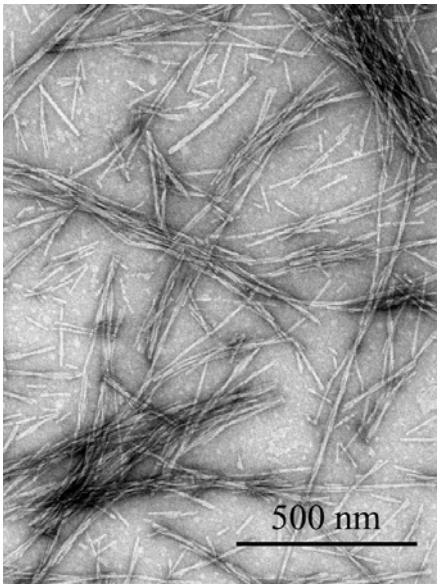

Figure 3.5

Time-dependent CD spectra of Aβ(10-21)CyCy.

CD spectra of a 1.5 mM Aβ(10-21)CyCy solution in 25mM MES buffer (pH 4.3). Negative peak at 208nm and positive peak at 275nm are developed in solution over incubation.

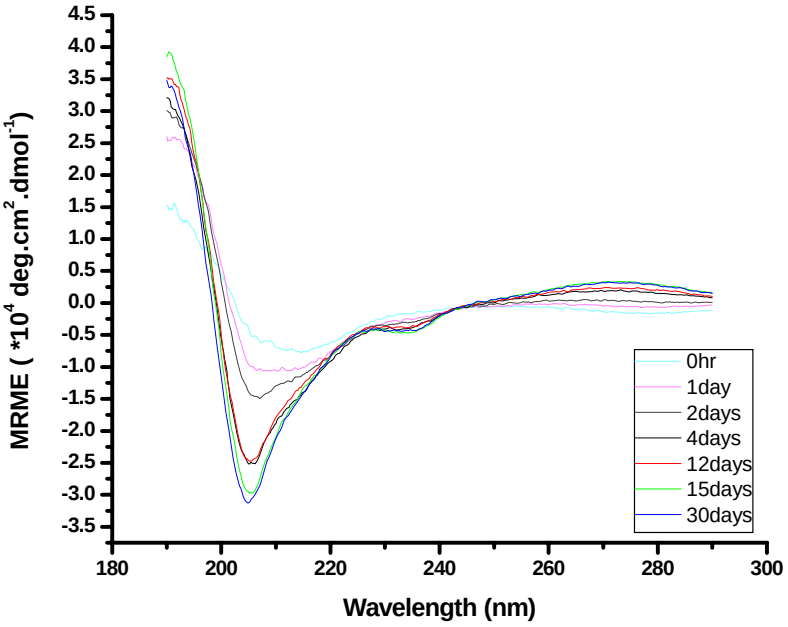

Figure 3.6

FT-IR spectra of Aβ(10-21)CyCy

After one month incubation, the sample was centrifuged at 16,110xg for 30 min and the pellet and supernatant were dried by lyophilization and FT-IR spectra were recorded qindividually. The pellet, blue; and the supernatant, red.

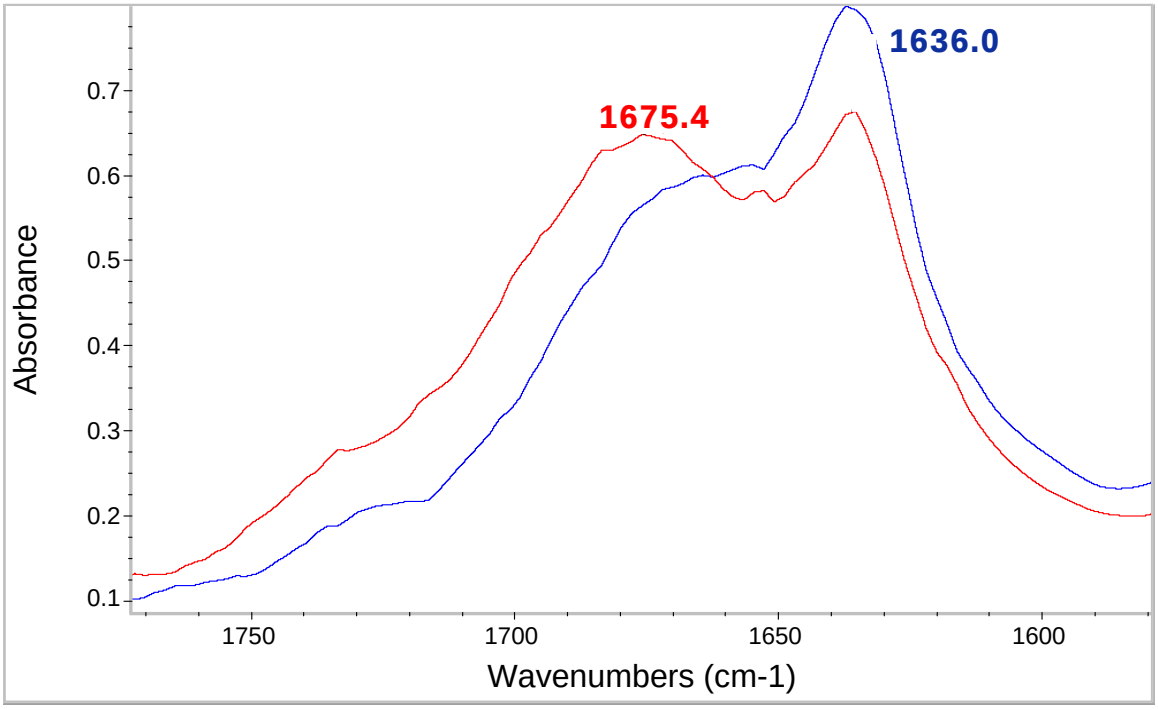

Infraed absorption (IR) spectroscopy has been extensively used for peptide conformational assignments (Hilbich, Kisterswoike et al. 1991; Wood, Maleeff et al. 1996), and Aβ(10-21)CyCy was further investigated by FT-IR (Figure 3.6). Mature fibrils were pelleted by centrifugation to remove non-assembled monomers. The pellet showed the amide carbonyl stretch (type II) at 1636 cm^{-1}, further supporting the CD assignment of β sheet secondary structure in the fibrils.

Does Cytosine accelerate self-assembly?

The effect of cytosine moiety on the rate of Aβ(10-21) assembly was followed by small angle neutron scattering (SANS). Both Aβ(10-21) and Aβ(10-21)CyCy were dissolved in 25mM MES buffers at pH 5.5, condition under which both peptides self-assemble into fibrils. The formation of large aggregates was also directly monitored by SANS. In order to acquire data within a reasonable time frame, experiments were performed at an initial peptide concentration of 3.3 mM. As seen in Figure 3.7, SANS intensity increased in the low Q region over time, indicating the formation of large particles. The SANS intensity at Q = 0.03 $Å^{-1}$, the region of best signal-to-noise and most appropriate for the expected fibril sign, was plotted as a function of aging time. For Aβ(10-21), a nucleation phase lasted several hours followed by a persistent growth phase and a plateau in 8 hours. For Aβ(10-21)CyCy, a nucleation phase was undetectable. Taken together, it was shown that cytosine moiety incorporation accelerates amyloid formation of Aβ(10-21).

Figure 3.7

Small Angle Neutron Scattering (SANS) Aβ(10-21) and Aβ(10-21)CyCy over time.

A. Small angle neutron scattering intensity I(Q) over time as a function of momentum transfer ($Q= 4\pi\sin\theta/\lambda$) of 3.3mM Aβ(10-21).

B. Small angle neutron scattering intensity I(Q) over time as a function of momentum transfer ($Q= 4\pi\sin\theta/\lambda$) of 3.3mM Aβ(10-21)CyCy.

C. Plot of I(Q) at $Q=0.03\text{Å}^{-1}$ as a function of time in Aβ(10-21) (blue) and in Aβ(10-21)CyCy (red).

A

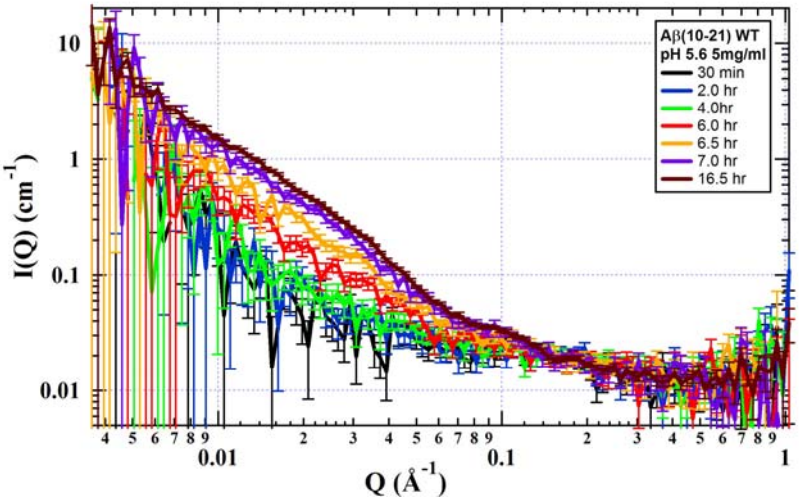
Aβ(10-21) WT
pH 5.6 5mg/ml
30 min
2.0 hr
4.0hr
6.0 hr
6.5 hr
7.0 hr
16.5 hr
I(Q) (cm^{-1})
Q (Å^{-1})

B

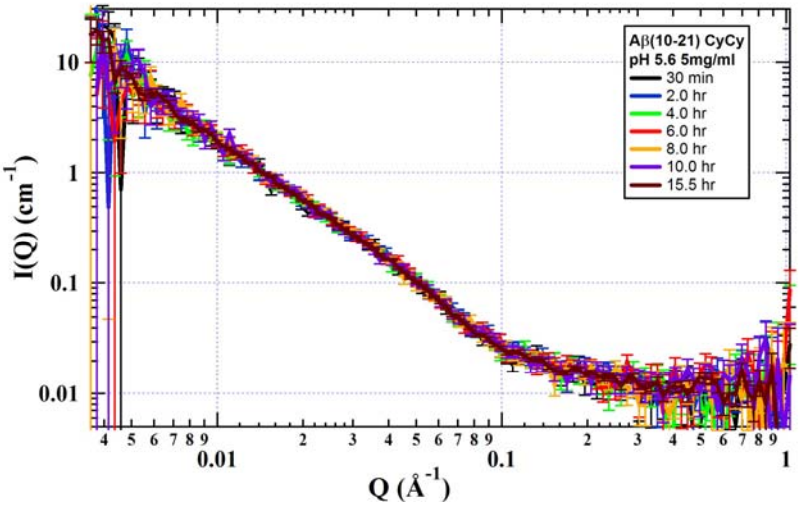
Aβ(10-21) CyCy
pH 5.6 5mg/ml
30 min
2.0 hr
4.0 hr
6.0 hr
8.0 hr
10.0 hr
15.5 hr
I(Q) (cm^{-1})
Q (Å^{-1})

C

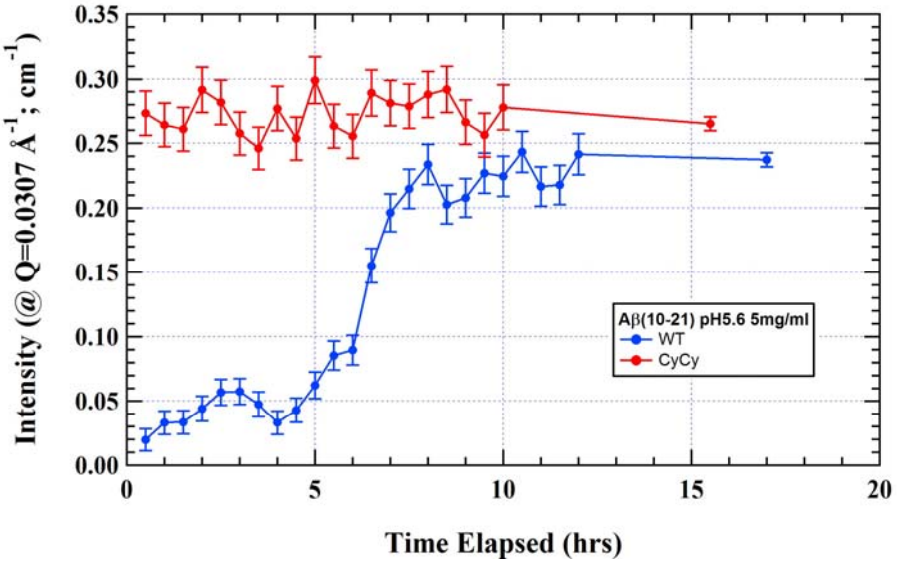
Aβ(10-21) pH5.6 5mg/ml
WT
CyCy
Intensity (@ Q=0.0307 Å^{-1}; cm^{-1})
Time Elapsed (hrs)

Do the Aβ(10-21) and Aβ(10-21)CyCy assemblies have the same structure?

Though the mature fibrils formed by Aβ(10-21)CyCy and Aβ(10-21) have similar morphologically similar, the fibril assembly pathways may be distinct. To investigate intermediates in the self-assembly pathway, Aβ(10-21)CyCy was prepared at a peptide concentration as low as 0.1 mM. As seen by AFM (Figure 3.8), at 0 hr, small particles were observed initially that appeared fuse to form large particles, at least on the AFM grid, to line up to form short assemblies with heights of 2 ± 1 nm (Figure 3.8A). Such fusing events have also been observed in other amyloid fibril assembly pathways (Seilheimer, Bohrmann et al. 1997). Over time, smooth fibrils with height of 4 ± 1 nm appeared (Figure 3.8B). Finally smooth fibrils twisted to form mature fibril with height of 8 ± 1 nm.

Point Mutation at His13 and His14 of Aβ(10-21)

Since zinc-binding to His13 and His14 in Aβ(10-21) is through inter-sheets interactions, point mutations of His13 and His14 may have important effects on the conformation of the peptide and consequently on the rate of fibril growth. To investigate the specificity, we examine the effect of substitution of cytosinyl-alanine, glutamine and phenylalanine for histine at poistion 13 and 14 in Aβ(10-21). As shown in the molecular dynamic simulation, at pH values around the pKa of cytosine (~4.2), a third H-bond could form between the two cytosines along β sheet lamination dimension and stabilize the fibril formation. If the two cytosines are protonated, charge repulsion is expected to disturb assembly; and indeed, Aβ(10-21)CyCy did not assemble at pH 2. As a control, the QQ dyad in Aβ(10-21)H13QH14Q could hydrogen bond as in CyCy, but independent

of pH. FF dyad in Aβ(10-21)H13FH14F would also accelerate fibril formation independent of pH. Based on this analysis, substitutions of H with amino acids Q and F were synthesized. Purified Aβ(10-21)QQ and Aβ(10-21)FF were dissolved in 40% actenitrile/water solution (due to the solubility issue) and allowed to assemble at various pHs. Significant β-sheet signature, with a minimum at 220 nm by CD, appeared right after the sample dissolved, indicating an increased propensity toward amyloid formation. Both Aβ(10-21)QQ and Aβ(10-21)FF self-assembled at a broad pH range from 2 to 7 (Figure 3.9 and Figure 3.10). Fibrils were observed by AFM with 8 ± 1 nm in height for both of the congeners (Table 3.2). Based on the above data, 13 and 14 positions in Aβ(10-21) appears structurally flexible and able to accommodate a variety of amino acids substitutions. Besides, previous research of the effects of hydrophobic amino acids (Phe, Ile, Val, or Tyr) on peptide self-assembly showed that morphology is delicately determined by the interactions between hydrophobic residues, especially the aromatic interactions between Phe residues (Matsumura, Uemura et al. 2004). In our study, according to the HPLC retention time and solubility, CyCy are less hydrophobic than QQ and FF dyads, and as hydrophilic as HH dyad, however, Aβ(10-21)CyCy has greater propensity to self-assembly into fibrils than Aβ(10-21), especially at pH 4 or lower, under which condition cytosine will be protonated and the positive charges on the side chain will destabilize the sheet-sheet lamination. It suggests that hydrophobic packing is not only driving force for amyloid self-assembly, though this interaction is very important.

Figure 3.8 Morphology Development of Aβ(10-21)CyCy

(A) 0 days, particles with height 1-2 nm

(B) 4days, particles grows into the fibrils with height of 3-4 nm

(C) 8 days, most of particles disappear, the fibrils mature with height increases to 8-9 nm

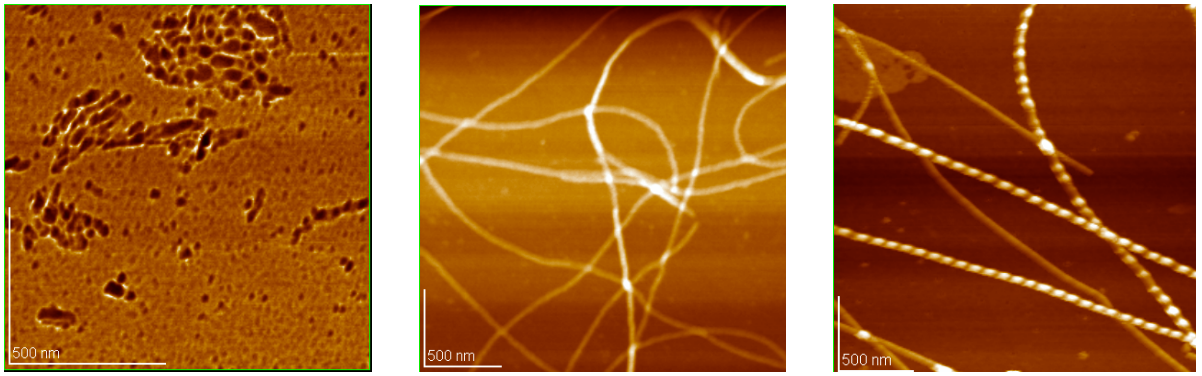

Figure 3.9

CD spectra and AFM of Aβ(10-21)QQ self-assembly under different pH

A, B, C, CD spectra of 1.5mM Aβ(10-21)QQ in 40% acetontrile/water with pH adjusted to 2.0, 3.3, 7.2.

D, E, F, AFM of 1.5mM Aβ(10-21)QQ in 40% acetontrile/water with pH adjusted to 2.0, 3.3, 7.2.

A **B** **C**

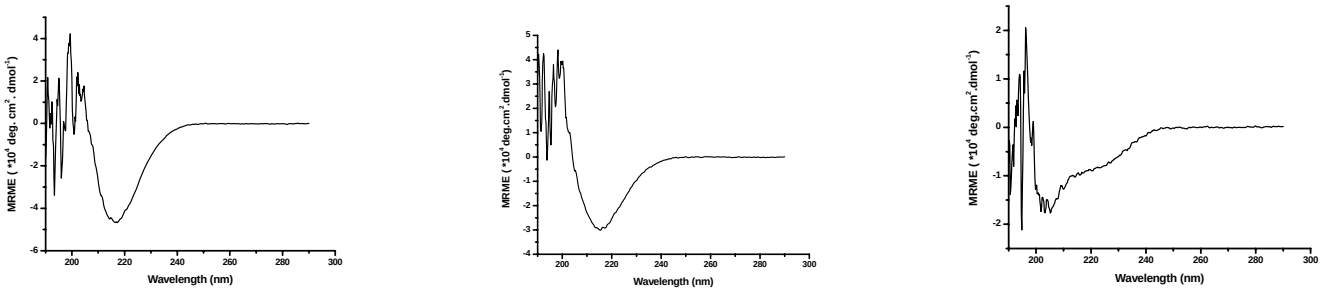

D **E** **F**

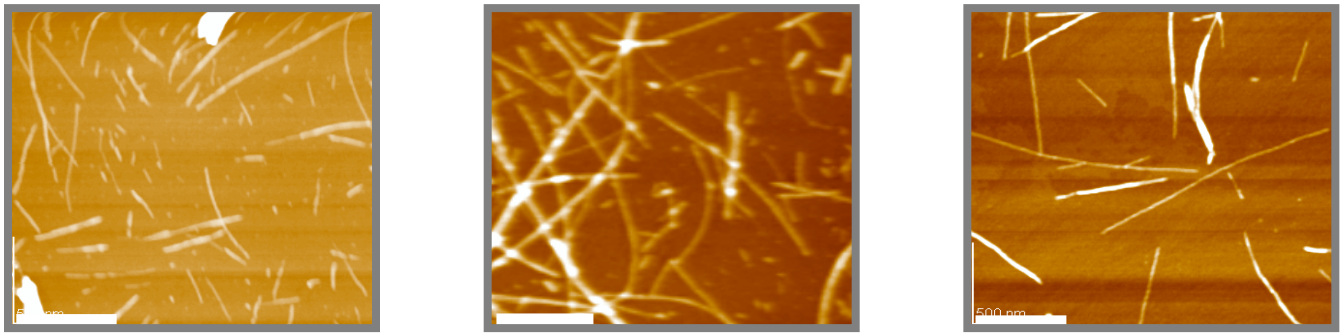

Figure 3.10

CD spectra and AFM of Aβ(10-21)FF self-assembly under different pH

A, B, C, CD spectra of 1.5mM Aβ(10-21)FF in 40% acetontrile/water with pH adjusted to 2.0, 3.3, 7.2.

D, E, F, AFM of 1.5mM Aβ(10-21)FF in 40% acetontrile/water with pH adjusted to 2.0, 3.3, 7.2.

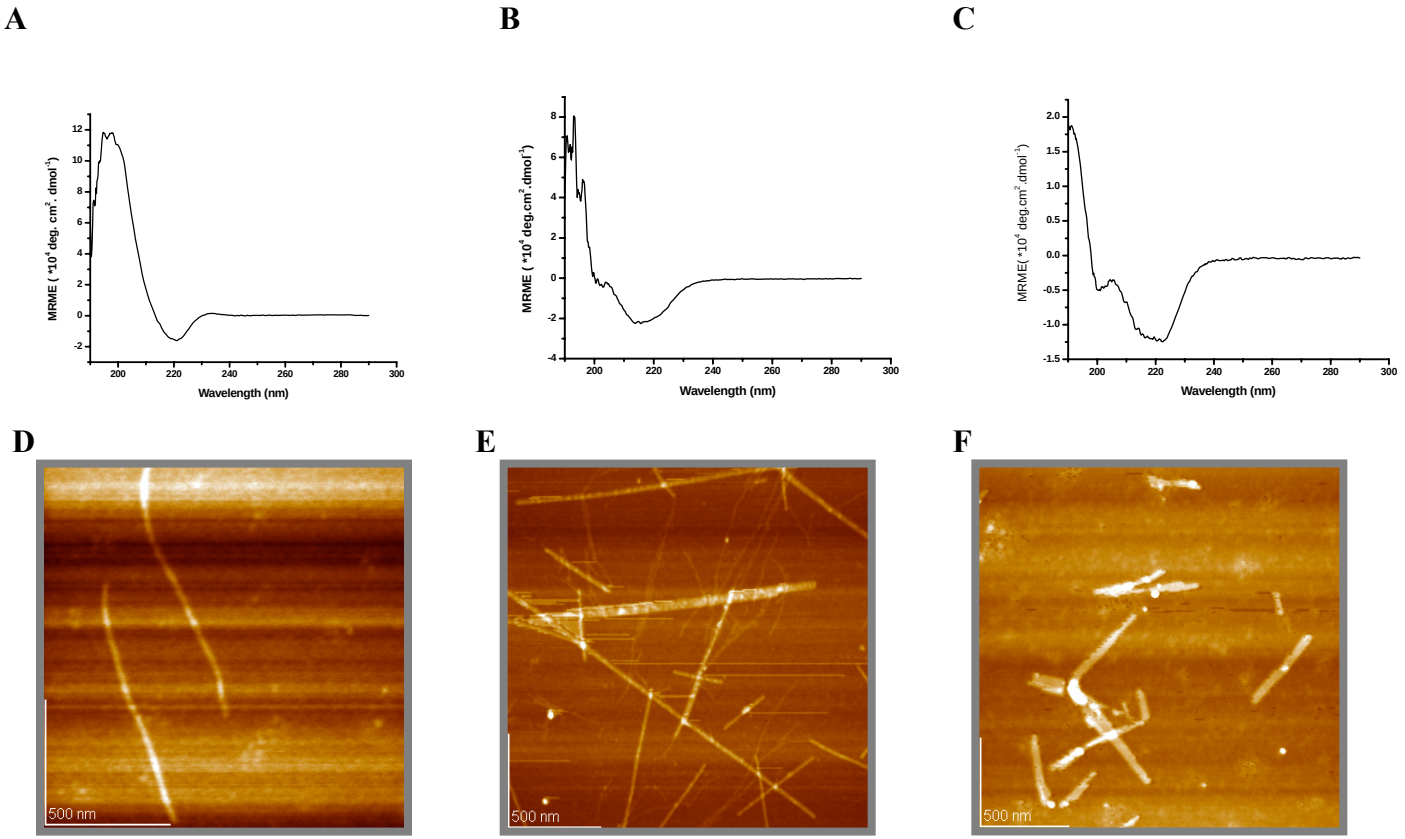

Investigation of the surfaces of nucleobases modified amyloid fibrils

Aβ(10-21)CyCy Acts as templates for metal deposition

Nucleobase modified amyloid beta peptide could be a good candidate for assisting the bottom-up assembling of nanostructure due to the following reasons. First of all, peptide-based nanomaterials have particular advantage in tailored molecular design, availability of a variety of functional groups, low toxicity, biodegradability and ability of self assembly into desired structural scaffold. With easily modified self-assembled surfaces and relatively high stability, synthetic amyloid fibrils were tested for the possibility as templates. In turn, this study would provide structural information of amyloid fibril surfaces. Secondly, due to the unique self-recognition properties, nucleobases could be a robust sensing or positioning component. For example, DNA molecules were used to template the metal nanoparticles into nanoclusters or nanowires (Braun, Eichen et al. 1998; Petty, Zheng et al. 2004).

Hg^{2+} and Ag^{+} ions have been found to be very effective in binding the nucleotide bases and there is no evidence showing that these metal ions bind phosphate (Eichhorn 1973; Marzilli 1977). Hg^{2+} has strong affinity for AT rich DNA and Ag^{+} for GC rich DNA. Specifically, silver forms complexes with purines or pyrimidines via nitrogen or π–electron coordination of the bases. Taking the advantage of great affinity of Ag^{+} ions for nucleobases, we test the possibility of growing silver nanoparticles with Aβ(10-21)CyCy as templates. If the cytosine moieties expose on surfaces of Aβ(10-21)CyCy fibrils, they would act as template to direct the deposition of Ag^{+} ions. Once localized, these silver cations can be reduced to form nanoparticles following the contour of the template. Following procedures described in the materials and methods section, silver

nitrate solution was first mixing with Aβ(10-21)CyCy solutions at various Ag^+ to peptide ratios. The peptide solution remains transparent after mixing with $AgNO_3$ solution. However, addition of $NaBH_4$ solution resulted in immediate precipitation and solution turns into brown or black depends on the concentration of $AgNO_3$, indicating the formation of silver particles. The silver-peptide binding was studied by UV-Vis spectra. No significant UV absorbance change with Ag^+: peptide ratio of 1:1. At Ag^+: peptide ratio of 5:1, the cytosine absorption maximum at 274 nm decreased from 0.869 to 0.854 upon Ag+ complexation, at which wavelength indicated the absorbance of cytosine bases (Figure 3.11). Following reduction of the bound ions, further spectral changes occur. Absorption peak at 274 nm shifts to 270 nm, and the absorbance increases to 1.14. These changes in the UV absorption might indicate the silver ions and nanoclusters associate with the bases. According to previous research on DNA-silver binding, this blue shift may be attributed to new, overlapping electronic bands for small silver clusters, which are known to absorb in this spectral region (Petty, Zheng et al. 2004). Reduction of the Ag^+ bound to the peptide results in a new absorption peak occurred in the visible region of the spectrum. The transition has λmax at 416 nm at 2 min after adding the BH^{4-}. Theoretical and low-temperature spectroscopic studies suggested electronic transitions for small silver clusters, in particular Ag_2 and Ag_3, are expected in this spectral region (Marchetti, Muenter et al. 1998; Bonacic-Koutecky, Pittner et al. 1999). Through TEM images shown in Figure3.12, several continuous silver coated fibrils were observed, however, the majority of the fibrils remained uncoated. This heterogeneous coating is probably due to the self-nucleation of Ag nanoparticles (Fu, Wang et al. 2003). On the same grids, the binding of individual Ag particles were also observed. Together, these

results suggest that it may be feasible to control the formation of nanoclusters using nucleobases modified amyloid peptide as template.

Aβ(10-21)ThTh Self-Assembly Under Different pH and Preliminary Data on DNA Binding

ThTh dyad in Aβ(10-21)ThTh could accelerate fibril formation independent of pH change. To test this hypothesis, Aβ(10-21)ThTh were incubated in 25mM MES buffers at pH 3.3, 4.3, 5.5 and 7.2 respectively. TEM revealed Aβ(10-21)CyCy self-assembled into fibril like structure under these pH conditions right after the peptides dissolved (Figure 3.13). The fibrils at pH 7.2 are clearly shorter and tend to bundle together as shown in TEM. Small-angle X-ray scattering (SAXS) was used to delineate the solution structure of the supermolecular assembly of Aβ(10-21)ThTh. The X-ray scattering cross section I(Q) for Aβ(10-21)ThTh samples in 25 mM MES buffer at different pH was shown in Figure 3.14A, and the data were interpreted using a modified Guinier analysis which involves plotting $\ln[Q \cdot I(Q)]$ versus Q^2 (Figure 3.14B). Table 2 presents the cross-sectional radius at different pH. Similar to Aβ(10-35) and Aβ(10-21)CyCy, the radius of the rods increases rapidly with increasing pH. At pH 7.2, the radius of the rod-like particles increased enormously, reaching a value of 152.0 ± 1.4 Å. The fibrils are large and polydispersed, and the large radius indicates that at this pH fibril-fibril association was dominant leading to complex network of structures, which is consistent with the observation of TEM. The sample at pH 7.2 was also unstable and formed precipitates over time.

Figure 3.11

UV-Vis spectra of Aβ(10-21)CyCy to association with Ag+ and Ag nanoclusters.

A (black line), 0.15mM peptide solution; B (red line), peptide with 0.75mM Ag^+ (5 Ag^+:2 bases); C (green line), 2 min after adding 1 BH_4^-:1 Ag^+ to the peptide/Ag^+ solution.

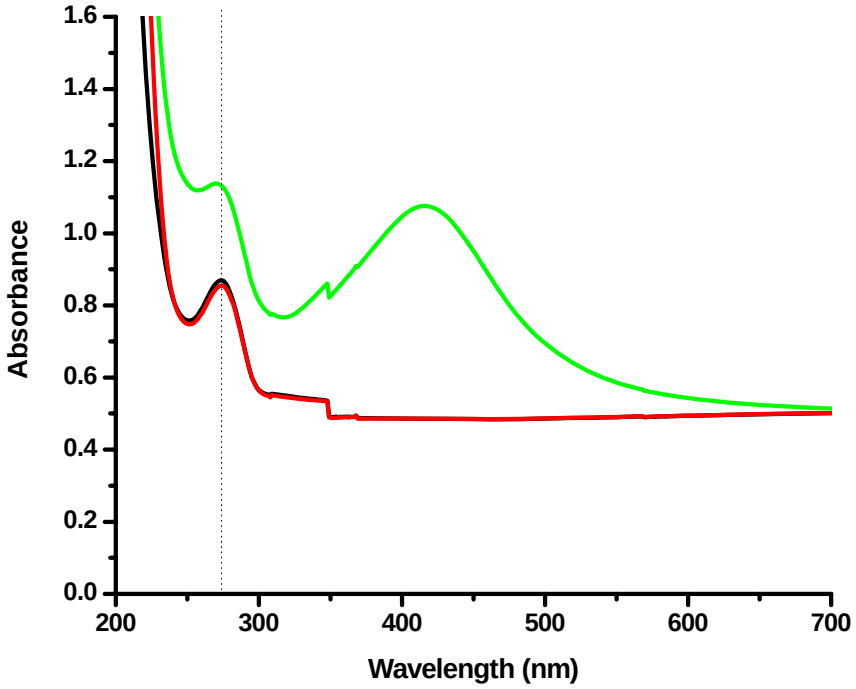

Figure 3.12

Sivler nanoparticle binding on Aβ(10-21)CyCy fibrils.

TEM images 1.5mM Aβ(10-21)CyCy in 25mM MES at pH3.3. Ag^{+}: peptide ratio of 5:1 at different spots. Scale bar, 167nm.

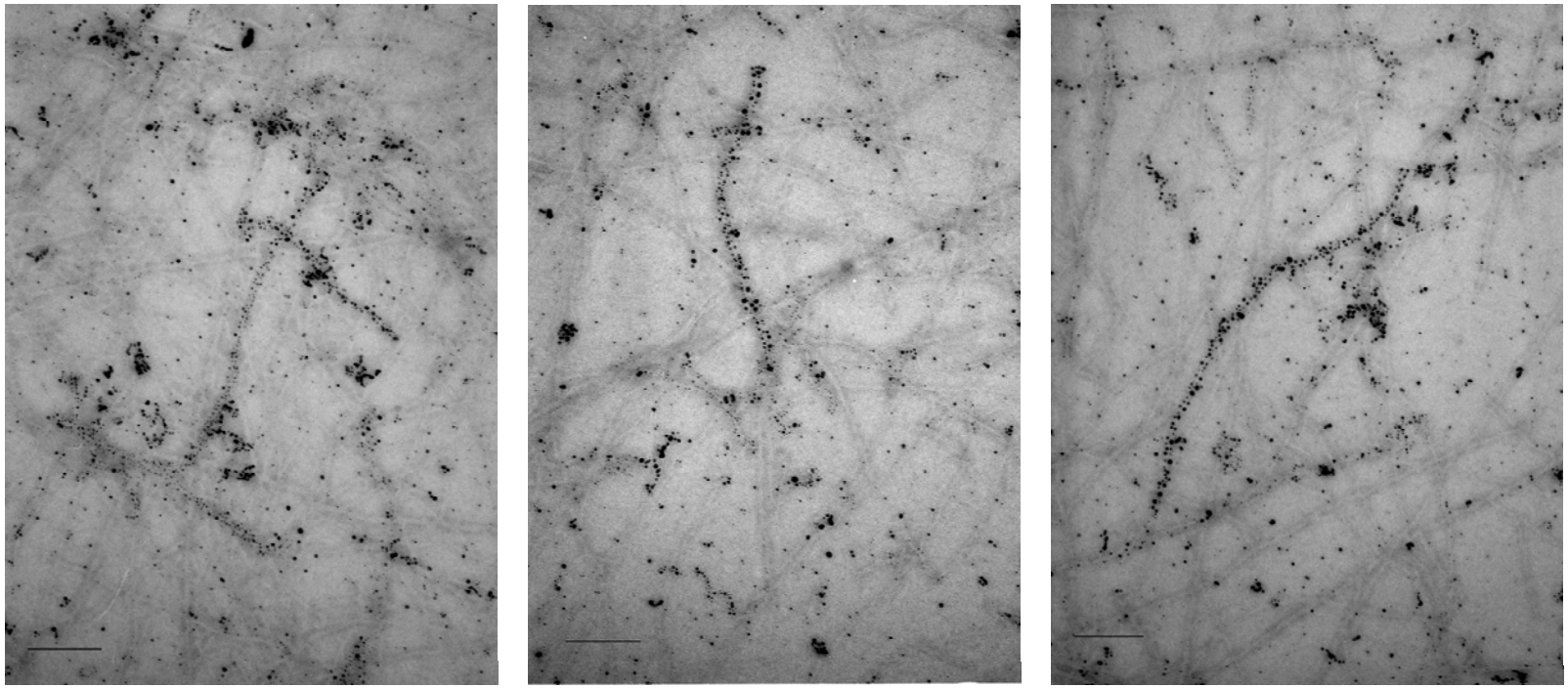

Table 3.3 Radius of the rods of Aβ(10-21)ThTh as function of pH.

pH	3.3	4.3	5.5	7.2
Rc (Å)	28.58±0.03	27.9±0.04	49.2±0.2	107.5±1.0
R (Å)	40.42±0.04	39.46±0.06	69.6±0.3	152.0±1.4

If the structure of Aβ(10-21)ThTh fibrils is similar to Aβ(10-35) fibrils as the molecular dynamic simulation suggests, that is, consist of laminated sheets twisting along the fibril axis, then there will be thymine bases exposing on the surface of fibril. Then it is possible to use Aβ(10-21)ThTh as template to bind DNA. Therefore, we tested the binding of Aβ(10-21)ThTh with oligodeoxyadenosine, (dAp)n. As Aβ(10-21)ThTh solution at pH 7.2 was unstable and formed precipitates over time, solutions of Aβ(10-21)ThTh at pH 5.5 were used to study the Aβ(10-21)ThTh-polyA binding by CD. 1.5 mM Aβ(10-21)ThTh in 25 mM MES buffer (pH 5.5) was diluted in half and make Aβ(10-21)ThTh: polyA ratio of 6:1. $(dAp)_2$, (dAp)4, $(dAp)_6$, $(dAp)_{12}$ and $(dAp)_{24}$ was used to test if there is chain-length-specific binding. Spectra of Aβ(10-21)ThTh mixing with polyA was taken first and then substracted the poly A curve to compare with the Aβ(10-21)ThTh curve. As shown in figure 3.15, if there is binding between the Aβ(10-21)ThTh and polyA, then the substraction CD curve will not overlap with CD curve of Aβ(10-21)ThTh. This preliminary data suggested there is some interaction occuring between the peptide and polyA. Further investiagation on sequence- and chain-length-specific reading of a Aβ(10-21)ThTh template is needed.

Figure 3.13

TEM images of Aβ (10-21)ThTh fibrils

TEM images of 1.5mM Aβ(10-21)ThTh in 25mM MES buffer with pH adjusted to 3.3 (A), 4.3 (B), 5.5 (C) and 7.2 (D) .

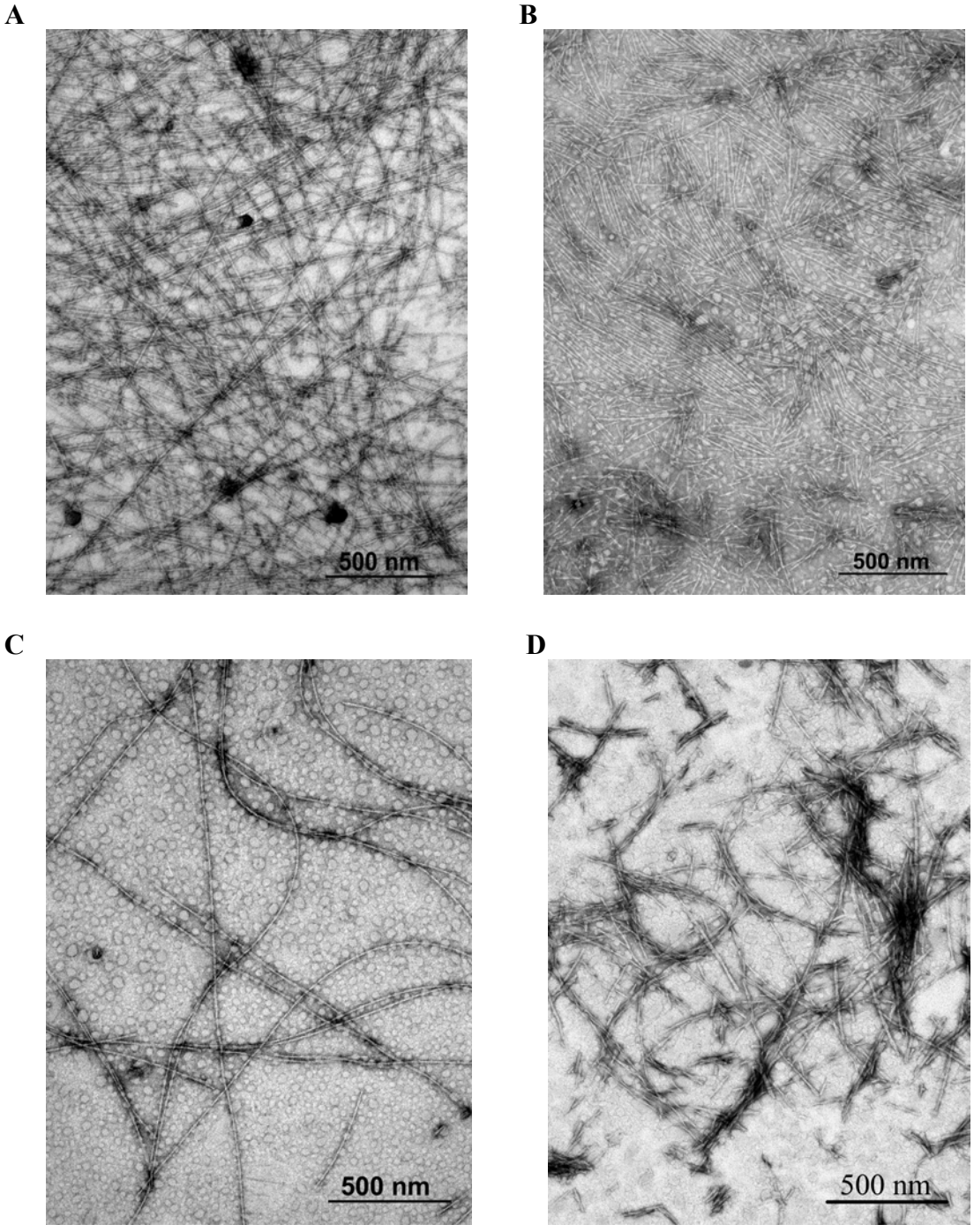

Figure 3.14

Small Angle X-ray Scattering (SAXS) of Aβ(10-21)ThTh.

A. Small angle X-ray scattering intensity I(Q) as a function of momentum transfer (Q= 4πsinθ/λ) of 1.5 mM Aβ(10-21)ThTh in 25mM MES at pH3.3, 4.3, 5.5, 7.2.

B. Modified Guinier Analyses for scattering profile of Aβ(10-21)ThTh shown in figure 3.15A.

A

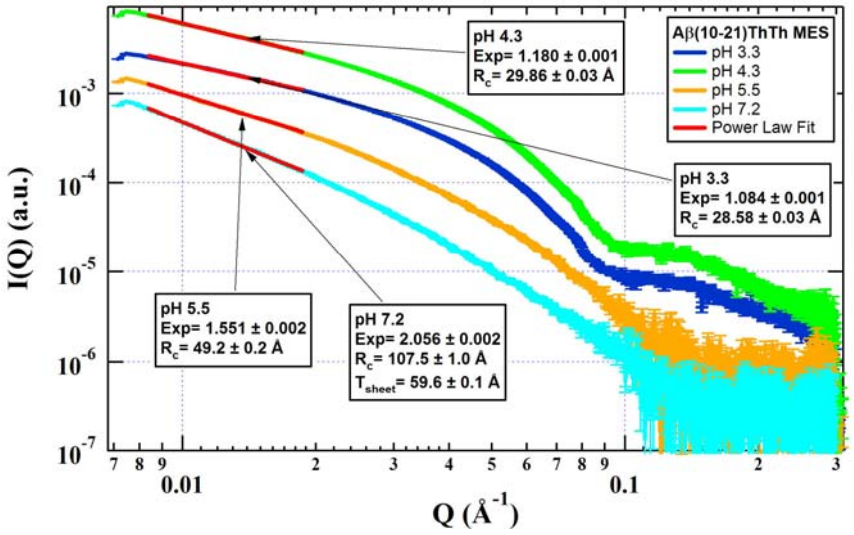

B

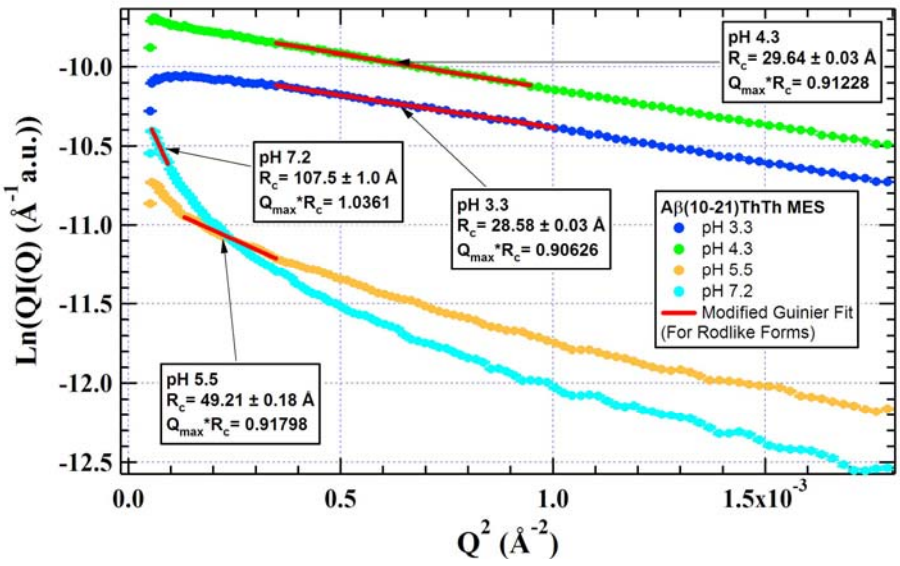

Figure 3.15

CD spectra of Aβ(10-21)ThTh mixing with polyA.

CD spectra of 1.5 mM Aβ(10-21)ThTh in 25mM MES buffer (pH 5.5) was diluted in half to make a Aβ(10-21)ThTh: polyA ratio of 6:1. Spectra of Aβ(10-21)ThTh mixing with polyA was taken first and then substracted the poly A curve to compare with the Aβ(10-21)ThTh curve.

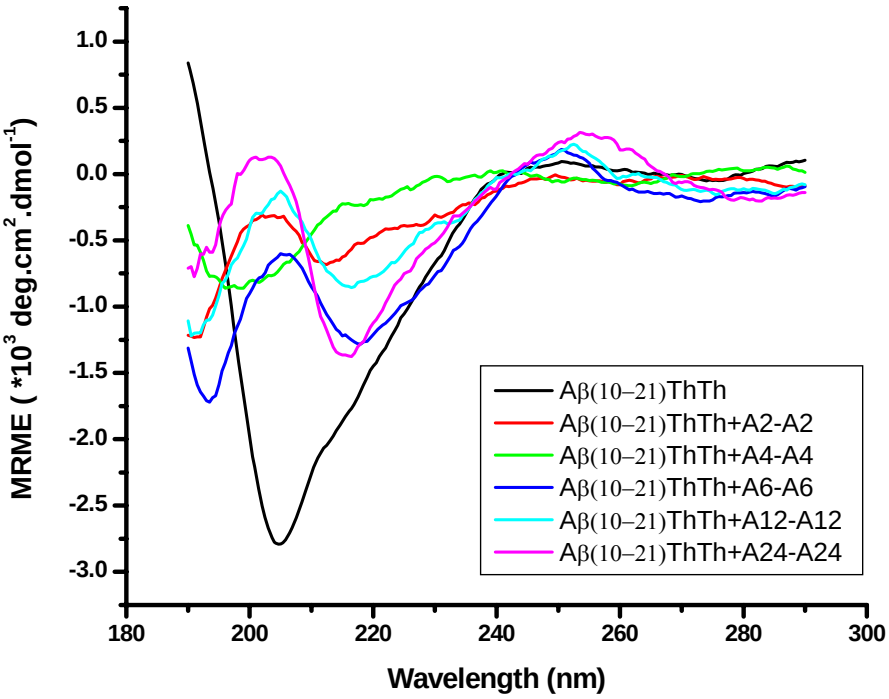

DISCUSSION

Here we showed that nucleobase modified amyloid peptide, Aβ(10-21)CyCy, is sufficient to form homogeneous amyloid fibrils. As expected, reaction conditions for the modified system Aβ(10-21)CyCy vary from native Aβ(10-21). Aβ(10-21)CC forms fibrils readily at pH 4, fibrils form at one tenth the concentration of Aβ(10-21), and the fibrils have the appearance of the Zn^{2+}-induced nucleation, forming relatively short and dense fibrils. The most striking difference exists between the pH required for fibril formation (pH of ~4 for Cy---Cy modified versus 5.5 for the native) suggesting a protonated state for the pyrimidines. Cytidine incorporation provides an additional element to explore the assembly pathway, extend the conditions for assembly, and stabilize fibril architecture.

Several observations suggest that cytosine incorporation induces Aβ(10-21) nucleation, specifically: 1) cytosine incorporation at the amino acid side chain increases assembly rate, 2) cytosine incorporation induces significantly denser and shorter fibrils at the same peptide concentration of Aβ(10-21) wild type without alternating fibril width. This suggests that it is possible to find conditions that differentially alter nucleation and propagation rates, and hence opens the possibility of further probing the mechanism of amyloid self-assembly. This work is the first successful demonstration of incorporation of nucleobases into the amyloid peptide self-assembly system.

The aggregation properties of Aβ(10-21)CyCy and Aβ(10-21) were compared in several ways. CD and FTIR spectroscopy suggest the confirmations of the two peptides are nearly identical in their folded states. TEM and AFM revealed the fibril formed by the two peptides have similar dimension. Cross-seeding experiment suggested that the

two peptides would use their shared sequence in similar way to engage in amyloid folding and the conformation at fibril growth end is quite similar.

Although Aβ(10-21)CyCy, Aβ(10-21)QQ and Aβ(10-21)FF form fibrils with similar dimension, they response to pH change differently and therefore reflect different side chain properties. Mutations associated with modest change in side chain hydrophobicity, charge and dipole monent, were observed to have great impact on fibril growth kinetics and stability. A critical question in the research of nucleobase modified amyloid peptide is the role nucleobase playing in the process of peptide folding. Does the nucleobase have inter-sheet contacts as the model predicts? How does the side chain packing contribute to accelerated amyloid fibril formation? Why does the nucleobase incorporation only accelerate fibril formation but not alter the assembly structure? Understanding the structure details of nucleobase incorporation would be helpful to explore the factors affecting amyloid self-assembly and factors controlling the assembly kinetics and morphology.

We have utilized Aβ(10-21)CyCy templates for synthesizing silver nanoclusters. By adjusting the $AgNO_3$ concentration, reducing time and reducing reagent concentration, Base-specific interactions could be a significant feature of these nanoclusters, as suggested from the absorbance maximus shifts in the UV-Vis spectra for the cytosine bases. Further investigation of Aβ(10-21)CyCy templates for silver nanoculsters using fluorescence, absorption, electrospray ionization mass, and NMR spectra would be valuable to clarify the binding mechanism and provide insight into the surface properties of Aβ(10-21)CyCy.

MATERIALS AND METHOD

Peptide Synthesis

Peptide was synthesized on a Rainin Symphony Quartet peptide synthesizer using standard FMOC chemistry. The detailed procedure was described in Chapter 2. The peptide was then purified using a Waters Delta 600 HPLC with Zorbax 300SB-C18 preparative HPLC column (21.2 mm x 25 cm) and eluted at 10 mL/min, room temperature with a linear gradient from H_2O/MeCN (90:10) with 0.1% TFA to H_2O/MeCN (60:40) with 0.1% TFA over 30 min. The peptide fractions were collected, rotary evaporated to remove MeCN/TFA, then frozen and lyophilized. Lyophilized peptide was stored at 4°C until required. The product was confirmed by MALDI-TOF mass spectral analysis: Aβ(10-21)WT (MALDI: $[M+3H^+]$ 1518.73, cal: $[M+H^+]$ 1515.77), Aβ(10-21)CyCy (MALDI: $[M+2H^+]$ 1604.21, cal: $[M+H^+]$ 1602.79) Aβ(10-21)QQ (MALDI: $[M+H^+]$ 1497.82, cal: $[M+H^+]$ 1497.75), Aβ(10-21)FF (MALDI: $[M+3H^+]$ 1539.39, cal: $[M+H^+]$ 1535.84).

Fibril Formation

Aβ(10-21) and Aβ(10-21)CyCy were dissolved in distilled deionized H_2O, then 50mM MES buffer in equal volume as distilled deionized H_2O was added in, making a solution with final concentration is 25mM MES buffer. Due to the solubility issue, Aβ(10-21)QQ and Aβ(10-21)FF were dissolved in distilled 40% acetonitrile solution. The peptide solution was sonicated for 10 min and centrifuged at 16,110xg for 10 min to

remove preformed aggregates. The supernatant was used as the peptide stock solution and incubated at room temperature if not specified.

Circular Dichroism Spectroscopy (CD)

CD spectrum was recorded at JASCO-810 CD spectropolarimeter at room temperature. Typically, spectra between 190 nm and 290 nm were collected with a 0.1mm path length cell, with a step size of 0.2 nm and a speed of 100 nm/s. Three spectra were recorded for each sample and averaged automatically.

Melting Curve by Circular Dichroism Spectroscopy (CD)

CD spectrum was recorded at JASCO-810 CD spectropolarimeter at room temperature. Typically, spectra between 190 nm and 290 nm were collected with a 0.1mm path length cell, with a step size of 0.2 nm and a speed of 100 nm/s. Starting temperature is 20ºC and ending temperature is 90ºC. The temperature is raised at 2ºC/min and equilibrium time 30 s. Three spectra were recorded for each sample and averaged automatically.

FT-IR Spectroscopy

Solution of mature fibrils was centrifuged at 16,110xg for 30 min, then the supernatant was removed and precipitate was lyophilized. The dried powder was mixed with KBr as a pellet for IR analysis. KBr background was deducted from each sample measurement. IR spectra were collected on a Nicolet MAGNA-IR 560 Spectrometer E. S. P. instrument operated at 2 cm^{-1} resolution. 100 scans were averaged to obtain a spectrum.

Transmission Electron Microscopy (TEM)

An aliquot of 8μL peptide solution was put on carbon-coated 200 mesh copper grid (Electron Microscopy Science, Hatfield, PA), allowed to settle for one minute. Excess solution was wicked away with filter paper. Then, 2% uranyl acetate solution as staing reagent was put to the grid for 1 minute. The excess staining solution was wicked away. All samples were stored in a desiccator before study. Electron micrographs were obtained using Hatachi Hitachi H-7500 transmission electron microscope operating at 75 kV at Neurology Microscopy Core Laboratory.

Atomic Force Microscopy (AFM)

Samples were diluted to desired concentration and 20 uL of the solution was placed on a clean silicon chip for one minute, excess solution was removed with filter paper and the chip was rinsed with distilled H_2O. Tapping mode analysis on a JEOL JSPM-4210 employed ultra-sharp non-contact silicon cantilevers with typical frequencies between 240 and 350 KHz (MikroMasch, Wilsonville, OR).

Small Angle Neutron Scattering (SANS)

Small Angle Neutron Scattering (SANS) experiments were performed at the time-of flight small angle neutron scattering diffractometers (SAND) at the Intense Pulsed Neutron Scource of Argonne National Laboratory. This instrument provides a range of momentum transfer ($Q= 4\pi\sin\theta/\lambda$), where θ is half the scattering angle and λ is the wavelength of incoming neutrons) of 0.0035 to 0.6 $Å^{-1}$ in a single measurement.

Aβ(10-21) (5mg/ml) and Aβ(10-21)CyCy (5mg/ml) was dissolved in 99.9% D_2O with 25 mM MES buffer at pH 5.6. Data were collected with samples in 2mm path length quartz cells.

Small Angle X-ray Scattering (SAXS)

Small-angle X-ray scattering (SAXS) was used to delineate the solution structure of the supramolecular assembly of Aβ(13-21)CyCy. Experiments were done at the 12-ID beam line at the APS. Small-angle scattering intensity, *I(Q)*, can be described by

$$I(Q) = I_0 \, n \, (\Delta\rho)^2 \, V^2 \, P(Q) + I_b$$

For a dilute system of particles, where I_0 is an instrument constant, n, the number density of particles, $\Delta\rho$, the difference in scattering length density (contrast) between the particles and solvent, V, the volume of particles, I_b, the flat background and $P(Q)$ is the particle form factor. The scattering vector, $Q = (4\pi/\lambda) \sin(\theta)$, where λ is the X-ray wavelength and 2θ is the scattering angle.

Aβ(10-21)CyCy Acts as templates for metal deposition

Silver nitrate (J. T. Bakers, 99.9%) and sodium borohydride (Aldrich, 98%) were used as received. The silver nanoclusters were synthesized by first mixing sliver nitrate solution with the Aβ(10-21)CyCy solution at room temperature and then adding $NaBH_4$ followed by vigorous shaking. Visible absorption spectra were acquired using a Cary UV- 1000 spectrometer.

Aβ(10-21)ThTh Acts as templates for DNA binding

PolyA was purchased from SigmaGenosys and was tested by UV, HPLC and MALDI before using. PolyA was dissolved in water and make final concentration of 0.125 mM. 1.5 mM Aβ(10-21)ThTh in 25 mM MES buffer (pH 5.5) was diluted in half and make Aβ(10-21)ThTh: polyA ratio of 6:1. Spectra of Aβ(10-21)ThTh mixing with polyA was taken by CD.

CHAPTER 4

EXPLORING AMYLOID LAMINATION BY NUCLEASEBASE INCORPORATION IN Aβ(13-21)

INTRODUCTION

The kinetics and morphological analysis on Aβ(10-21)CyCy in chapter 3 suggested that cytosine incorporation increased the rate of nucleation, but did not alter fibril propagation. Side chains of tyrosine, glutamate acid and valene resideues at the N-terminal might complicate the cytosine-cytosine interaction which is in the middle of peptide strand. Therefore, a shorter fragment Aβ(13-21), CyCyQKLVFFA was considered. Further, substitution of lysine 16 with alanine was performed in order to amplify the hydrophobicity and amphiphilicity of the peptide, an important feature of self-assembly. The peptide, CyCyQALVFFA was prepared for the investigation.

Previous studies indicated that Aβ(13-21) is an amphiphilic fragment in which self-assembly can be modulated by metal ions. Zn^{2+} incorporation not only increased the self-assembly rate but also dramatically modulated amyloid morphology (Dong, Shokes et al. 2006). In the absence of Zn^{2+}, Aβ(13-21)K16A forms typical amyloid fibrils; in the presence of Zn^{2+}, the self-assembly rate was accelerated and the morphology was altered profoundly. Zn^{2+} incorporation increased the lamination and induced ribbon and tube formation. As seen in Aβ(10-21), nucleobase incorporation accelerated the self-assembly as Zn^{2+} does. Here I chose to test whether in Aβ(13-21), nucleobase incorporation could be used to increase the sheet-sheet interaction.

RESULTS

Aβ(13-21)CyCy Forms Homogenous Nanotubes

The nine-residue peptide Aβ(13-21)CyCy, NH_2-CyCyQALVFFA-NH_2, was synthesized via standard FMOC solid phase protocols. The C termini capped, and the free N-terminus ensured the amphiphilicity. Aβ(13-21)CyCy 0.3 mM was dissolved in 25 mM MES buffer and pH was adjusted to 4.2, approximately the pKa of cytosine. Immediately after the peptide was dissolved in solution, the CD spectrum showed negative ellipticity at ~195 nm, and positive ellipticity at 207 nm and 270 nm (Figure 4.1A). While the spectrum is not that typically expected for protein secondary structure because of the cytosine chromophore, IR spectra revealed a strong amide I absorption at 1636 cm^{-1}, indicating the presence of H-bonded, β sheet rich structures (Figure 4.1B).

Figure 4.1 Secondary structure of Aβ(13-21)CyCy monitored by CD and FT-IR.

(A) CD sectra of a 0.3 Aβ(10-21)CyCy solution in 25mM MES buffer (pH 4.3).

(B) IR spectra of a 0.3 Aβ(10-21)CyCy solution in 25mM MES buffer (pH 4.3).

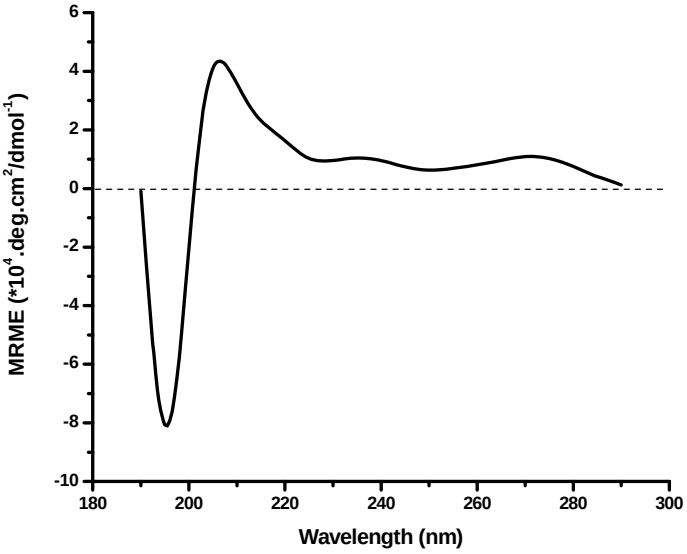

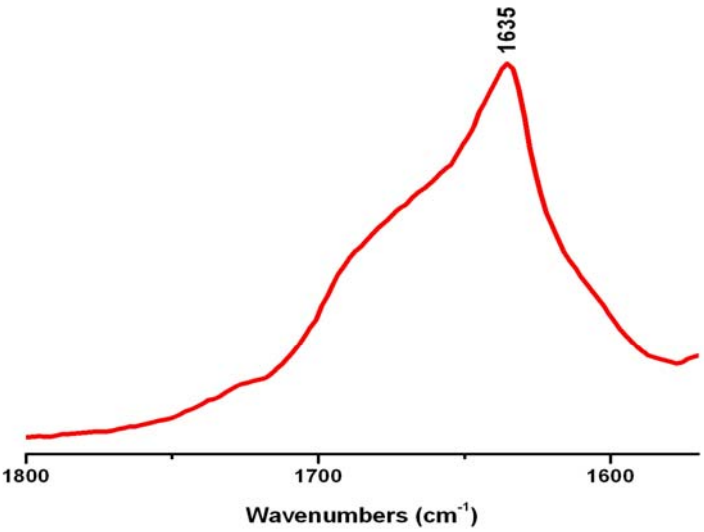

Transmission Electron Microscopy (TEM) analysis were most consistent with homogenous nanotubes. The dark line in the contour has been a characteristic feature of these peptide nanotubes (Lu, Jacob et al. 2003) and these show a width of about 30 nm when dried on TEM grids (Figure 4.2). This size is significantly larger than the normal amyloid fibrils, and the sharp white edges observed for each assembly, suggested hollow properties being visualized by the negative uranyl acetate staining. In contrast to other polydisperse nanotubes, the lengths are generally short.

Small-angle X-ray scattering (SAXS) experiments were performed at the 12-ID beam line in the Advanced Photon Sources (APS) at Argonne National Laboratory. Small-angle scattering intensity, *I(Q)*, can be described by

$$I(Q) = I_0 \, \mathrm{n} \, (\Delta\rho)^2 \, \mathrm{V}^2 \, P(Q) + I_\mathrm{b}$$

In this expression, for a dilute system of particles, I_0 is an instrument constant, n is the number density of particles, $\Delta\rho$ is the difference in scattering length density (contrast) between the particles and solvent, V is the volume of particles, I_b is the flat background, and $P(Q)$ is the particle form factor. The scattering vector, $Q = (4\pi/\lambda) \sin(\theta)$, where λ is the X-ray wavelength and 2θ is the scattering angle. The hollow circular cylindrical form factor, similar to Aβ(16-22) nanotubes (Lu, Jacob et al. 2003), was used to fit the scattering data from the particles. Figure 4.3 shows a monodisperse hollow circular cylinder fit to the peptide solution at pH 4.3. Best fit to the data yields a tube with an outer radius of 12.7 nm and a wall thickness=3.8 nm, while the length is too large to be determined by the SAXS. Therefore, the SAXS measurement is mostly constituent with

Figure 4.2

TEM image of Aβ(13-21)CyCy.

Aβ(13-21)CyCy was dissolved in 25 mM MES to make final peptide concentration 0.3 mM with pH adjusted to pH 4.3. Scale bar, 250 nm.

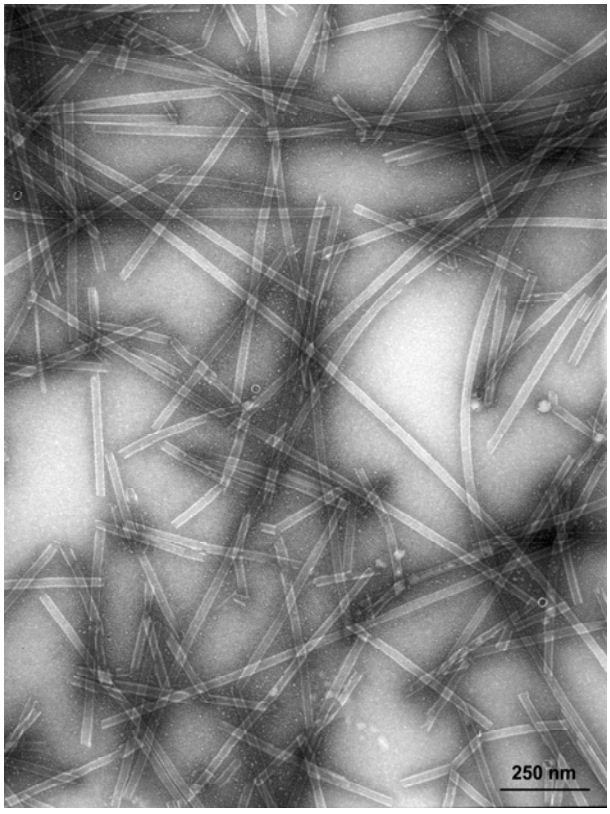

Aβ(13-21)CyCy self-assembled into peptide nanotubes with a highly homogeneous outer radius and wall thickness (Figure 4.3).

pH dependence of nanotube formation

Aβ(13-21)CyCy (0.3mM) was allowed to assemble in 25 mM MES buffer across a range of pH values. As shown in the TEM images in Figure 4.4, little assembly occurs at low pH, however at pH 3.3 and 4.3, in the range of the expected pKa of cytosine, Aβ(13-21)CyCy rapidly forms large homogenous hollow tubes seen with the Zn^{2+}-induced assembly of the native peptide. At pH 5.5, the assembly is more heterogeneous with the appearance of more typical 10 nm fibrils and ribbons. This pH dependent morphology is consistent with the hyphothesis that around the pKa of cytosine, a third hydrogen bond will form between two nucleobases and futher stabilize the sheet/sheet lamination to direct formation of tubular structures instead of filbrils. Aβ(13-21)CyCy also forms tubes at higher pH, pH 6-8, however, the tubes are not stable under these conditions and tends to precipitate over time.

Thermodynamic stability of Aβ(13-21)CyCy tubes

The thermodynamic stability of the Aβ(13-21)CyCy mature nanotubed was evaluated by CD. 0.3 mM of the tube solution was heated from 20 °C to 80 °C at 2 °C/min and spectra were recorded every 2 °C (Figure 4.5A). The spectra showed that the CD signal gradually weakened as the temperature increased. Since ellipiticity at 270 nm is representative of the transition dipole of cytosine base, we plot the ellipiticity change over temperature change at this wavelength.

Figure 4. 3

Small angle x-ray scattering (SAXS) measurement for Aβ(13-21)CyCy.

Small angle x-ray scattering (SAXS) and the tubular form factor fits (red) of 0.3 mM Aβ(13-21)CyCy assemblied in 25 mM MES buffer at pH 4.3. The data was fit by using the form factor for a hollow cylinder.

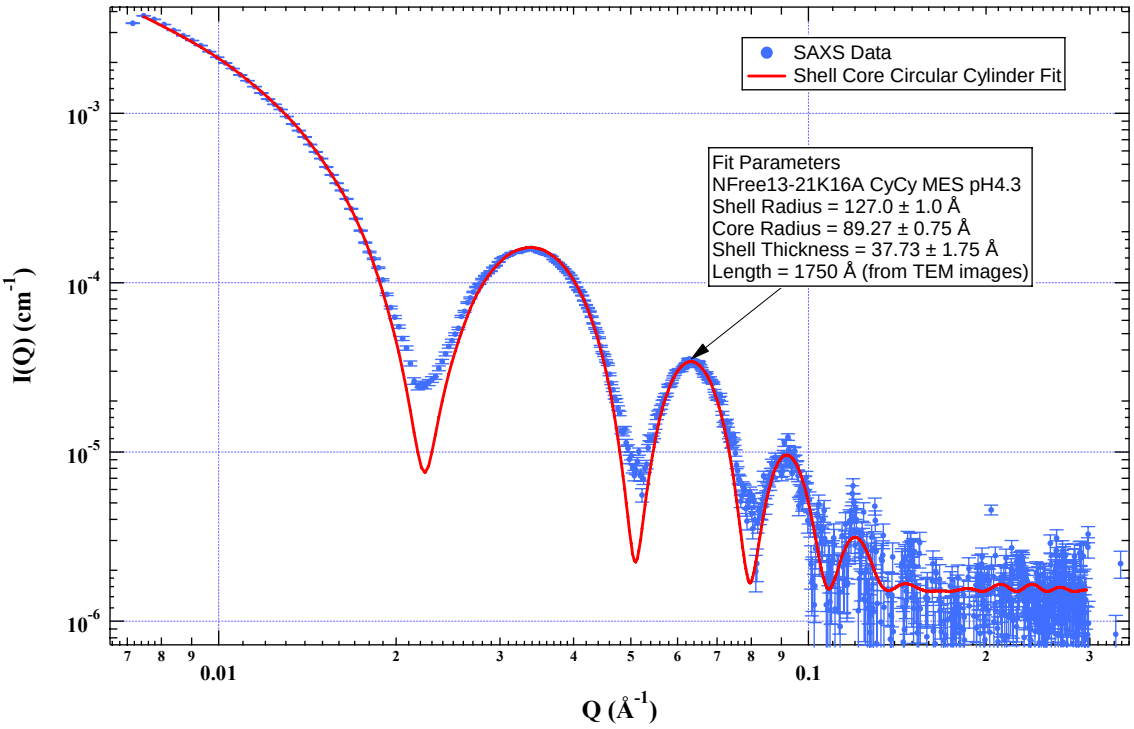

Figure 4.4

TEM images of Aβ(13-21)CyCy assembled at different pH.

TEM images of Aβ(13-21)CyCy (0.3 mM) assembled in 25 mM MES buffer at pH: A, pH=2.0; B, pH=3.3; C, pH=4.3; D, pH=5.5 (scale=200 nm).

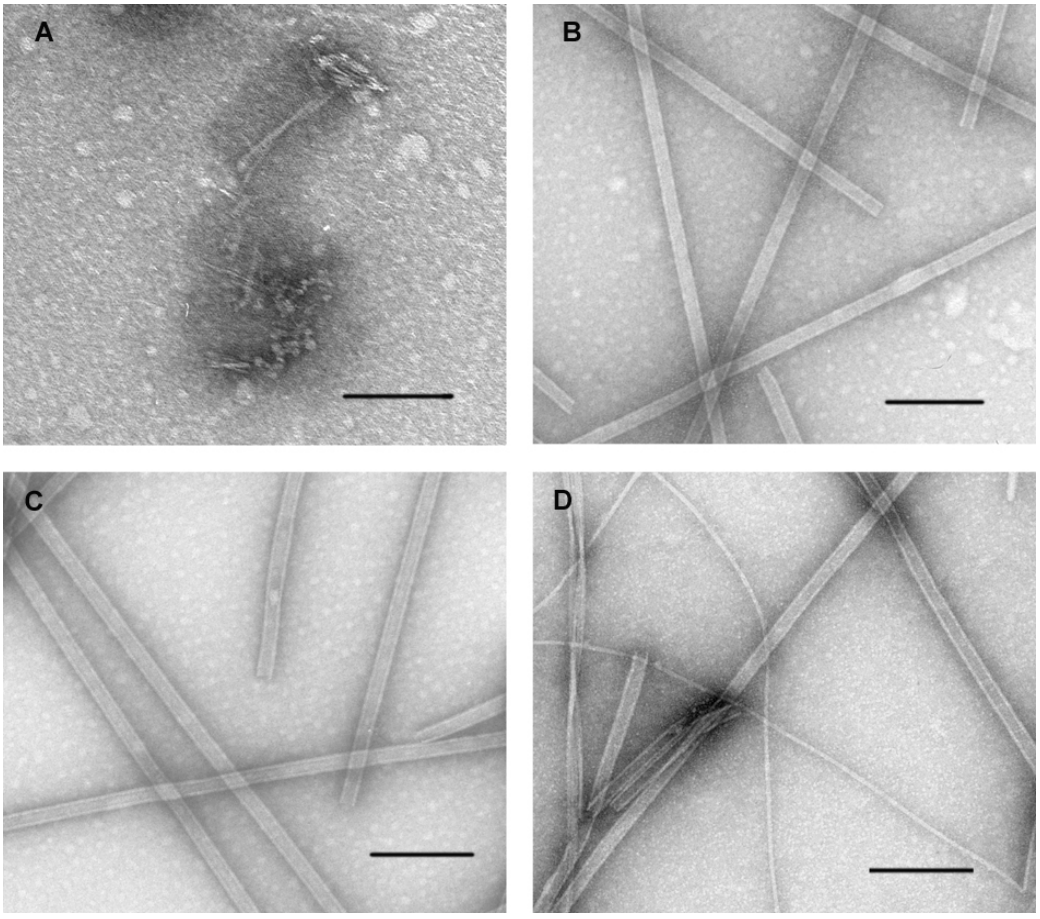

Figure 4.5

Aβ(13-21)CyCy nanotubes thermal stability monitored by CD.

The intensity of the ellipiticity at 207 nm and 270 nm gradually decreased with increased temperature, showing the melting temperature at 72.0 °C.

A

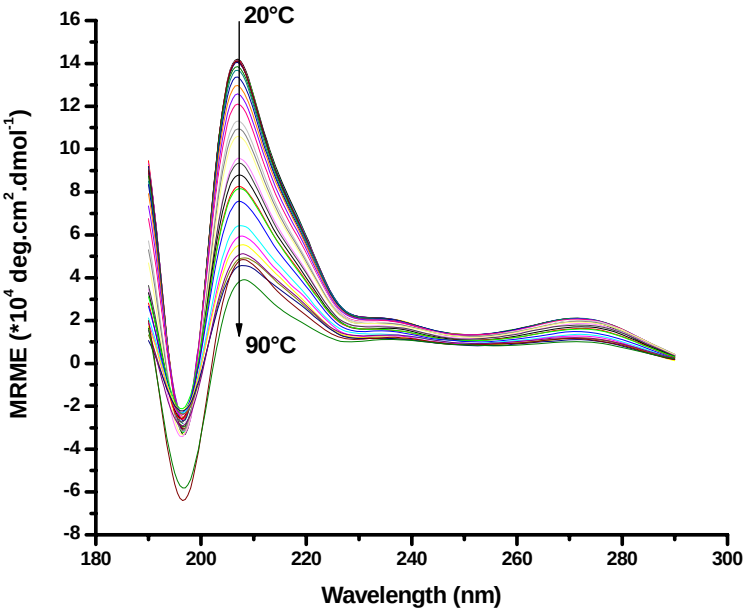

B

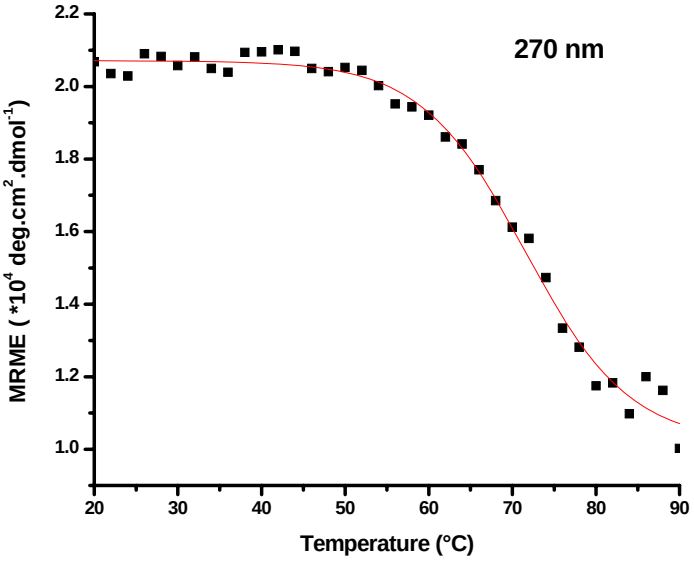

Plot of the ellipiticity at 270 nm showed a clear sigmoidal dependence and a melting temperature at ~72.0 °C (Figure 4.5 B, C). The melting process however was not reversible, and this lack of reversibility was also observation in Aβ(16-22) self-assembly (Lu, Jacob et al. 2003).

Previous temperature-dependent studies of alanyl PNA self-pairing showed intensity decrease of Cotton effect in CD spectra is correlated with UV melting curve, which indicated the disassociation of base-pairing between alanyl PNA strands (Diederichsen and Schmitt 1996). Similar CD intensity decrease at 270 nm was observed in Aβ(10-21)CyCy as the temperature increased, which suggested base pairing between cytosine moieties through the lamination dimension.

X-ray diffraction and Electron Diffraction suggest cross-β peptide arrays

As for amyloid fibrils, a "cross-beta" pattern has been observed in amyloid fibrils formed by many proteins with different sequence and therefore implying a common structure feature. That is, X-ray diffraction revealed reflections at 4.7 Å and 10.6 Å corresponds to the distance between peptide strands in the H-bonding direction within the sheet and between laminated sheets (Kirschner, Abraham et al. 1986; Inouye, Fraser et al. 1993; Serpell, Berriman et al. 2000).

Lyophilized Aβ(13-21)CyCy nanotubes with Na_2SO_4 alignment was used for structure study. Diffraction data obtained by the powder diffractometer (WAXS) at Argonne National Laboratory revealed several bands: 3.4 Å, 3.7 Å, 3.8 Å, 4.6 Å and 10.3 Å (Figure 4.6). The sharp peaks at 3.4 Å, 3.7 Å and 3.8 Å in the samples correspond mostly to the Na_2SO_4 crystallites. The two broad peaks corresponding to a cross-beta diffraction pattern of amyloid type peptide assembly. The d spacings are 4.6 Å and 10.3

Å. Comparing to the supernatant curve, the stronger intensity of the precipitate curve suggested that majority of the self-assembled structures have been spun down through centrifugation. Consequently, though nanotubes show remarkable morphological difference from fibrils, they possess the same cross-β structures.

The observation by WAXS was confirmed by electron diffraction. Electron diffraction on a Na_2SO_4 aligned nanotubes revealed the typical amyloid cross-β signature at 4.7 Å (Figure 4.7) Eight different spacings were observed in the electron diffraction pattern: d1= 4.7 Å, d2= 3.9 Å, d3= 3.6 Å, d4= 2.8 Å, d5=2.4 Å, d6=2.3 Å, d7=1.9 Å and d8=1.8 Å. Among these reflections, d5 was assigned as the harmonic of d1, and d6 was assigned as second harmonic of d1. Reflections at d2, d3 and d4 were assigned to Na_2SO_4, d7 and d8 was assigned to harmonic of d2 and d3 respectively. No spacing larger than 10 Å was probed due to the shorter wavelength of electrons compared to the X-ray beam. The overall diffraction pattern was similar to that reported for previous aligned amyloid fibrils (Makin, Serpell 2004).

Test for Cy/Cy Association

The model for nanotubes formed by Aβ(13-21) with Zn^{2+} incorporation and Aβ(16-22) suggested that the peptide nanotubes result from dramatic stabilization of β-sheets lamination (Lu, Jacob et al. 2003; Dong, Shokes et al. 2006). As indicated by the Molecular Dynamic simulation, cytosine bases on two adjacent β strands of two adjacent β-sheets could interact with each other to stabilize the sheet-sheet lamination. To test this hypothesis, single Cy substitution, Aβ(13-21)H13Cy or Aβ(13-21)H14Cy, was prepared for study. If the Cy/Cy association occurs along the lamination direction, the single Cy

Figure 4.6

Wide Angle X-ray Scattering (WAXS) of Aβ(13-21)CyCy

Sample of 1.5 mM Aβ(13-21)CyCy was incubated in 25 mM MES at pH 3.3, the maturation of the sample was monitored by CD. Na_2SO_4 solution was added to the peptide solution and making final Na_2SO_4 concentration as 20 mM. The solution was centrifuged. The supernatant was separated from the precipitate and lyophilized. In the WAXS fitting curve, the peaks correlated to Na_2SO_4 crystalline phases are 3.8 Å, 3.7 Å and 3.4 Å. The peaks correlated to the peptide cross β structure are 10.3 Å and 4.6 Å.

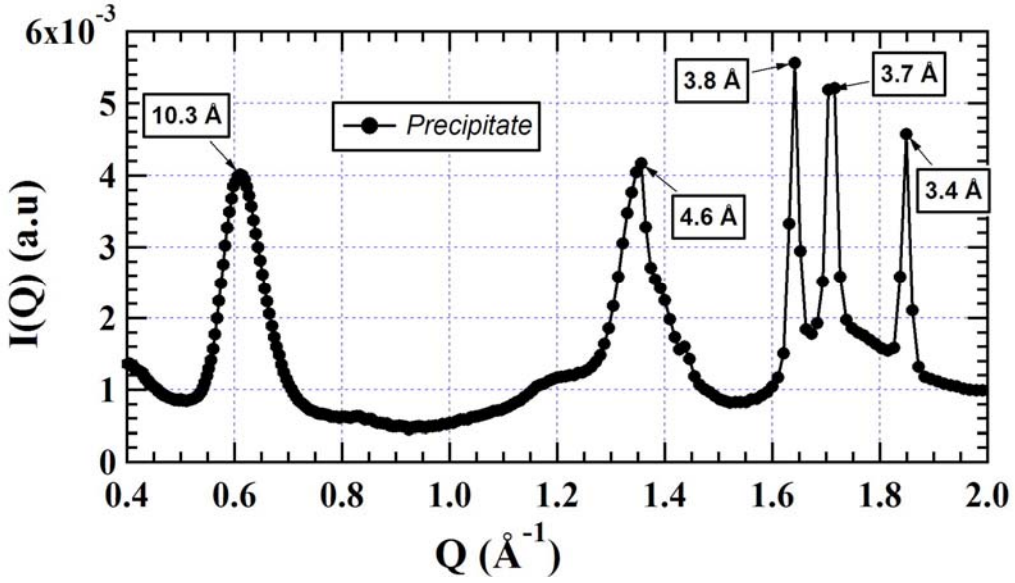

Figure 4.7

Electron Diffraction Pattern of Aβ(13-21)CyCy nanotube bundles.

The mature Aβ(13-21)CyCy nanotubes were bundled by sulfate ions and deposited on a TEM grid. The numbers on the arcs indicate the calculated d-spacings (Å).

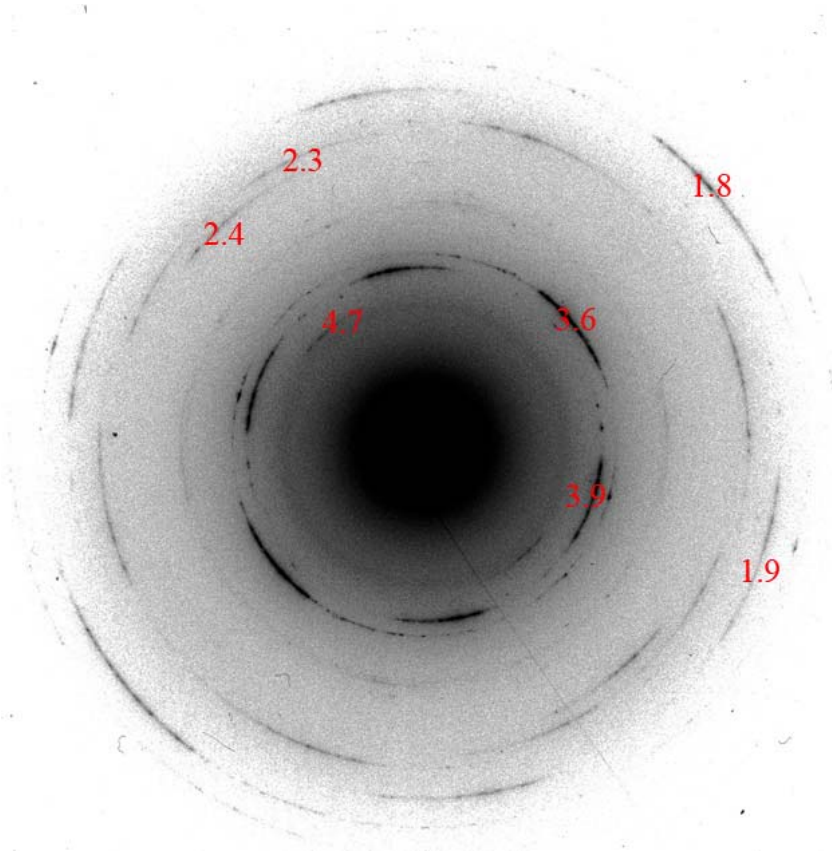

substitution would not be sufficient to stabilize the sheet-sheet lamination and therefore disrupt nanotube structure. If the Cy/Cy association occurs along the β-sheet hydrogen bonding direction, the single Cy substitution would not affect sheet lamination and therefore would not affect nanotube structure. Under the same solution and pH conditions, Aβ(13-21)H13Cy or Aβ(13-21)H14Cy gives only fibrils and no larger assemblies (Figure 4.8). This suggests cytosine moiety is required at both 13 and 14 position. The hydrogen bonding interaction between the side chain nucleobase pair should occur along the sheet lamination direction. Lack of tubular structure in the assembly of H13Cy and H14Cy supports this view that the inter-sheet nucleobase interaction is the key for nanotube formation.

Free N-termnus plays a role in stabilizing the Aβ(13-21)CyCy Nanotubes

Study of N-termnus of Aβ(16-22) suggested that exposure of the positive charge is essential for nanotube assembly, and burial of the positive charge would destabilize the structure (Lu, 2005). To further investigate the importance of the N-terminal charge on nucleobase incorporated nanotube assembly, the peptide N-terminus was acetylated, leaving only two possible sites for protonation, the two cytosine bases, under these acidic conditions.

Immediately after dissolved of Ac-CyCyQALVFFA-NH_2 at 0.3mM concentration at room temperature, the CD spectrum showed similar Cotton effect as NH_2-CyCyQALVFFA-NH_2, with negative ellipiticity at ~195 nm, and positive ellipiticity at 207 nm and 270 nm (Figure 4.9A). However, the CD intensity is less than the free N-termini Aβ(13-21)CyCy, which may associate with less assemblies in the solution. IR

Figure 4.8

TEM image of Single Cy incorporation in Aβ (13-21).

Each peptide (0.3 mM) was dissolved in 25 mM MES buffer. Aβ (13-21)H13Cy: A: pH 3.3, B: pH 4.3 and C: pH 5.5. Aβ (13-21)H14Cy: D: pH 3.3, E: pH 4.3 and F: pH 5.5. Scale: 250 nm.

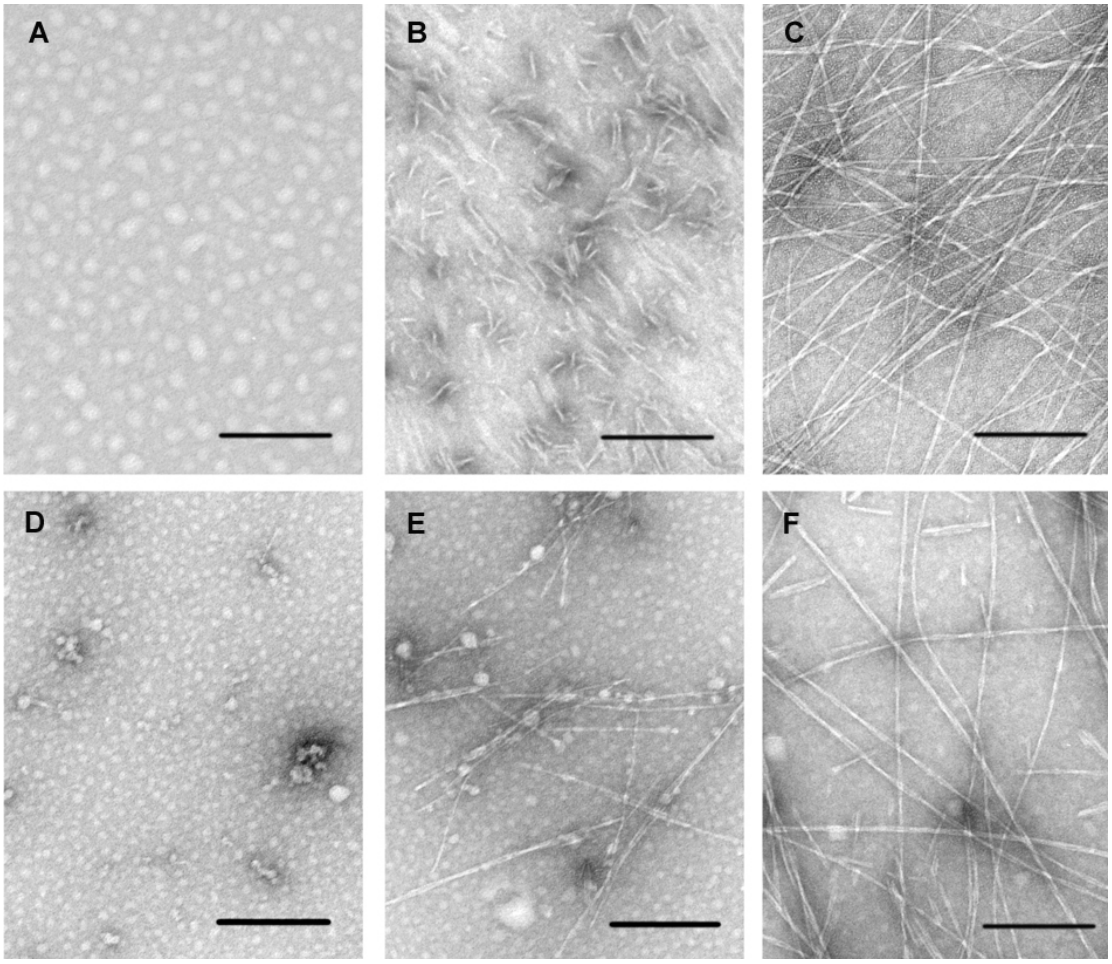

Figure 4.9

Secondary structure of Aβ(13-21)CyCy (Ac-CyCyQALVFFA-NH_2) monitored by CD and FT-IR.

(A) 0.3 mM NC-Aβ(13-21)CyCy in H_2O. Secondary structure of monitored by CD

(B) Mature nanotube of NC-Aβ(13-21)CyCy was pelleted and lyophilized. Secondary structure of Aβ(13-21)CyCy monitored by FT-IR

A

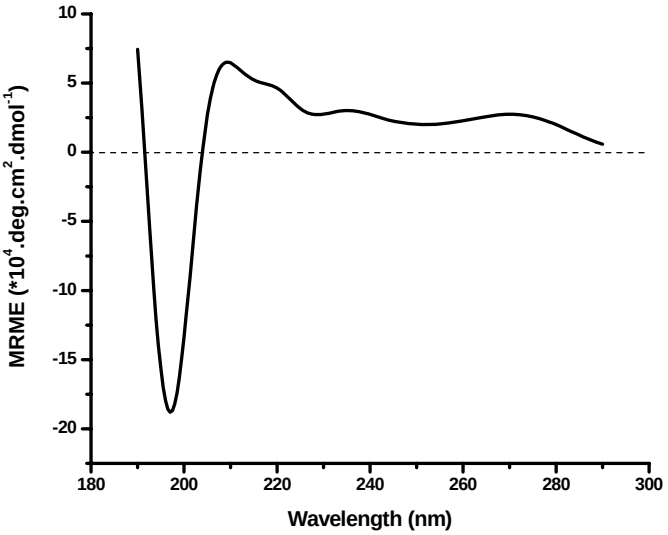

B

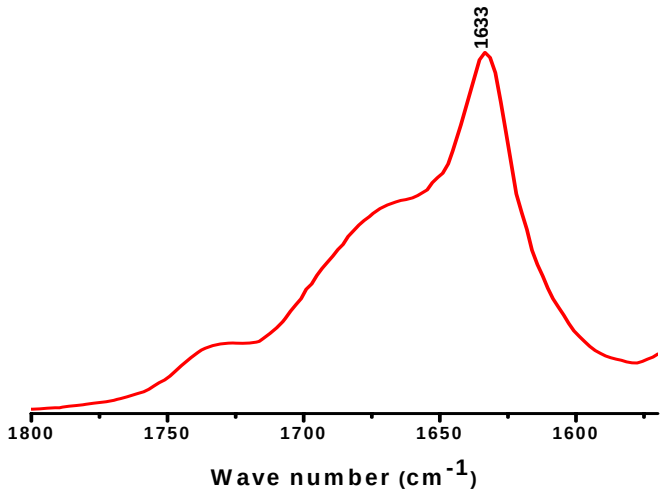

analysis confirmed that the assemblies formed by N-terminus capped congeners maintain the β-sheet structure, with the diagnostic amide I transition at 1633 cm^{-1} (Figure 4.9B).

TEM analysis revealed nanotubes with width of 36 ± 1 nm (Figure 4.10A), and a contour length range from 5 μm to 15 μm. The dark line in the contour has been a characteristic feature of these peptide nanotubes (Lu, Jacob et al. 2003), suggesting the hollow properties being visualized by the negative uranyl acetate staining. Over time, the short nanotubes disappeared and long, thin fibril like structure formed (Figure 4.10B). After 20 days at room temperature, the majority of the species revealed by TEM were long-twisted fibrils (Figure 4.10C). By contrast, the nanotubes formed by the NH_2-Aβ(13-21)CyCy (at pH 3.3 or pH 4.3) were stable for at least one year at room temperatue. SAXS measurement was best fit to peptide nanotubes with outer radius of 16.7 nm and wall thickness of 5.1 nm (Figure 4.11). The low amplitude of the experiment curve may result from the lower nanotube content in the solution as compared with its free-N termni counterpart.

Single Cy substitution, Ac-HCyQALVFFA-NH_2, or Ac-CyHQALVFFA-NH_2, under the same solution and pH conditions, give only fibrils and no larger assemblies (Figure 4.11). This result is consistent with N-terminus free Aβ(13-21)H13Cy or Aβ(13-21)H14Cy which lacks the ability to form nanotubes and further support the argument that the cytosine moiety is required at both 13 and 14 position. The inter-sheet nucleobase interaction is the key for nanotube formation.

Figure 4.10

TEM of Aβ(13-21)CyCy (Ac-CyCyQALVFFA-NH_2) overtime.

Sample of 0.3mM peptide in H_2O incubated at room temperature. A. 0hr sample; B. 10 days sample; C, 20days sample.

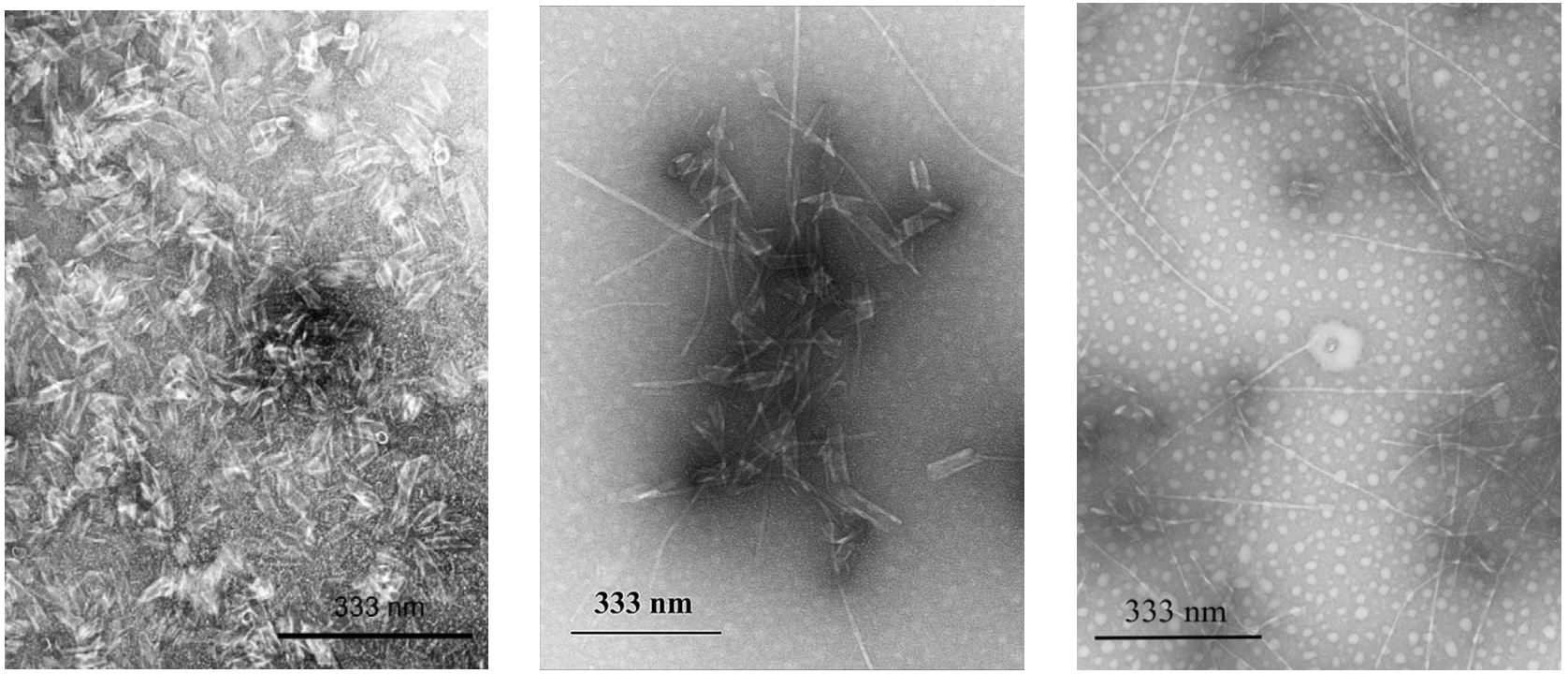

Figure 4. 11

Small angle x-ray scattering (SAXS) and the tubular form factor fits (red) of Aβ(13-21)CyCy (Ac-CyCyQALVFFA-NH_2) assemblied in H_2O.

Small angle x-ray scattering (SAXS) and the tubular form factor fits (red) of 0.3 mM Aβ(13-21)CyCy assemblied in H_2O at room temperature. The data was fit by using the form factor for a hollow cylinder.

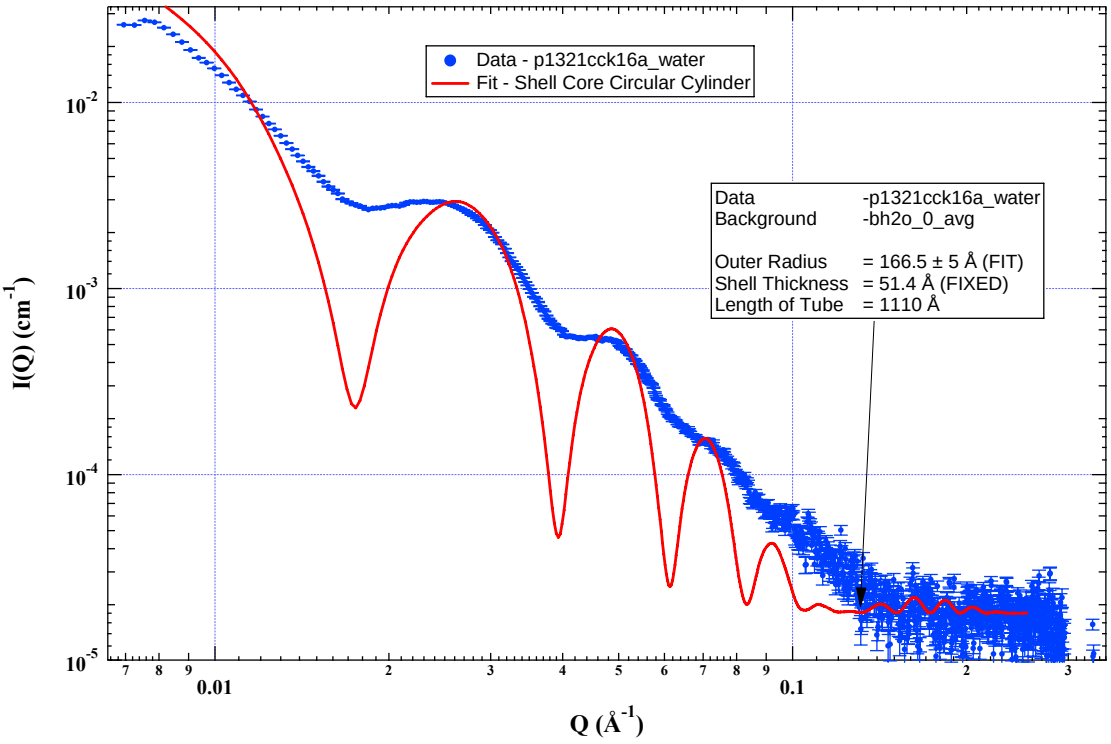

Figure 4.12

TEM image of Single Cy incorporation in Aβ (13-21) (Ac-CyCyQALVFFA-NH_2)

A. 0.3mM Aβ (13-21)H13Cy in H2O at room temperature;

B. 0.3mM Aβ (13-21)H14Cy in H2O at room temperature.

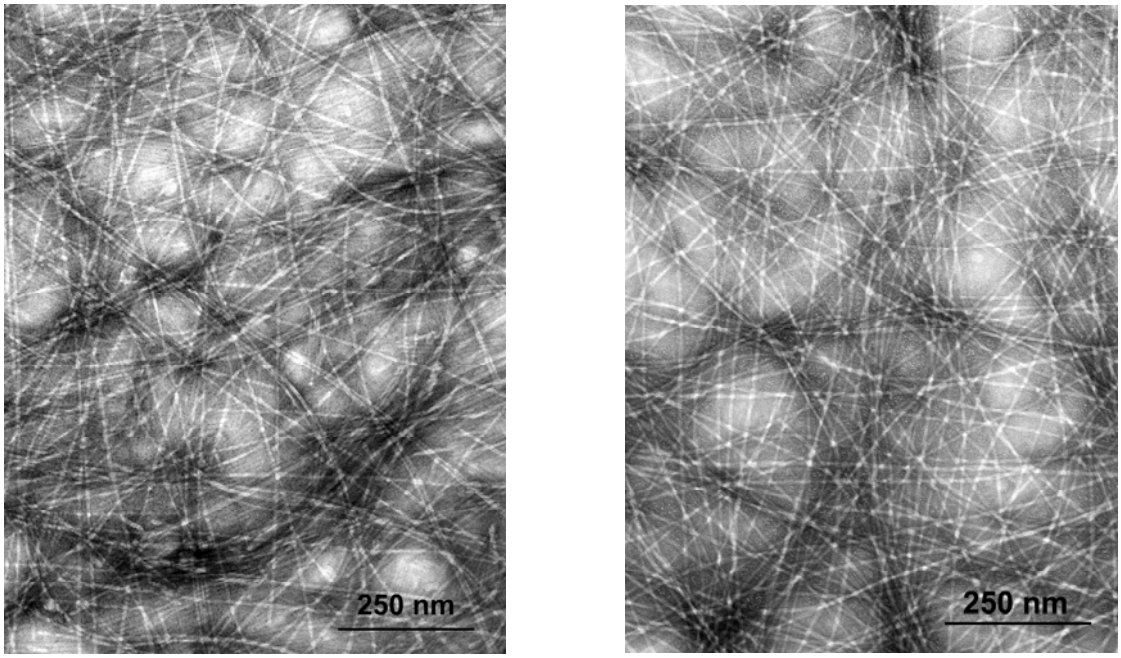

Aβ(13-21)CyCy Nanotube Acts as templates for metal deposition

The uniqueness of the nanotube formed by Aβ(13-21)CyCy arises from its tubular structure and the inherent subtlety in the structure, which is the cytosine base arrangement in the nanotubes. Since the nanotubes are composed of laminated β-sheets and possess cross-β structures, the arrangement of cytosine base in the nanotube probably follows certain repeat pattern or arrays. This nucleobase arrangement pattern along with the nano-scale dimension, the high thermal stability make the nucleobase modified peptide nanotubes a very unique material with promising applications. As described in Chapter 3, Ag^+ has strong affinity for GC rich DNA. I tested the possibility of growing silver nanoparticles with Aβ(13-21)CyCy as templates. The silver nanoparticles were generated following the same procedure described in Chapter 3. In figure 4.13A some of the nanotubes were completely covered with Ag nanoparticles, while some of them were barely covered. On the same grids, large aggregations of individual Ag particles were also observed (Figure 4.13A). The coexistence of continuous Ag-coated structures (Figure 4.13B) and barely coated structure could be explained in two ways. One possibility is due to the self-nucleation of silver nanoparticles as reported for Pd nanoparticles (Fu 2003). The other plausible explanation is that since Ag^+ has strong affinity for cytosine base, the different degree of silver nanoparticle coverage probably reflect the degree of exposure of cytosine on the nanotube surface are different. In some nanotubes, the majority of cytosine base are exposed on the surface, while for others, the majority of cytosine base are buried inside. The reason account for this phenomenon remains unclear and studied are undergoing. By adjusting the $AgNO_3$ concentration,

Figure 4.13

TEM image of Silver Nanoparticles binding on Aβ (13-21)CyCy Nanotubes (NH_2-CyCyQALVFFA-NH_2).

A. 0.3mM Aβ (13-21)CyCy in 25mM MES at pH3.3. Ag^+: peptide concentration ratio of 10:1. Once the Ag^+ was mixed with peptide solution, equal molar of $NaBH_4$ to Ag^+ was added into the solution reducing the Ag^+ to nanoparticles.

B. Enlargement image of one peptide nanotube covered with silver nanoparticles.

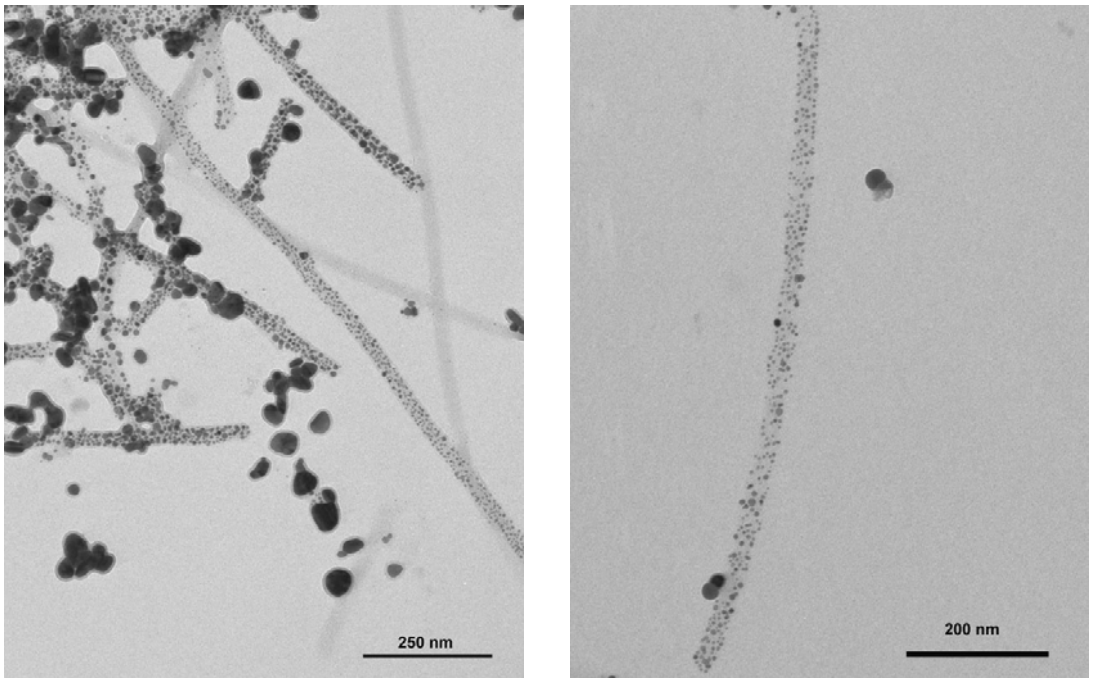

A **B**

the reducing time and reducing reagent concentration, it is possible to control the coating density and manufacture silver nanowires.

DISCUSSION

Aβ(13-21)CyCy forms homogeneous peptide nanotube under acidic conditions through rational design. The shortening of peptide length from Aβ(10-21) simplify the amphiphilic pattern of the peptide sequence and remove the defects or disorders in the assembled structure, resulting in the large extent lamination and nanotube structure as Aβ(16-22) does. The self-assembly rate of Aβ(13-21)CyCy depends on the solvent, pH and temperature.

The ability of forming nanotubes by acetyl capped Aβ(13-21)CyCy suggested that although N-terminus charge plays an important role in stabilizing the nanotubes in solution, it is not the determinant factor of nanotube formation. Instead, the Cy/Cy association is crucial for the nanotube structure formation. The transition from nanotubes to fibril of N-termini capped Aβ(13-21)CyCy suggest although amyloid fibrils and ribbons/nanotubes are morphologically distinct, they are cable of interchanging morphologically.

The uniqueness of the nanotube formed by Aβ(13-21)CyCy arises from its tubular structure and the inherent subtlety in the structure, which is the cytosine base arrangement in the nanotubes. Since the nanotubes are composed of laminated β-sheets and possess cross-β structures, the arrangement of cytosine base within the nanotube is

probably highly ordered. This nucleobase arrangement pattern along with the nano-scale dimension, the high thermal stability make the nucleobase modified peptide nanotubes a very unique material with promising applications. Such robust and homogenous self-assembling nanotubes with nucleobases at the terminus may offer a unique functionalized and easily accessible scaffold for nanotechnology. Further characterization on the structure will be essential to understand the self-assembly process of ordered nanostructure and extend the applications.

MATERIALS AND METHODS

Synthesis and Purification of Aβ(13-21)CyCy Congeners

Aβ(13-21)CyCy, NH_2-CyCyQALVFFA-NH_2, with the N-terminus leaving free and the C-terminus capped, was synthesized following the protocol described in chapter 2. Cy13, Cy14, Gln15 and Ala16 were double coupled. The peptide was then purified using a Waters Delta 600 HPLC with Zorbax 300SB-C18 preparative HPLC column (21.2mm x 25cm) and eluted at 15 mL/min, room temperature with a linear gradient from H_2O/MeCN (9:1) with 0.1% TFA to H_2O/MeCN (3:2) with 0.1% TFA over 30min. Aβ(13-21)H13Cy and Aβ(13-21)H14Cy were prepared following the same protocol. The product was confirmed by MALDI-TOF mass spectral analysis: Aβ(13-21)CyCy (MALDI: $[M+2H^+]$ 1155.39, cal: $[M+H^+]$ 1153.27). Aβ(13-21)H13Cy (MALDI: $[M+H^+]$ 1111.68, cal: $[M+H^+]$ 1111.26). Aβ(10-21)H14Cy (MALDI: $[M+H^+]$ 1111.72, cal:

[$M+H^+$] 1111.26).

Ac-Aβ(13-21)CyCy-NH_2, CH_3CO-CyCyQALVFFA-NH_2, with both the N-terminus and C termini capped, was synthesized following the standard protocol except that . The product was confirmed by MALDI-TOF mass spectral analysis: NC-Aβ(13-21)CyCy (MALDI: [$M+H^+$] 1195.78, cal: [$M+H^+$] 1196.32). NC-Aβ(13-21)H13Cy (MALDI: [$M+H^+$] 1153.77, cal: [$M+H^+$] 1153.29). NC-Aβ(10-21)H14Cy (MALDI: [$M+H^+$] 1153.72, cal: [$M+H^+$] 1153.29).

Sample Preparation

The purified peptide was dissolved in distilled de-ionized H_2O with sonication for 10 min and centrifugation at 16,110 xg for 10 min to remove preformed aggregates. The supernatant was used as the peptide stock solution. The supernatant peptide stock was diluted to the desired solution conditions with 50 mM MES buffer at the required pH. Eventually, final peptide concentration was 0.3 mM in the presence of 25mM MES buffer at pH 3-7.

Circular Dichroism Spectroscopy (CD)

CD spectrum was recorded at JASCO-810 CD spectropolarimeter at the indicated temperature. Typically, spectra between 190 nm and 290 nm were collected with a 0.1 mm path length cell, with a step size of 0.2 nm and a speed of 100 nm/s. Three spectra were recorded for each sample and averaged automatically.

Melting curves were obtained by starting temperature is 20 ºC and ending temperature is 90 ºC. The temperature is raised at 2 ºC/min and equilibrium time 30 s. Three spectra were recorded for each sample and averaged automatically.

FT-IR Spectroscopy

Mature peptide nanotubes were aligned with 20 mM Na_2SO_4 solution, centrifuged at 16,110xg for 30 min, then the supernatant was removed and precipitate was lyophilized to dryness. The dried powder was mixed with KBr and pressed into a pellet for IR analysis. IR spectra were collected on a Nicolet MAGNA-IR 560 Spectrometer instrument operated at 2 cm^{-1} resolution. 100 scans were averaged to obtain a spectrum and KBr background was deducted from each sample measurement.

Transmission Electron Microscopy (TEM)

8 μL of the peptide solution was put on carbon-coated 200 mesh copper grid (Electron Microscopy Science, Hatfield, PA), allowed to settle for one minute, and excess solution was wicked away with filter paper. Then, 2% uranyl acetate solution as a negative staing reagent was applied to the grid for 1 minute and wicked away as above. All samples were stored in a desiccator before analysis. Electron micrographs were obtained using Hatachi Hitachi H-7500 transmission electron microscope operating at 75 kV in the Neurology Microscopy Core Laboratory or the IMMF at department of chemistry.

Small Angle X-ray Scattering (SAXS)

SAXS experiments were carried out at room temperature on the 12-ID beam-line of Argonne National Laboratory's Advanced Photon Source (APS). Data were collected using a 15 cm × 15 cm, high-resolution, position-sensitive, nine element-tiled, CCD mosaic detector and exposure time was approximately 0.5 seconds for each measurement.

Typically, five successive measurements were recorded for each sample and then averaged to obtain a final scattering profile. Sample to detector distance was ~2 m and energy of X-ray radiation was set to 12 keV. A Biologic SFM 400 stopped-flow apparatus with a 1.0 mm diameter cylindrical quartz capillary of 0.01–0.02 mm wall thickness was mounted at the beam-line. About 100 μl peptide solution was delivered into the quartz capillary and exposed to the X-ray beam. Samples were measured under constant gas flow conditions to reduce potential radiation damage. No evidence of sample changes was seen over the time interval of exposure. The measurement of each sample was preceded by a measurement of the same buffer solution used in protein sample preparation. The buffer measurements provided a check on beam properties and the cleanliness of the sample cell between sample measurements as well as the means for background subtraction.

Data Analysis. The SAXS data were reduced following routine procedures at 12-ID and the analysis of the data were carried out using the macros developed on Igor Pro platform at the Intense Pulsed Neutron Source, Argonne National Laboratory. The reduced data were averaged over the 10 measurements for further analysis in Igor Pro. Small angle scattering intensity, $I(Q)$, can be described by

$$I(Q) = I_0 \, \mathrm{n} \, (\Delta\rho)^2 \, \mathrm{V}^2 \, P(Q) + I_\mathrm{b}$$

----- Eq. 4-1

for a dilute system of scattering particles where I_0 is an instrument constant, n is the number density of particles, $\Delta\rho$ is the difference in scattering length density (contrast) between particles and solvent, V is the volume of particles, I_b is the flat background

intensity, and $P(Q)$ is the particle form factor. Q is the momentum transfer given by $Q = (4\pi/\lambda)\ sin\ (\theta/2)$ where λ is the neutron or x-ray wavelength and θ is the scattering angle. Several models were investigated, but only P(Q) for hollow cylindrical particles accurately fit the data.

$$P(Q) = \int_0^1 \left(\frac{1}{1 - \left(R_2 / R_1 \right)^2} \right)^2 \left[\frac{2J_1\left(QR_1 \left(1 - x^2\right)^{0.5} \right)}{QR_1 \left(1 - x^2\right)^{0.5}} - \frac{\left(R_2 / R_1 \right)^2 2J_1\left(QR_2 \left(1 - x^2\right)^{0.5} \right)}{QR_2 \left(1 - x^2\right)^{0.5}} \right]^2 \left(\frac{Sin\left(QHx/2 \right)}{QHx/2} \right)^2 dx$$

----- Eq. 4-2

Here R_1 is the outer radius, R_2 the inner radius; H the height of the cylinder and $J_1(x)$ is the Bessel function of the first order.

Powder Diffraction (or Wide Angle X-ray Scattering, WAXS)

Powder samples in 1.5mm diameter quartz capillary tubes were measured at the same facility of SAXS at Argonne National Laboratory's Advanced Photon Source (APS). with a shorter camera length and X-rays with E = 18 keV. The peaks in the plot $I(Q)$ versus Q are related to real-space distance d by the relation $d=2\pi/Q$. While intense, sharp and narrow peaks imply high degree of repetition, the weak and broad peaks relate to a low degree of repetition of the corresponding length scale. Mature peptide nanotubes were aligned with 20 mM Na_2SO_4 solution, centrifuged at 16,110xg for 30 min, then the supernatant was removed and precipitate was lyophilized to dryness. The dried powder was used for powder diffraction measurement.

Electron Diffraction

Mature peptide nanotubes were bundled with 10 mM Na_2SO_4 solution. An aliquot (8 μl) of the solution was applied to TEM grids, allowed to settle for one minute, and

excess solution was wicked away with filter paper. The diffraction pattern was recorded by a Philips 410 transmission electron microscope under the diffraction mode. The d-spacing was calculated by $d=\lambda L/R$, where R represents the distance from the central bright spot to one of the rings, L represents the camera length and λ is the wavelength of the electron (80 kV: 0.00435 nm). The instrument camera length was calibrated using the aluminum polycrystalline standard (purchased from Electron Microscopy Science). The instrument camera length was calculated to be 720 mm.

CHAPTER 5

STRUCTURAL CHARACTERIZATION OF NANO-TUBES BY ISOTOPE-EDITED IR AND SSNMR

INTRODUCTION

Aβ(13-21)CyCy can self-assemble into nanotubes, and specific structure changes in the peptide highlighted the importance of inter-sheet contacts in nanotube formation. Although CD spectra of the nanotube appear did not appears representation of typical β-sheet secondary structure, IR analyses have suggested that the peptides are oriented β-sheets in the nanotubes. In addition, X-ray diffraction shows the same cross-β structure as amyloid fibrils. As the nucleobases decorated amyloid peptide nanotubes have potential applications as a novel bio-material, understanding the structure of this assembly at a molecular level would be essential. Therefore, several structural questions need to be addressed:

1. What is the peptide orientation/position within a sheet?
2. What is the driving force defining sheet lamination, and

3. Energetically, what controls the pathway forwards self-assembly?

Due to the para-crystalline and insoluble nature of amyloid, these assemblies are not suitable for structural characterization by X-ray crystallography or solution NMR, the two principal approaches to biomolecular structure determination. As alternatives, isotope-edited IR (IE-IR) and solid-state NMR (ss-NMR) methods are frequently applied recently to define the structural models for amyloid peptide assemblies.

Infrared spectroscopy is a powerful tool for analyzing the secondary structure of proteins and peptides. Recent advance in FT-IR spectroscopy has shown more detailed local structure information can be obtained by using isotope labeling approach. When an isotope label is introduced into the peptide backbone, the isotope-induced shift can be calculated using a simple harmonic oscillator model (where k is the force constant and μ is the reduced mass):

$$\nu = \frac{1}{2\pi}\sqrt{\frac{k}{\mu}}$$

The increased mass of an isotope label causes a shift of absorption frequency to lower wavenumbers, isolates the individual vibration and thus yields accurate structural data on the labeled site. Isotope-edited IR technique has been applied to locate the β-sheet organization and the alignment of residues within the β-sheet in amyloid proteins (Halverson, Sucholeiki et al. 1991; Silva, Barber-Armstrong et al. 2003; Hiramatsu, Goto et al. 2005). As for the ^{13}C label incorporation, the carbonyl amide I band shifts to lower frequency while the remaining ^{12}C carbonyl amide I shifts to a higher frequency. The magnitude of ^{13}C carbonyl stretch shift depends on the coupling efficiency, the more strongly the β-sheet regions are coupled, the more significant the shift to higher

frequency. An anomalous intensity increase of the ^{13}C carbonyl stretch is often observed in the anti-parallel β-sheet arrangement; such anomalous intensity increase is not obvious for parallel β-sheet arrangement (Brauner, Dugan et al. 2000; Kubelka and Keiderling 2001; Paul, Wang et al. 2004).

RESULT

Isotope Edited FT-IR

To probe the peptide arrangement within β-sheet, isotope-edited IR (IE-IR) technique is applied. Three 1-^{13}C labeled Aβ(13-21)CyCy peptides were characterized respectively, [A16, 1-^{13}C], [L17, 1-^{13}C], and [V18, 1-^{13}C] (Figure 5.1). The amide I bond split into two distinct transitions with ^{13}C band shift to lower frequency while the residual ^{12}C carbonyls shift to higher frequency. All of the 1-^{13}C labels showed weak absorption intensities around 1610-1605 cm^{-1}, and ^{12}C carbonyls shift to 1638-1641 cm^{-1}. For instance, the 1-^{13}C label on Leu17 residue absorbs at 1606 cm^{-1} and the absorption maximum of ^{12}C carbonyl shifts from 1635 to 1641 cm^{-1}. [L17, 1-^{13}C]-Aβ(13-21)K16A amyloid fibrils, with 1-^{13}C carbonyl absorbs at 1605 cm^{-1} and the absorption maximum of ^{12}C carbonyl shifts from 1628 to 1637 cm^{-1}, and this peptide has been confirmed by SSNMR to be a parallel in-register beta sheet arrangements. [L17, 1-^{13}C]-Aβ(13-21)K16A also shows a weak ^{13}C absorption intensity, while [L17, 1-^{13}C]-Aβ(16-22), only two amino acids shorter than Aβ(13-21)K16A but forming amyloid fibrils with an anti-parallel in-register β sheet structure, shows an anomalous increase in the intensity of the

Figure 5.1.

Isotope-edited FTIR of Aβ(13-21)CyCy.

Spectra of Aβ(13-21)CyCy nanotubes as KBr pellets with Red: unlabeled, Green: [16-^{13}C]-Ala, Blue: [17-^{13}C]-Leu, Black: [18-^{13}C]-Val IR.

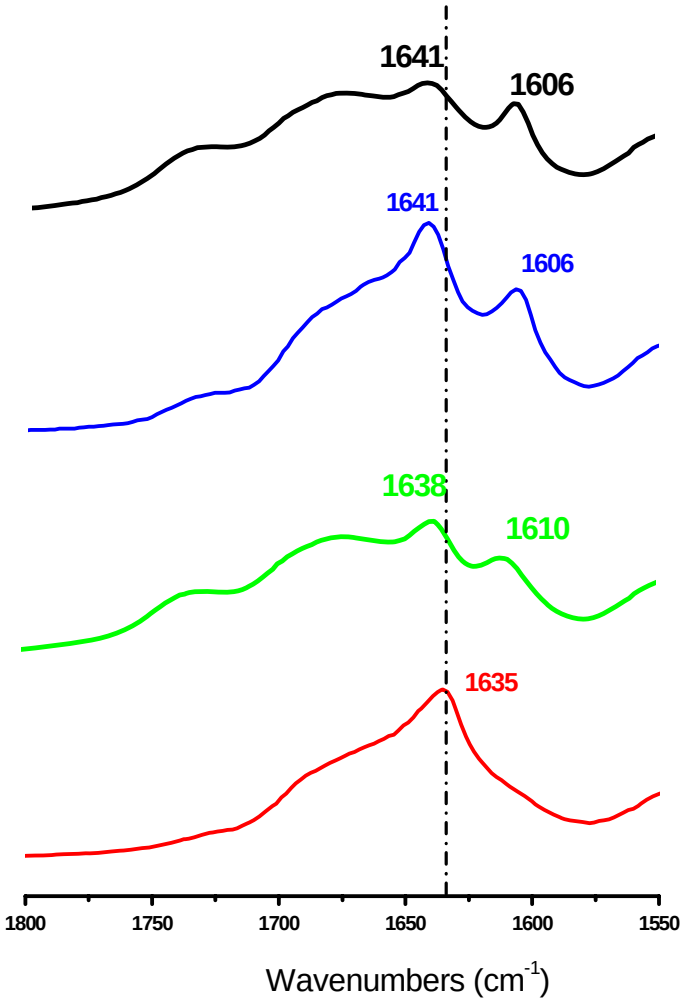

^{13}C peak (ref). These observations suggest that Aβ(13-21)cc-NH_2 assembled as a parallel β-sheets.

Peptide Organization Study by Solid-state NMR

Further characterization of peptide organization in the nanotube was conducted by using solid state NMR (SSNMR). Standard solid-state NMR techniques such as REDOR and DRAWS can measure ^{13}C-^{15}N distances up to 5Å and ^{13}C-^{13}C distances of 5Å. The nanotubes formed by Aβ(13-21)CyCy in 25mM MES buffer at pH4.3 were analyzed by $^{13}C\{^{15}N\}$ REDOR experiment which directly measures the distance between selected ^{13}C and ^{15}N isotopes in Aβ(13-21)CyCy. The sample was prepared by mixing two peptides of Aβ(13-21)CyCy, labeled with [^{15}N]A16-[1-^{13}C]F20 and [3-^{13}C]A16 respectively, at 1:1 molar ratio. This labeling scheme was designed to distinguish parallel in-register versus antiparallel out-of-registry arrangement (either one, two or three residue shift) in a single $^{13}C\{^{15}N\}$ REDOR experiment (Figure 5.2). If the peptides are parallel in-register β along one sheet, [3-^{13}C]A16 (methyl carbon) and [^{15}N]A16 are proximal (Figure 5.2 A, left). While in an anti-parallel two residue shifted orientation, [^{15}N]A16 and [1-^{13}C]F20 are directly hydrogen bonded (Figure 5.2 A, right).

The REDOR experiment measures the heteronuclear dipolar coupling by applying two π-pulses in each rotor cycle to dephase rotational echoes. The REDOR experiment consists of the full-echo spectrum and the dephased (S) spectrum. Using ^{13}C-^{15}N as an example, in the S spectrum, the heteronuclear dipolar coupling is reintroduced by applying π-pulses on the ^{15}N channel. In the $^{13}C\{^{15}N\}$ REDOR difference spectrum, ΔS, the distance between ^{13}C and ^{15}N nuclei is obtained through calculating the difference in

signal intensity of a ^{13}C spectrum with and without ^{15}N π-pulses. As shown in the ^{13}C full-echo spectrum of Aβ(13-21)CyCy (Figure 5.2B, bottom), the resonance at 20ppm and 170ppm was assigned to [3-^{13}C]Ala and [1-^{13}C] Phe respectively. In Figure 5.2B, both [3-^{13}C]Ala and [1-^{13}C]Phe appear in the ΔS specturm, suggesting both [3-^{13}C]Ala16 and [1-^{13}C]Phe are proximal to [^{15}N]A16. The [3-^{13}C]A16-{^{15}N}A16 REDOR dephasing curve was fit either as a parallel in-register arrangement, with 5.6Å and 5.5Å for the distances between [3-^{13}C]A16 and [^{15}N]A16 and a ^{15}N-^{13}C-^{15}N angle of 129° (Figure 5.2C, solid red line and Figure 5.2D); or a parallel one residue out of register arrangement, with 7.2Å and 4.9Å for the distances between [3-^{13}C]A16 and [^{15}N]A16 and a ^{15}N-^{13}C-^{15}N angle of 111° (Figure 5.2C, solid black line and Figure 5.2E). As scanning time increased, fitting of the dephasing curve suggested parallel one residue out of register arrangement was more plausible. The [1-^{13}C]F20-{^{15}N}A16 REDOR dephasing curve was fit to an anti-parallel two residue out of register arrangement, with 4.2Å and 5.5Å for the distances between [1-^{13}C]F20 and [^{15}N]A21 and an ^{13}C-^{15}N-^{13}C angle of 155° (Figure 5.2F, solid black line and Figure 5.2G). Fitting of REDOR dephasing curve also indicate 59% of the peptides of the self-assembled structure in the SS-NMR sample adopt parallel arrangement while 41% adopt anti-parallel arrangement.

TEM images of the ssNMR sample showed that some fibrils coexist with the nanotubes (Figure 5.3), therefore sample heterogeneity accounts for the SSNMR results, that is, the nanotubes adopt one peptide orientation and the fibrils adopt the other peptide orientation. The reason for the heterogeneity of the sample most probably is related to the sample preparation. In comparison with the non-isotope labeled Aβ(13-21)CyCy

Figure 5.2 $^{13}C\{^{15}N\}$ REDOR spectra and dephasing curves of Aβ(13-21)CyCy

A. Schematic representation of the relative position of [3-^{13}C]A16 and [1-^{13}C]F20 labels (yellow) to [^{15}N]A16 label (blue) in parallel in-register (left) and anti-parallel two residue out-of-registry (right) arrangements. Red, oxygen; grey, carbon; light blue, nitrogen; green line, backbone hydrogen bonding; white line, detectable distance between ^{13}C and ^{15}N isotopes.

B. $^{13}C\{^{15}N\}$ REDOR NMR spectra at 392 Tr for Aβ(13-21)CyCy, formed by mixing two isotopic labeled peptides, [^{15}N]A16-[1-^{13}C]F20 and [3-^{13}C] A16.

C. $^{13}C\{^{15}N\}$ REDOR dephasing curves for parallel arrangement of Aβ(13-21)CyCy.

D. The fitting results of the red solid line and schematic representation of the relative position of [^{15}N]A16 label (blue) to [3-^{13}C]A16 (silver) in parallel in-register arrangement.

E. The fitting results of the black solid line and schematic representation of the relative position of [^{15}N]A16 label (blue) to [3-^{13}C]A16 (silver) in parallel one residue out of register arrangement.

F. $^{13}C\{^{15}N\}$ REDOR dephasing curves for anti-parallel arrangement of Aβ(13-21)CyCy.

G. The fitting results of the black solid line and schematic representation of the relative position of [^{15}N]A16 label (blue) to [1-^{13}C]F20 (green) in anti-parallel two residue out of register arrangement.

A

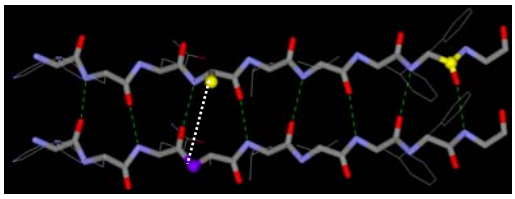

CyCyQALVFFA
CyCyQALVFFA

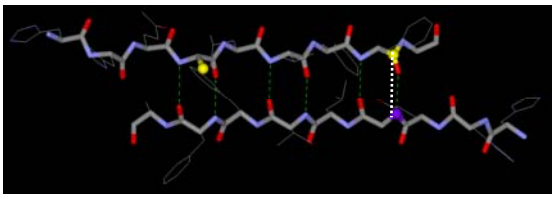

CyCyQALVFFA
AFFVLAQCyCy

B

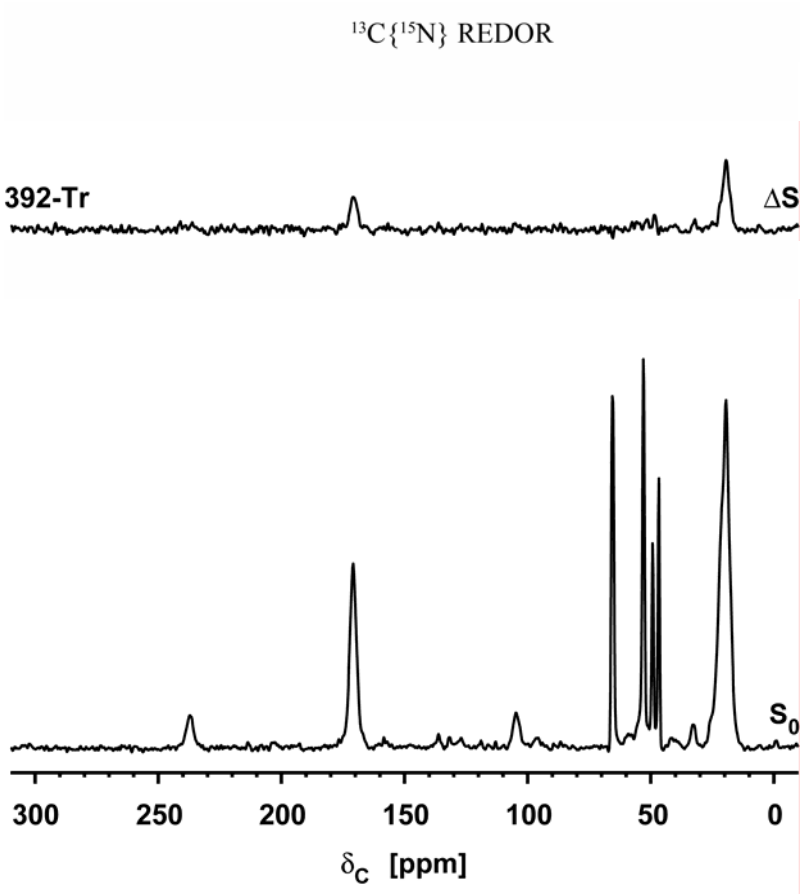

C

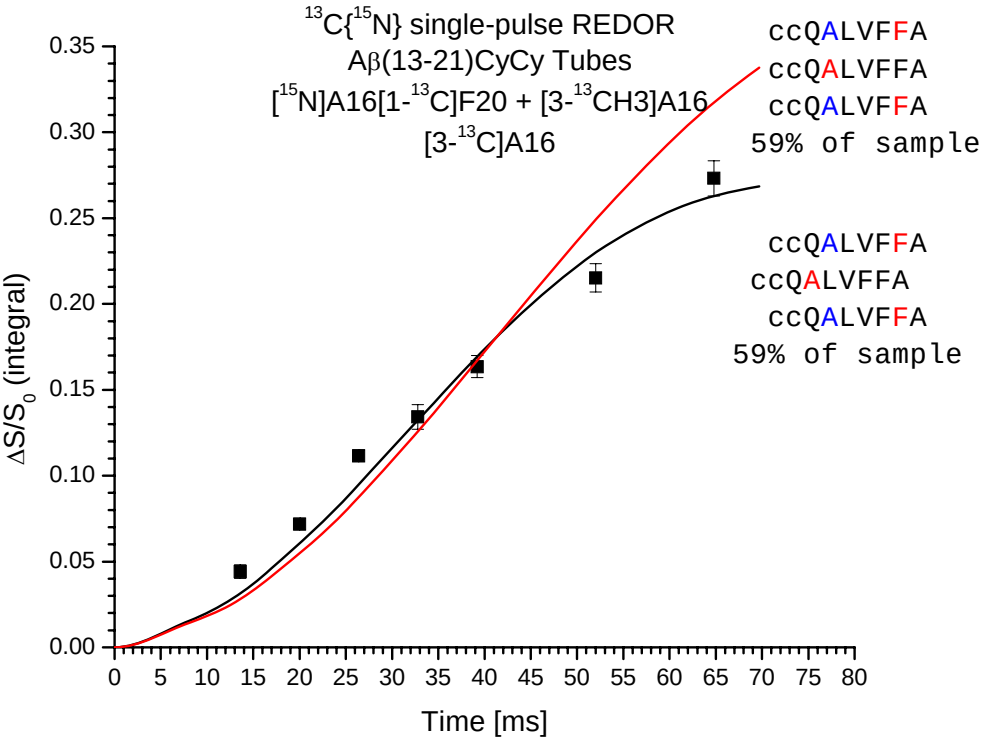
^{13}C{^{15}N} single-pulse REDOR
Aβ(13-21)CyCy Tubes
[^{15}N]A16[1-^{13}C]F20 + [3-^{13}CH3]A16
[3-^{13}C]A16
ccQALVFFA
ccQALVFFA
ccQALVFFA
59% of sample
ccQALVFFA
ccQALVFFA
ccQALVFFA
59% of sample
ΔS/S$_0$ (integral)
Time [ms]
0.00
0.05
0.10
0.15
0.20
0.25
0.30
0.35
0 5 10 15 20 25 30 35 40 45 50 55 60 65 70 75 80

D

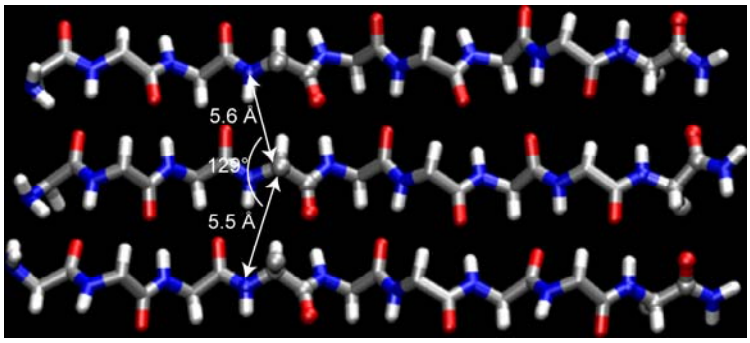
5.6 Å
129°
5.5 Å

E

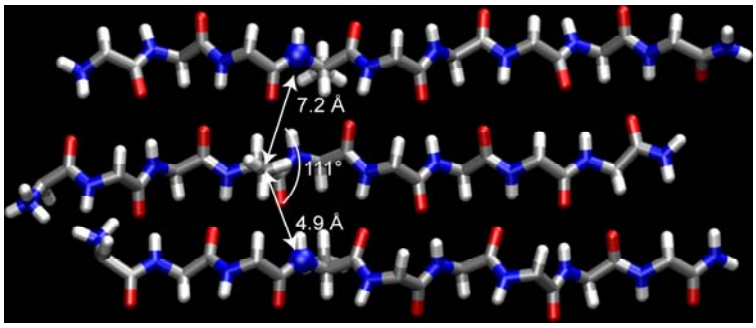
7.2 Å
111°
4.9 Å

F

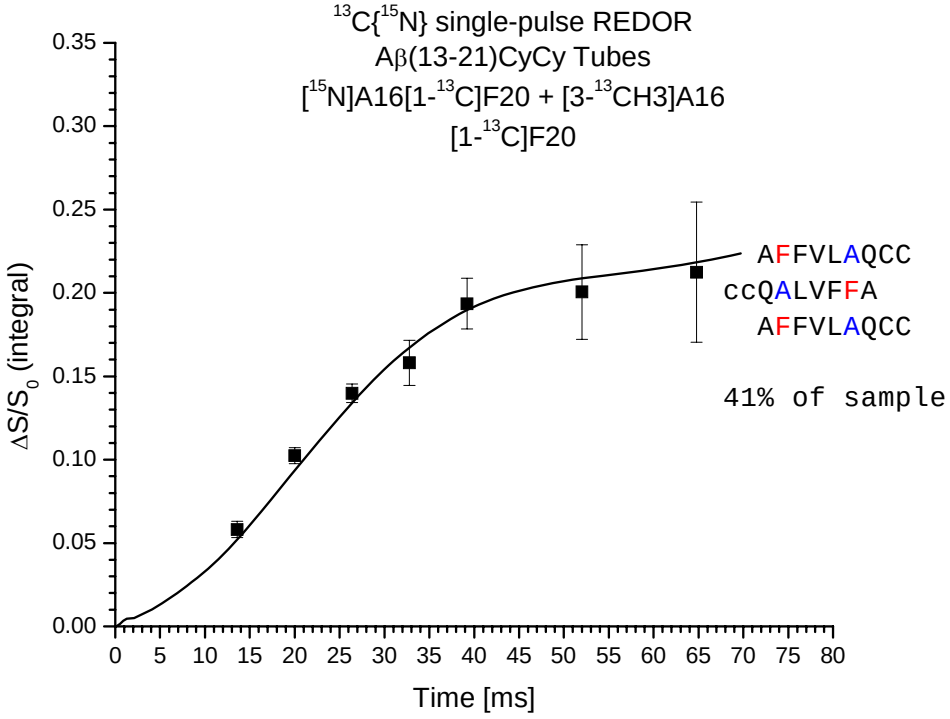
^{13}C{^{15}N} single-pulse REDOR
Aβ(13-21)CyCy Tubes
[^{15}N]A16[1-^{13}C]F20 + [3-^{13}CH3]A16
[1-^{13}C]F20
AFFVLAQCC
ccQALVFFA
AFFVLAQCC
41% of sample
ΔS/S$_0$ (integral)
Time [ms]
0.00
0.05
0.10
0.15
0.20
0.25
0.30
0.35
0 5 10 15 20 25 30 35 40 45 50 55 60 65 70 75 80

G

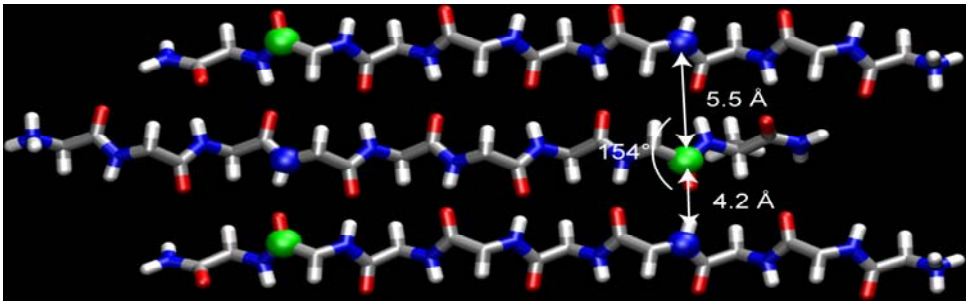
5.5 Å
154°
4.2 Å

Figure 5.3

TEM images of the SS-NMR sample

A. TEM image indicated the nanotube morphology in the SS-NMR sample. Peptides CyCyQ[^{15}N]ALVF[1-^{13}C]FA and CyCyQ[3-^{13}C]ALVFFA was mixed at 1:1 molar ratio, dissolved in 25mM MES at pH4.3 and final peptide concentration is 1.5 mM**.**

B. TEM image indicated the fibril morphology coexisting with nanotubes in the SS-NMR sample. Left image is the enlargement of rectangular region in the right image.

A.

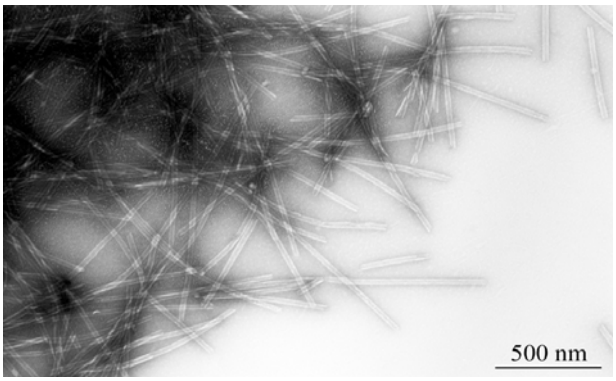

B

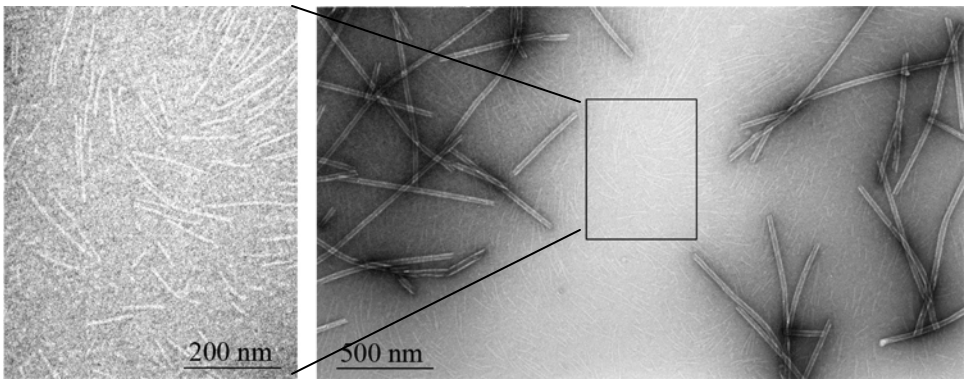

sample, sample preparation procedure was changed to ensure that the two peptides mix thoroughly at 1:1 molar ratio. Two extra steps were taken to prepare the sample. First, the two peptides are dissolved seperately in 0.1%TFA solution at pH 2, under which condition the peptide has a random coil structure. Then the peptide solutions were mixed and lyophilized. Secondly, the mixing peptide powder was dissolved in 25 mM MES buffer at pH 4.3 at 4°C and then allowed to incubate at room temperature. Temperatures as low as 4°C slow down the self-assembly of the peptide and therefore further guaranteed that the two peptides mixed well. However, the low temperature may also favor fibril formation over nanotube formation and similar phenomena was observed in Aβ(13-21)K16A with Zn^{2+} addition (Xu, 2007).

Probing the Cytosine Orientation by Linear Dichroism

Ultraviolet (UV) flow-oriented linear dichroism (LD) has been applied to study the structural arrangement of secondary structural elements recently. Thorough measuring the difference in absorbance of linearly polarized light parallel and perpendicular to an orientation direction, information on the orientation of transition dipole could be obtained (Dafforn, Rajendra et al. 2004; Rajendra, Damianoglou et al. 2006). If the LD signal is positive, it suggests the polarizations of the transition is more parallel along the direction of the orientation. If the LD signal is positive, it suggests the polarizations of the transition is more perpendicular to the direction of the orientation.

Mature nanotube formed by 0.3mM Aβ(13-21)CyCy in 25mM MES at pH4.3 was studied Ultraviolet ((UV) flow-oriented linear dichroism (LD) at Clemson University.

Figure 5.4

Linear Dichroism (LD) and Ultraviolet (UV) Spectra of Aβ(13-21)CyCy.

Mature nanotube formed by 0.3mM Aβ(13-21)CyCy in 25mM MES at pH4.3. In the spectra of UV (red), the peak at 207nm represents amide π-π* transition and the peak at 267 represents cytosine transition. In the spectra of LD (black), positive peak around 207nm suggested transition dipole more parallel tube axis; negative peak at 267nm suggested transition dipole more perpendicular to tube axis.

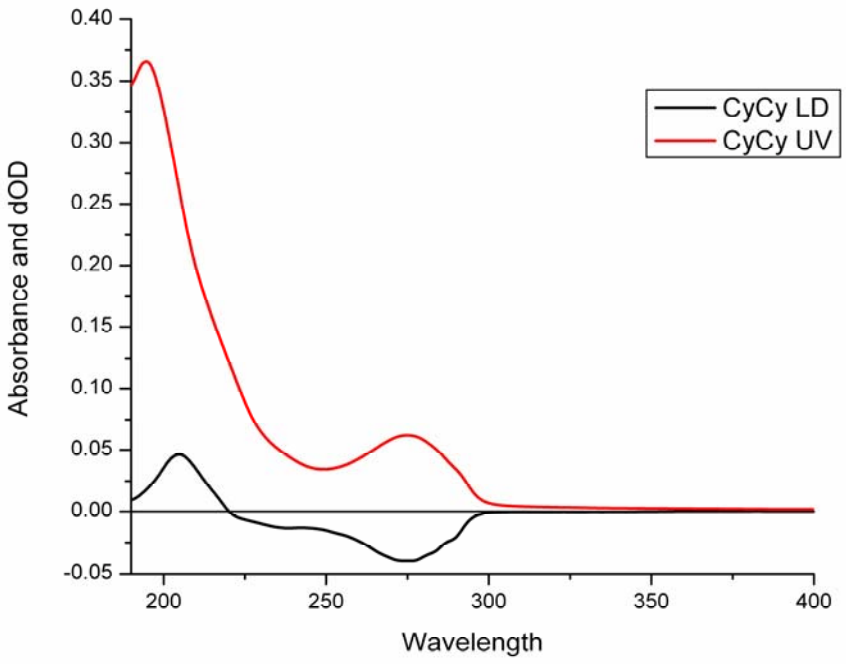

The nanotubes were aligned by using couette flow cell. As seen in Figure 5.4, after alignment of the nanotubes, two signals showed up in the LD spectra (black), positive signal at 207 nm suggested transition dipole are more parallel to tube axis; negative peak at 267nm suggested transition dipole more perpendicular to tube axis. While in the spectra of UV (red), the peak at 207nm represents amide π-π* transition and the peak at 267nm represents cytosine in-plane transition. Therefore, the hydron bonds of peptide backbone are more parallel to tube axis, and the bases are highly ordered in CyCy tubes which is more perpendicular to tube axis than parallel. This supports the model in which that the bases and side chain laminates are more perpindicular to tube axis, while hydrogen bonds are more parallel to tube axis.

DISCUSSION

Isotope edited FTIR result of Aβ(13-21)CyCy established a parallel β sheet arrangement of Aβ(13-21)K16A amyloid fibrils. SSNMR suggests two peptide arrangement patterns, a parallel β sheet organization and an anti-parallel β sheet organization, which probably results from the two morphologies. As the parallel SSNMR result is consistent with isotope edited FTIR data, we therefore hypothesis that the peptides in Aβ(13-21)CyCy nanotubes are in a parallel arrangement while the peptide that form fibrils are antiparallel arrangement. At this point, the peptide arrangement of the Aβ(13-21)CyCy nanotubes has not yet been defined, and the test for this hypothesis is undergoing.

The mutation data suggested that two cytosines are required to direct nanotube formation. Linear Dichroism indicated the hydron bonds of peptide backbone are more parallel to tube axis, and the bases are highly ordered in CyCy tubes which is more perpendicular to tube axis than parallel. As a result, the most likely place where Cy13 and Cy14 are in close proximity is along the lamination dimension. Therefore, we propose a model that the Aβ(13-21)CyCy nanotubes share a similar three-demensional architecture with the Aβ(13-21)CyCy fibrils and only the degree of lamination is significantly different, and the increased lamination model of Aβ(13-21)CyCy nanotube is consistent with the models of Aβ(16-22) nanotubes and Aβ(13-21) ribbons. In this model, cytosine base interaction is along β sheet lamination direction and stabilizes β–sheet lamination, inducing significant lamination growth and morphology of nanotubes (Figure 5.5A). According to isotope edited FT-IR and SSNMR measurement, the peptides in the nanotubes probably adopt the parallel one residue out of register arrangement. Therefore, cytosines orienting on one ends of laminated sheets. When the laminated sheets coil up forming nanotube, cytosines expose only on one face of the tube. The cytosine side-chains are perpendicular to the β–sheet hydrogen bonding direction based on LD measurement, along with the MD simulation and mutation study, the Cy/Cy association are along the lamination dimension. The fibrils in the SSNMR sample probably adopt the anti-parallel two residues out of register arrangement, cytosines orient on both ends of laminated sheets (Figure 5.5B).

Figure 5.5

Models of Nanotubes formed by Aβ(13-21)CyCy

A. Three dimensional architecture of peptide nanotubes. Left, β–sheets consisting of peptides with parallel one residue out of register arrangement are packed through side-chain/side-chain interactions along the lamination dimension (Blue, Cy; red, the other amino acids). The cytosine side chains are along the lamination dimension; right, the peptide nanotubes.

B. Three dimensional architecture of peptide fibrils. Left, the peptide fibrils; right, β–sheets consisting of peptides with anti-parallel two residues out of register arrangement are packed (Blue, Cy; red, the other amino acids). The cytosine side chains are along the lamination dimension.

A.

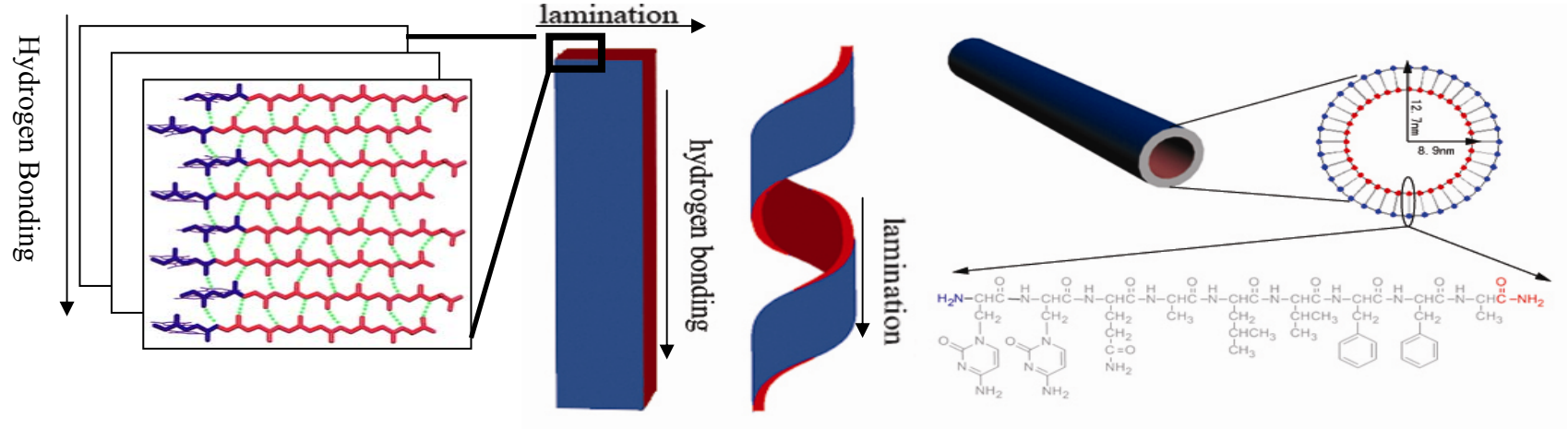
Hydrogen Bonding
lamination
hydrogen bonding
lamination
12.7nm
8.9nm

B

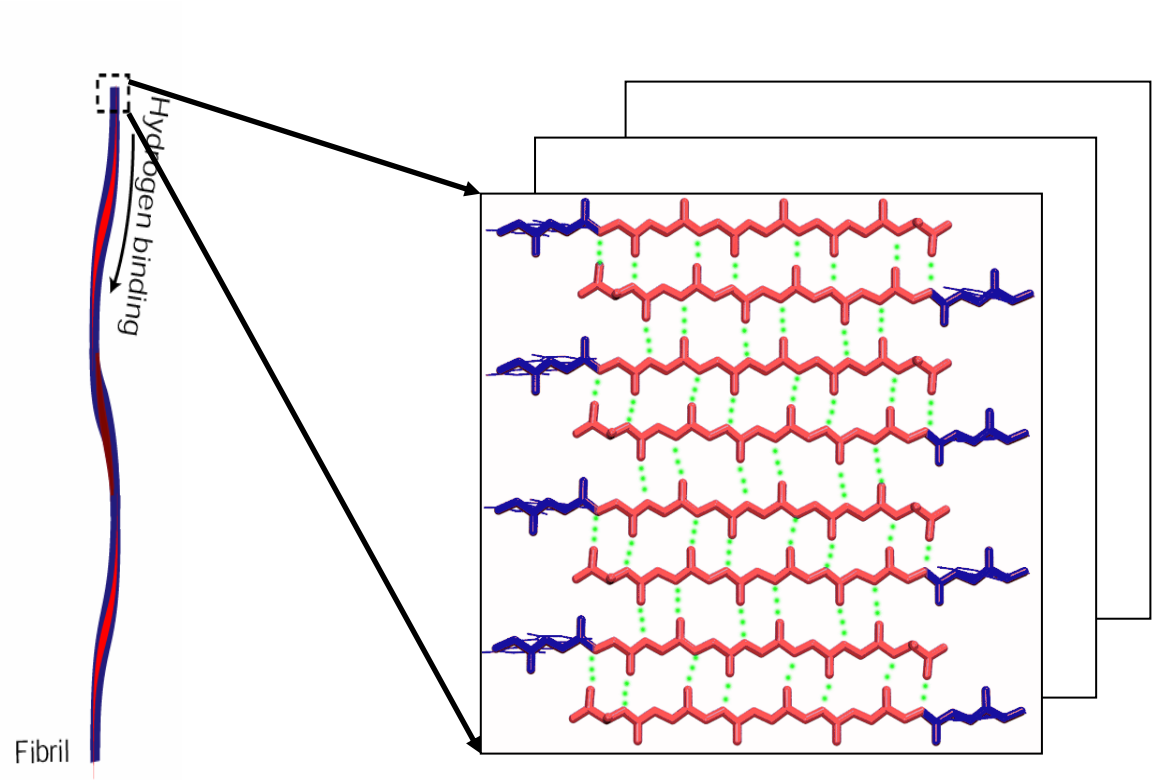

MATERIALS AND METHODS

FT-IR Spectroscopy

Isotope edited FTIR was performed on ^{13}C labeled peptides, Aβ(13-21)CyCy[-A16, 1-^{13}C], Aβ(13-21)CyCy[L17, 1-^{13}C] and Aβ(13-21)CyCy[F20, 1-^{13}C]. The isotope labeled peptide was synthesized by standard Fmoc peptide protocol. The sample solution was prepared following the same procedure as the non-labeled peptides. After maturation, mature peptide nanotubes were aligned with 20mM Na_2SO_4 solution, centrifuged at 16,110xg for 30 min, then the supernatant was removed and precipitate was lyophilized. The dried powder was mixed with KBr as a pellet for IR analysis. KBr background was deducted from each sample measurement. IR spectra were collected on a Nicolet MAGNA-IR 560 Spectrometer E. S. P. instrument operated at 2 cm^{-1} resolution. 100 scans were averaged to obtain a spectrum.

Solid-State NMR experiments (SSNMR)

SSNMR spectroscopy: ^{13}C observe, ^{15}N dephase REDOR (Gullion, 1988) NMR measurements were made on a Bruker Avance 600 MHz spectrometer operating with a ^{13}C frequency of 150.8 MHz and ^{15}N frequency of 60.3 MHz. All spectra were collected with a Bruker triple resonance probe. ^{13}C Magnetization was prepared by 2ms ^{1}H-^{13}C cross-polarization with a 50 kHz ^{13}C spin-lock pulse and a linear ramp on the ^{1}H spin-lock pulse from 50 kHz to 70 kHz. To compensate for pulse imperfections and ^{13}C homonuclear recoupling, ^{15}N π pulse were applied every half-rotor period and xy8 phase cycle (Gullion 1990). A single ^{13}C pulse was applied downed the middle of the REDOR

evolution period (single pulse REDOR). ^{13}C π Pulse widths were of 6μs and ^{15}N π pulse widths were 10.4 μs. EXORCYCLE phase cycling of the ^{13}C Hahn-echo refocusing pulse (Rance, 1983, Sinha 2004) and 95 kHz Spinal64 (Fung, 2000) and ^{1}H decoupling are used. Magic-angle spinning frequency was 10 kHz ± 2Hz. The exit temperature of the cooling and spinning air was kept below -1^{o} C to ensure that magic-angle spinning and RF heating did not denature the samples. ^{1}H-^{13}C and ^{1}H-^{15}N Cross-polarization spectra were taken before and after the REDOR experiment to ensure that the sample did not change. Peak integrals of the labeled carbon center band were used to provide the experimental REDOR data points. The error was calculated using the noise of each spectrum as the maximum deviation and multiplied by the square root of the number of points in the integral. The error bars on the experimental REDOR points represents 3 standard deviations.

Room temperature $^{13}C\{^{15}N\}$ REDOR results for [1-^{13}C,^{15}N] glycine were obtained, which was diluted 10:1 with natural abundance glycine. The calculated REDOR dephasing curve was calculated using the formula of Mueller (Mueller, 1995) and includes a correction for the natural abundance glycine carbonyls which do not dephase as they are not near an ^{15}N. To match the x-ray determined distance between 1-^{13}C and ^{15}N for single-pulse REDOR, a scaling factor of 0.706 must be applied to the data to account for the imperfect ^{13}C and ^{15}N π pulses. With this scaling factor, the REDOR determined ^{13}C-^{15}N internuclear distance is 2.5 Å ± 0.1 Å, which compares well to the x-ray determined distance of 2.49 Å (Marsh, 1958). This scaling factor was applied to the rest of the calculated REDOR curves. To ensure that this scaling factor did not change, $^{13}C\{^{15}N\}$ REDOR measurements were made on the diluted [1-^{13}C,^{15}N] glycine sample

before and after every sample measurements.

Sample preparation for $^{13}C\{^{15}N\}$ REDOR measurements:

Two peptides, Aβ(13-21)CyCy labeled with [^{15}N]A16-[1-^{13}C]F20 and [3-^{13}C]A16 repectively, were synthesized for SSNMR experiments. To ensure that equal molar ratios of the two peptides were mixed, peptides were first incubated in 0.1%TFA aqueous solution at pH 2 under which condition the peptides remain random coil structure and 25μl of the peptide was injected into HPLC analytical column.

The sample was prepared by mixing two peptides of Aβ(13-21)CyCy, labeled with [^{15}N]A16-[1-^{13}C]F20 and [3-^{13}C]A16 respectively, at 1:1 molar ratio. To ensure the two peptides mix thoroughly at 1:1 molar ratio, following procedures are taken. First, the two peptides were dissolved separately in 0.1%TFA solution at pH 2, under which condition the peptide remains random coil structure. The secondary structure was studied by CD. Second, the peptide solutions were mixed and lyophilized. Third, the mixed peptide powder was dissolved in 25mM MES buffer at pH 4.3 at 4 °C and then allowed to incubate at room temperature. Temperature as low as 4°C slow down the self-assembly of the peptide and therefore guarantee that the two peptides mixed well. Maturation of nanotubes were achieved at room temperature and confirmed by CD and TEM analysis. To prepare SSNMR sample, mature tubes were pelleted and lyophilized to make powders. To protect the samples from fragmentation caused by freezing and lyophilization (Figure 3.3B), mature fibrils were bundled and precipitated from 20 mL solutions by the addition of 20 mM Na_2SO_4. Bundled intact nantobues after lyophilization were confirmed with TEM.

Solid-State NMR experiments (SSNMR)

$^{13}C\{^{15}N\}$ REDOR calibration and curve fitting:

The following discussion is for the [1-^{13}C]F20 dephasing by [^{15}N]A16, and similar methods were used for calculation of all $^{13}C\{^{15}N\}$ REDOR curves. The calculated REDOR curves (Goetz and Schaefer 1997) for the *inter*strand distances account for the dephasing of a single observed spin (^{13}C) in the presence of two dephasing spins (^{15}N), but do not include any ^{15}N-^{15}N dipolar coupling. Therefore the calculated curves require two interstrand ^{13}C-^{15}N distances and an interstrand ^{15}N-^{13}C-^{15}N angle. For a H-bonded carbonyl-nitrogen spin pair, one distance will be ~ 4.2 Å and the other will be ~ 5.4 Å. The simulations also include a natural abundance correction for the unlabeled carbonyl carbons that are not close to an ^{15}N. These carbons will contribute to the ^{13}C full-echo spectrum but not to the REDOR difference spectrum; therefore, for a 1:1 mixture the maximum observed dephasing will be:

$$\frac{99}{99+(9+8)*1.1}=0.84$$

In the above calculation, it was assumed that the ^{13}C isotope enrichment is 99% and the natural abundance ^{13}C is 1.1%. Therefore the total ^{13}C signal (i.e. full-echo) is a sum of the labeled and natural abundant ^{13}C, and each Aβ(13-21)CyCy peptide has 9 carbonyl carbons. However, the carbonyl carbons of [^{15}N]A16 (which have a two bond ^{13}C-^{15}N distance of 2.42 Å) and of Q15 (a one bond ^{13}C-^{15}N distance of 1.325 Å) will also dephase and have a contribution to the REDOR difference spectrum of:

$$\frac{1.1}{99+(9+8)*1.1}=0.009$$

$$\left(0.84*\left(\frac{3}{12}\mathrm{REDOR}[r_1]+\frac{3}{12}\mathrm{REDOR}[r_2]+\frac{1}{12}\mathrm{REDOR}[r_1 r_2)]\right)+0.009*\left(\mathrm{REDOR}[1.325]+\mathrm{REDOR}[2.42]\right)\right)*0.706$$

Finally as there is a 1:1 mixture of ^{13}C:^{15}N labeled peptides, there will be a binomial distribution of peptides so that only 6/12 of the ^{13}C will only be coupled to a single ^{15}N (i.e. an isolated spin-pair), 3/12 with a ^{13}C-^{15}N distance of r_1 and 3/12 with a distance of r_2. 1/12 of the ^{13}C will be surrounded by two ^{15}N. The calculated REDOR curve ($\Delta S/S_0$) then is:

Where REDOR[x] is the REDOR curve for an isolated ^{13}C-^{15}N spin-pair with a distance of x Å using the formula of Mueller (Mueller, 1995) and REDOR[x y] is the three-spin REDOR curve with ^{13}C and ^{15}N distances of x Å and y Å, and an ^{15}N-^{13}C-^{15}N angle calculated using the formula of Goetz (Goetz,1997). In the case where there is a non-equal-molar ratio of ^{13}C and ^{15}N labeled peptides, $\Delta S/S_0$ becomes:

$$\left(0.84*\left(\frac{p(2+p)}{3(1+p)^2}*\frac{99}{99+(9+8*p)*1.1}\mathrm{REDOR}[r_1]+\frac{p(2+p)}{3(1+p)^2}*\frac{99}{99+(9+8*p)*1.1}\mathrm{REDOR}[r_2]+\frac{p^2}{3(1+p)^2}*\frac{99}{99+(9+8*p)*1.1}\mathrm{REDOR}[r_1 r_2]\right)+\frac{1.1*p}{99+(9+8*p)*1.1}*\left(\mathrm{REDOR}[1.325]+\mathrm{REDOR}[2.42]\right)\right)*0.706$$

Where p is the ratio of ^{15}N to ^{13}C labeled peptides and is equal to 1 for an equal-molar ^{13}C:^{15}N mixture. When p = 1, this simplifies to the previous equation.

Linear Dichroism

Flow linear dichroism spectra were recorded using a Jasco J-715 circular dichroism spectropolarimeter adapted for flow linear dichroism (LD) measurements at Clemeson University. The LD cell is a cylindrical capillary flow cell, consisting of two

coaxial cylinders, one of which is a capillary and the other is a quartz rod. The annular gap between the rotating capillary and the stationary rod is filled with the sample, and upon rotation of the capillary a shear force is induced across the sample to cause significant orientation but not a turbulent flow. Sample of 0.3 mM Aβ(13-21)CyCy in 25 mM MES at pH4.3 was used for LD study. The nanotube morphology was confirmed by TEM. To orient the tube sample we rotate the cell at 3000 rpm and wait for 15 mins until the LD comes to equilibrium. Absorbance and CD baselines were collected in the same cuvette. For LD, the sample in the same couette flow cell without rotation (0 rpm) was used as backbound for baseline substraction, under which condition the tube sample are disordered and do not have an LD.

CHAPTER 6

CONCLUSION AND PESPECTIVE

The folding of proteins into a compact three-dimensional structure with precision and fidelity is one of the most significant examples of biological self-assembly. Protein folding plays a crucial role in generating biological activity and regulating cellular growth and differentiation. Failure of folding properly is the origin of many pathological conditions. As an intriguing example of protein misfolding, amyloid diseases including Alzheimer's disease, prion diseases and diabetes, share the pathological feature of aggregated misfolded protein deposits. These 'protein-misfolding diseases' might be linked by common principles, therefore understanding the driving force and mechanism of protein misfolding may help to find common targets for therapeutic intervention.

Although being identified as misfolded toxic protein structure for many years, amyloid fibers recently have been found in bacteria, fungi, insects, invertebrates and humans that are functional (Coustou, Deleu et al. 1997; Iconomidou, Vriend et al. 2000; Mackay, Matthews et al. 2001; Chapman, Robinson et al. 2002; Fowler, Koulov et al.

2006). For example, curli, the extracelluar amyloid fibrils produced by *Escherichia coli*, is a major component of bacteria biofilm (Chapman, Robinson et al. 2002). Pmel17 fibrils template the formation of melanin in eukaryotes (Berson, Theos et al. 2003). These naturally occurred amyloid fibrils with positive function provide insight into potential applications as biomaterials for coating surface or templating reactions.

Elucidation of the structure, the assembly pathway and the regulatory factors of amyloid fibrils would be crucial for both the disease therapy and bionanotechnology application. In this dissertation, self-assembly of several short peptides originating from amyloid-β peptide was investigated and was specifically probed with nucleaobases incorporation.

The Synthesis of β-(cytosine-1-yl)alanine is successful, and for the first time, nucleobases are successfully incorporated into amyloid beta peptide side chain. The nucleo-amino acid monomers are characterized by ^{1}H NMR, ^{13}C-NMR, IR, MS and thermal analysis. The synthesis route of nucleobase modified Aβ peptide under Fmoc protocol is successfully developed by our group. We have designed and synthesized a series of nucleobase modified Aβ peptide based on the method described above.

My analysis suggested that nucleobase modified amyloid peptide, Aβ(10-21)CyCy-NH_2, is sufficient to form homogeneous amyloid fibrils. Cytosine nucleaobase incorporation in Aβ(10-21) reduced the nucleation phase and initiation of sheet-sheet contacts is crucial for the formation of nucleus. In order to simplify possible geometric constraints on assembly, Aβ(13-21)CyCy was designed to exposure of the CyCy dyad at peptide N-terminus. The results established that Aβ(13-21)cc-NH_2 forms homogenous nanotubes around the pKa of cytosine. The fibrils formed by Aβ(10-21)CyCy and

nanotubes formed by Aβ(13-21)CyCy possess remarkably similar structural elements to those of the normal assembled amyloid fibrils, such as cross-β diffraction pattern, CR binding and β-sheet secondary structures. Formation of homogenous stable nanotubes by Aβ(13-21)CyCy was clearly pH-dependent.

Isotope edited FTIR result of Aβ(13-21)CyCy established a parallel β sheet arrangement of Aβ(13-21)K16A amyloid fibrils. SSNMR suggests two peptide arrangement patterns, a parallel β–sheet organization and an anti-parallel β–sheet organization, which probably results from the two clear morphologies. SSNMR results are consistent with isotope edited FTIR result so far. Therefore, we hypothesis that the peptides in Aβ(13-21)CyCy nanotubes are parallel arrangement while the peptide that form fibrils are antiparallel arrangement. Combination of structural analysis and Linear Dichroism results, argues that the cytosine base interaction is along the β–sheet lamination, inducing significant lamination growth and stabilizing the morphology of nanotubes.

These nucleobase modified amyloid peptides now have potential applications in the design of synthetic materials. Peptide self-assembly can be controlled by varying the the length of the peptide, and functional groups exposed on the surfaces can be tailored with different nucleobases. For example, fibrils formed by Aβ(10-21)CyCy and nanotubes of Aβ(13-21)CyCy could be used as templates for synthesizing silver nanoclusters. Fibrils formed by Aβ(10-21)ThTh can associate with polyA, and therefore has potential as a DNA template. The nucleobases decorated amyloid fibrils and nanotubes could be assembled under physiological pH, which may be applied in the biological assays, such as gene delivery or PNT-membrane interactions. Moreover, the

self-assembly could be controlled by pH, temperature and solvent condition, and result in different structural isomers. These studies have set the good base for more extensive development of peptide self-assembly for novel material development.

REFERENCE

Aggeli, A., I. A. Nyrkova, et al. (2001). "Hierarchical self-assembly of chiral rod-like molecules as a model for peptide beta -sheet tapes, ribbons, fibrils, and fibers." *Proc. Natl. Acad. Sci. U S A* **98**(21): 11857-62.

Andreu, J. M. and S. N. Timasheff (1986). "The Measurement of Cooperative Protein Self-Assembly by Turbidity and Other Techniques." *Methods Enzymol.* **130**: 47-59.

Arnold, L. D., T. H. Kalantar, et al. (1985). "Conversion of Serine to Stereochemically Pure Beta-Substituted Alpha-Amino-Acids Via Beta-Lactones." *J Am Chem Soc* **107**(24): 7105-7109.

Arnold, L. D., R. G. May, et al. (1988). "Synthesis of Optically Pure Alpha-Amino-Acids Via Salts of Alpha-Amino-Beta-Propiolactone." *J. Am. Chem. Soc.* **110**(7): 2237-2241.

Atwood, C. S., R. D. Moir, et al. (1998). "Dramatic aggregation of Alzheimer A beta by Cu(II) is induced by conditions representing physiological acidosis." *J. Biol. Chem.* **273**(21): 12817-12826.

Balbach, J. J., Y. Ishii, et al. (2000). "Amyloid fibril formation by A beta(16-22), a seven-residue fragment of the Alzheimer's beta-amyloid peptide, and structural characterization by solid state NMR." *Biochemistry* **39**(45): 13748-13759.

Berson, J. F., A. C. Theos, et al. (2003). "Proprotein convertase cleavage liberates a fibrillogenic fragment of a resident glycoprotein to initiate melanosome biogenesis." *J. Cell Biol.* **161**(3): 521-533.

Benzinger, T. L. S., D. M. Gregory, et al. (1998). "Propagating structure of Alzheimer's beta-amyloid((10-35)) is parallel beta-sheet with residues in exact register." *Proc. Natl. Acad. Sci. U S A* **95**(23): 13407-13412.

Bonacic-Koutecky, V., J. Pittner, et al. (1999). "An accurate relativistic effective core potential for excited states of Ag atom: An application for studying the absorption spectra of Ag^{-n} and $Ag^{-n(+)}$ clusters." *J. Chem. Phys.* 110(8): 3876-3886.

Braun, E., Y. Eichen, et al. (1998). "DNA-templated assembly and electrode attachment of a conducting silver wire." *Nature* **391**(6669): 775-778.

Brauner, J. W., C. Dugan, et al. (2000). "C-13 isotope labeling of hydrophobic peptides. Origin of the anomalous intensity distribution in the infrared amide I spectral region of beta-sheet structures." *J. Am. Chem. Soc.* **122**(4): 677-683.

Brown, A. M., D. M. Tummolo, et al. (1997). "Selective aggregation of endogenous beta-amyloid peptide and soluble amyloid precursor protein in cerebrospinal fluid by zinc." *J. Neurochem.* **69**(3): 1204-1212.

Burkoth, T. S., T. L. S. Benzinger, et al. (1999). "Self-assembly of A beta((10-35))-PEG block copolymer fibrils." *J. Am. Chem. Soc.* **121**(32): 7429-7430.

Burkoth, T. S., T. L. S. Benzinger, et al. (2000). "Structure of the beta-amyloid((10-35)) fibril." *J. Am. Chem. Soc.* **122**(33): 7883-7889.

Bush, A. I., W. H. Pettingell, et al. (1994). "Rapid Induction of Alzheimer a-Beta Amyloid Formation by Zinc." *Science* **265**(5177): 1464-1467.

Chapman, M. R., L. S. Robinson, et al. (2002). "Role of Escherichia coli curli operons in directing amyloid fiber formation." *Science* **295**(5556): 851-855.

Coustou, V., C. Deleu, et al. (1997). "The protein product of the het-s heterokaryon incompatibility gene of the fungus Podospora anserina behaves as a prion analog." *Proc. Natl. Acad. Sci. U S A* **94**(18): 9773-9778.

Curtain, C. C., F. Ali, et al. (2001). "Alzheimer's disease amyloid-beta binds copper and zinc to generate an allosterically ordered membrane-penetrating structure containing superoxide dismutase-like subunits." *J. Biol. Chem.* **276**(23): 20466-20473.

Dafforn, T. R., Rajendra, J. et al. (2004). "Protein fiber linear dichroism for structure determination and kinetics in a low-volume, low-wavelength coquette flow cell." *Biophys. J* . **86**(1)**:** 404-410.

Demers, D. B., E. T. Curry, et al. (1995). "Enhanced Pcr Amplification of Vntr Locus D1s80 Using Peptide Nucleic-Acid (Pna)." *Nucleic Acids Res.* **23**(15): 3050-3055.

Diederichsen, U. and H. W. Schmitt (1996). "Self-fairing PNA with alternating alanyl/homoalanyl backbone." *Tetrahedron Lett.* **37**(4): 475-478.

Diederichsen, U. (1996). "Pairing properties of alanyl peptide nucleic acids containing an amino acid backbone with alternating configuration." *Angew. Chem. Int. Ed.* **35**(4): 445-448.

Diederichsen, U. (1997). "Alanyl PNA: Evidence for linear band structures based on guanine-cytosine base pairs." *Angew. Chem. Int. Ed.* **36**(17): 1886-1889.

Diederichsen, U. and D. Weicherding (1999). "Interactions of amino acid side chains with nucleobases in alanyl-PNA." *Synth lett.* 917-920.

Dobson, C. M. (2002). "Protein-misfolding diseases: Getting out of shape." *Nature* **418**(6899): 729-730.

Dong, J., C. S. Atwood, et al. (2003). "Metal binding and oxidation of amyloid-beta within isolated senile plaque cores: Raman microscopic evidence." *Biochemistry* **42**(10): 2768-73.

Dong, J. J., K. Lu, et al. (2006). "Controlling amyloid growth in multiple dimensions." *Amyloid* **13**(4): 206-215.

Dong, J. J., J. E. Shokes, et al. (2006). "Modulating amyloid self-assembly and fibril morphology with Zn(II)." *J. Am. Chem. Soc.* **128**(11): 3540-3542.

Doniach, S. (2001). "Changes in biomolecular conformation seen by small angle X-ray scattering." *Chem. Rev.* **101**(6): 1763-1778.

Dueholm, K. L., M. Egholm, et al. (1994). "Synthesis of Peptide Nucleic-Acid Monomers Containing the 4 Natural Nucleobases - Thymine, Cytosine, Adenine, and Guanine and Their Oligomerization." *J. Org. Chem.* **59**(19): 5767-5773.

Eaton, W. A. and J. Hofrichter (1995). "The Biophysics of Sickle-Cell Hydroxyurea Therapy." *Science* **268**(5214): 1142-1143.

Egholm, M., O. Buchardt, et al. (1993). "Pna Hybridizes to Complementary Oligonucleotides Obeying the Watson-Crick Hydrogen-Bonding Rules." *Nature* **365**(6446): 566-568.

Eichhorn, G. L. (1973). Complexes of Nucleosides and Nucleotides. Inorganic Biochemistry. Vol. 2, Chapter 33.

Fraser, P. E., J. T. Nguyen, et al. (1992). "Fibril Formation by Primate, Rodent, and Dutch-Hemorrhagic Analogs of Alzheimer Amyloid Beta-Protein." *Biochemistry* **31**(44): 10716-10723.

Fowler, D. M., A. V. Koulov, et al. (2006). "Functional amyloid formation within mammalian tissue." *PloS Biol.* **4**(1): 100-107.

Fu, X. Y., Y. Wang, et al. (2003). "Assemblies of metal nanoparticles and self-assembled peptide fibrils - Formation of double helical and single-chain arrays of metal nanoparticles." *Adv. Mater.* **15**(11): 902-906

Garzon-Rodriguez, W., M. Sepulveda-Becerra, et al. (1997). "Soluble amyloid A beta-(1-40) exists as a stable dimer at low concentrations." *J. Biol. Chem.* **272**(34): 21037-21044.

Gazit, E. (2002). "A possible role for pi-stacking in the self-assembly of amyloid fibrils." *FASEB J.* **16**(1): 77-83.

Ghadiri, M. R., J. R. Granja, et al. (1993). "Self-Assembling Organic Nanotubes Based on a Cyclic Peptide Architecture." *Nature* **366**(6453): 324-327.

Goetz, J. M. and J. Schaefer (1997). *J. Magn. Reson.* **127**: 147-154.

Gorbitz, C. H. (2003). "Nanotubes from hydrophobic dipeptides: pore size regulation through side chain substitution." *New J. Chem.* **27**(12): 1789-1793.

Griffiths, J. M., T. T. Ashburn, et al. (1995). "Rotational Resonance Solid-State Nmr Elucidates a Structural Model of Pancreatic Amyloid." *J. Am. Chem. Soc.* **117**(12): 3539-3546.

Halverson, K. J., I. Sucholeiki, et al. (1991). "Location of Beta-Sheet-Forming Sequences in Amyloid Proteins by Ftir." *J. Am. Chem. Soc.* **113**(17): 6701-6703.

Hanvey, J. C., N. J. Peffer, et al. (1992). "Antisense and Antigene Properties of Peptide Nucleic-Acids." *Science* **258**(5087): 1481-1485.

Harper, J. D. and P. T. Lansbury (1997). "Models of amyloid seeding in Alzheimier's disease and scrapie: Mechanistic truths and physiological consequences of the time-dependent solubility of amyloid proteins." *Annu. Rev. Biochem* **66**: 385-407.

Hartgerink, J. D., E. Beniash, et al. (2001). "Self-assembly and mineralization of peptide-amphiphile nanofibers." *Science* **294**(5547): 1684-1688.

Hartgerink, J. D., J. R. Granja, et al. (1996). "Self-assembling peptide nanotubes." *J. Am. Chem. Soc.* **118**(1): 43-50.

Hilbich, C., B. Kisterswoike, et al. (1991). "Aggregation and Secondary Structure of Synthetic Amyloid Beta-A4 Peptides of Alzheimers-Disease." *J. Mol. Biol.* **218**(1): 149-163.

Hiramatsu, H., Y. Goto, et al. (2005). "Structural model of the amyloid fibril formed by beta(2)-microglobulin #21-31 fragment based on vibrational spectroscopy." *J. Am. Chem. Soc.* **127**(22): 7988-7989.

Hoffmann, M. F. H., A. M. Bruckner, et al. (2000). "Specific purine-purine base pairing in linear alanyl-peptide nucleic acids." *HeIv. Chim. Acta* **83**(9): 2580-2593.

Holmes, T. C., S. de Lacalle, et al. (2000). "Extensive neurite outgrowth and active synapse formation on self-assembling peptide scaffolds." *Proc. Natl. Acad. Sci. U S A* **97**(12): 6728-6733.

Huang, X. D., C. S. Atwood, et al. (1997). "Zinc-induced Alzheimer's A beta 1-40 aggregation is mediated by conformational factors." *J. Biol. Chem.* **272**(42): 26464-26470.

Husby, G., T. Stenstad, et al. (1994). "Interaction between Circulating Amyloid Fibril Protein Precursors and Extracellular Tissue Matrix Components in the Pathogenesis of Systemic Amyloidosis." *Clin. Immunol. Immunopathol.* **70**(1): 2-9.

Iconomidou, V. A., G. Vriend, et al. (2000). "Amyloids protect the silkmoth oocyte and embryo." *FEBS Lett.* **479**(3): 141-145.

Inouye, H., P. E. Fraser, et al. (1993). "Structure of Beta-Crystallite Assemblies Formed by Alzheimer Beta-Amyloid Protein Analogs - Analysis by X-Ray-Diffraction." *Biophys. J .* **64**(2): 502-519.

Jarrett, J. T. and P. T. Lansbury (1992). "Amyloid Fibril Formation Requires a Chemically Discriminating Nucleation Event - Studies of an Amyloidogenic Sequence from the Bacterial Protein Osmb." *Biochemistry* **31**(49): 12345-12352.

Jarrett, J. T. and P. T. Lansbury (1993). "Seeding One-Dimensional Crystallization of Amyloid - a Pathogenic Mechanism in Alzheimers-Disease and Scrapie." *Cell* **73**(6): 1055-1058.

Jensen, K. K., H. Orum, et al. (1997). "Kinetics for hybridization of peptide nucleic acids (PNA) with DNA and RNA studied with the BIAcore technique." *Biochemistry* **36**(16): 5072-5077.

Kelly, J. W. (1996). "Alternative conformations of amyloidogenic proteins govern their behavior." *Curr. Opin. Chem. Biol.* **6**(1): 11-17.

Kirschner, D. A., C. Abraham, et al. (1986). "X-Ray-Diffraction from Intraneuronal Paired Helical Filaments and Extraneuronal Amyloid Fibers in Alzheimer-Disease Indicates Cross-Beta Conformation." *Proc. Natl. Acad. Sci. U S A* **83**(2): 503-507.

Kirschner, D. A., H. Inouye, et al. (1987). "Synthetic Peptide Homologous to Beta-Protein from Alzheimer-Disease Forms Amyloid-Like Fibrils Invitro." *Proc. Natl. Acad. Sci. U S A* **84**(19): 6953-6957.

Konno, T., K. Murata, et al. (1999). "Amyloid-like aggregates of a plant protein: a case of a sweet-tasting protein, monellin." *FEBS Lett.* **454**(1-2): 122-126.

Kubelka, J. and T. A. Keiderling (2001). "The anomalous infrared amide I intensity distribution in C-13 isotopically labeled peptide beta-sheets comes from extended, multiple-stranded structures. An ab Into study (vol 123, 6142, 2001)." *J. Am. Chem. Soc.* **123**(33): 8163-8163.

Lakdawala, A. S., D. M. Morgan, et al. (2002). "Dynamics and fluidity of amyloid fibrils: A model of fibrous protein aggregates." *J. Am. Chem. Soc.* **124**(51): 15150-15151.

Lansbury, P. T., P. R. Costa, et al. (1995). "Structural Model for the Beta-Amyloid Fibril Based on Interstrand Alignment of an Antiparallel-Sheet Comprising a C-Terminal Peptide." *Nat. Struct. Biol.* **2**(11): 990-998.

Lapatsanis, L., G. Milias, et al. (1983). "Synthesis of N-2,2,2-(Trichloroethoxycarbonyl)-L-Amino Acids and N-(9-Fluorenylmethoxycarbonyl)-L-Amino Acids Involving Succinimidoxy Anion as a Leaving Group in Amino-Acid Protection." *Synthesis* (8): 671-673.

Lattman, E. E. (1994). "Small-Angle Scattering Studies of Protein-Folding." *Curr. Opin. Chem. Biol.* **4**(1): 87-92.

Lamm, M. S., K. Rajagopal, et al. (2005). "Laminated morphology of nontwisting beta-sheet fibrils constructed via peptide self-assembly." *J. Am. Chem. Soc.* **127**(47): 16692-700.

Lee, J. P., E. R. Stimson, et al. (1995). "H-1-Nmr of a-Beta Amyloid Peptide Congeners in Water Solution - Conformational-Changes Correlate with Plaque Competence." *Biochemistry* **34**(15): 5191-5200.

Liu, S. T., G. Howlett, et al. (1999). "Histidine-13 is a crucial residue in the zinc ion-induced aggregation of the A beta peptide of Alzheimer's disease." *Biochemistry* **38**(29): 9373-8.

Lohse, P. (1992). "Synthese und Eigenschafen von oligomeren Nukleodipeptamidinium-Salzen." *Dissertation ETH Zurich* 148-153, 177-181.

Lohse, P., Oberhauser, B., Oberhauser-Hofbauser, B., Baschang, G., Eschenmoser, A. (1996). "Chemie von a-Aminonitrilne. XVII. Oligo(nukleodipeptamidinium)-Salze." *Croat. Chem. Acta* **69**(2): 535-562.

Lovell, M. A., J. D. Robertson, et al. (1998). "Copper, iron and zinc in Alzheimer's disease senile plaques." *J. Neurol. Sci.* **158**(1): 47-52.

Lu, K., Conticello, V. P., Lynn, D. G. (2004). "Templating Colloidal Metal Nanoparticle Assemblies: Use of the Aβ Amyloid Peptide Nanotube." *Mater. Res. Soc. Synp. Proc.* **V1.6.**

Lu, K., J. Jacob, et al. (2003). "Exploiting amyloid fibril lamination for nanotube self-assembly." *J. Am. Chem. Soc.* **125**(21): 6391-6393.

Mackay, J. P., J. M. Matthews, et al. (2001). "The hydrophobin EAS is largely unstructured in solution and functions by forming amyloid-like structures." *Structure* **9**(2): 83-91.

Marchetti, A. P., A. A. Muenter, et al. (1998). "Formation and spectroscopic manifestation of silver clusters on silver bromide surfaces." *J. Phys. Chem. B* **102**(27): 5287-5297.

Markus F. H. Hoffmann, A. M. B., Thomas Hupp, Bernd Engels and Ulf Diederichsen (2000). "Specific Purine-Purine Base Pairing in Linear Alanyl-Peptide Nucleic Acids." *HeIv. Chim. Acta* **83**: 2580-2593.

Marzilli, L. G. (1977). "Metal-Ion Interactions with Nucleic Acids and Nucleic Acid Derivatives." Progress in Inorganic Chemistry Vol.23: 255-378.

Matsumura, S., S. Uemura, et al. (2004). "Fabrication of nanofibers with uniform morphology by self-assembly of designed peptides." *Chem. Eur. J.* **10**(11): 2789-2794.

Mazor, Y., S. Gilead, et al. (2002). "Identification and characterization of a novel molecular-recognition and self-assembly domain within the islet amyloid polypeptide." *J. Mol. Biol.* **322**(5): 1013-1024.

Mehta, A., R. Jaouhari, et al. (1992). "Improved Efficiency and Selectivity in Peptide-Synthesis - Use of Triethylsilane as a Carbocation Scavenger in Deprotection of Tert-Butyl Esters and Tert-Butoxycarbonyl-Protected Sites." *Tetrahedron Lett.* **33**(37): 5441-5444.

Miura, T., K. Suzuki, et al. (2000). "Metal binding modes of Alzheimer's amyloid beta-peptide in insoluble aggregates and soluble complexes." *Biochemistry* **39**(23): 7024-7031.

Morgan, D. M., J. J. Dong, et al. (2002). "Metal switch for amyloid formation: Insight into the structure of the nucleus." *J. Am. Chem. Soc.* **124**(43): 12644-12645.

Nielsen, P. E. (1999). "Applications of peptide nucleic acids." *Curr. Opin. Biotechnol.* **10**(1): 71-75.

Nielsen, P. E., M. Egholm, et al. (1991). "Sequence-Selective Recognition of DNA by Strand Displacement with a Thymine-Substituted Polyamide." *Science* **254**(5037): 1497-1500.

Nyrkova, I. A., A. N. Semenov, et al. (2000). "Fibril stability in solutions of twisted beta-sheet peptides: a new kind of micellization in chiral systems." *Eur. Phys. J. B* **17**(3): 481-497.

O'Nuallain, B., A. D. Williams, et al. (2004). "Seeding specificity in amyloid growth induced by heterologous fibrils." *J. Biol. Chem.* **279**(17): 17490-17499.

Paul, C., J. P. Wang, et al. (2004). "Vibrational coupling, isotopic editing, and beta-sheet structure in a membrane-bound polypeptide." *J. Am. Chem. Soc.* **126**(18): 5843-5850.

Perry-OKeefe, H., X. W. Yao, et al. (1996). "Peptide nucleic acid pre-gel hybridization: An alternative to Southern hybridization." *Proc. Natl. Acad. Sci. U S A* **93**(25): 14670-14675.

Petkova, A. T., G. Buntkowsky, et al. (2004). "Solid state NMR reveals a pH-dependent antiparallel beta-sheet registry in fibrils formed by a beta-amyloid peptide." *J. Mol. Biol.* **335**(1): 247-260.

Petkova, A. T., Y. Ishii, et al. (2002). "A structural model for Alzheimer's beta-amyloid fibrils based on experimental constraints from solid state NMR." *Proc. Natl. Acad. Sci. U S A* **99**(26): 16742-16747.

Petty, J. T., J. Zheng, et al. (2004). "DNA-templated Ag nanocluster formation." *J. Am. Chem. Soc*. **126**(16): 5207-5212.

Porod, G. (1982). Small Angle X-ray Scattering Chapter 2. Academic Press, New York, NY.

Rajendra, J., Damianoglou A. et al. (2006). "Quantitation of protein orientation in flow-oriented unilamellar liposomes by linear dichroism." *Chem. Phys*. **326**(16): 210-220.

Reches, M. and E. Gazit (2003). "Casting metal nanowires within discrete self-assembled peptide nanotubes." *Science* **300**(5619): 625-627.

Reches, M., Y. Porat, et al. (2002). "Amyloid fibril formation by pentapeptide and tetrapeptide fragments of human calcitonin." *J. Biol. Chem.* **277**(38): 35475-35480.

Seilheimer, B., B. Bohrmann, et al. (1997). "The toxicity of the Alzheimer's beta-amyloid peptide correlates with a distinct fiber morphology." *J. Struct. Biol.* **119**(1): 59-71.

Selkoe, D. J. (1991). "The Molecular Pathology of Alzheimers-Disease." *Neuron* **6**(4): 487-498.

Semisotnov, G. V., H. Kihara, et al. (1996). "Protein globularization during folding. A study by synchrotron small-angle X-ray scattering." *J. Mol. Biol.* **262**(4): 559-574.

Serpell, L. C., J. Berriman, et al. (2000). "Fiber diffraction of synthetic alpha-synuclein filaments shows amyloid-like cross-beta conformation." *Proc. Natl. Acad. Sci. U S A* **97**(9): 4897-4902.

Shiraham.T and A. S. Cohen (1967). "High-Resolution Electron Microscopic Analysis of Amyloid Fibril." *J. Cell Biol.* **33**(3): 679-&.

Silva, G. A., C. Czeisler, et al. (2004). "Selective differentiation of neural progenitor cells by high-epitope density nanofibers." *Science* **303**(5662): 1352-1355.

Silva, R. A. G. D., J. Y. Nguyen, et al. (2002). "Probing the effect of side chains on the conformation and stability of helical peptides via isotope-edited infrared spectroscopy." *Biochemistry* **41**(51): 15296-15303.

Silva, R. A. G. D., W. Barber-Armstrong, et al. (2003). "The organization and assembly of beta-sheet formed by a prion peptide in solution: An isotope-edited FTIR study." *J. Am. Chem. Soc.* **125**(45): 13674-13675.

Song, Y. J., S. R. Challa, et al. (2004). "Synthesis of peptide-nanotube platinum-nanoparticle composites." *Chem. Commun.* (9): 1044-1045.

Sorimachi, K. and D. J. Craik (1994). "Structure Determination of Extracellular Fragments of Amyloid Proteins Involved in Alzheimers-Disease and Dutch-Type Hereditary Cerebral-Hemorrhage with Amyloidosis." *Eur. J. Biochem.* **219**(1-2): 237-251.

Sparks, D. L. and B. G. Schreurs (2003). "Trace amounts of copper in water induce beta-amyloid plaques and learning deficits in a rabbit model of Alzheimer's disease." *Proc. Natl. Acad. Sci. U S A* **100**(19): 11065-9.

Spencer, R. G. S., K. J. Halverson, et al. (1991). "An Unusual Peptide Conformation May Precipitate Amyloid Formation in Alzheimers-Disease - Application of Solid-State Nmr to the Determination of Protein Secondary Structure." *Biochemistry* **30**(43): 10382-10387.

Sticht, H., P. Bayer, et al. (1995). "Structure of Amyloid A4-(1-40)-Peptide of Alzheimers-Disease." *Eur. J. Biochem.* **233**(1): 293-298.

Suh, S. W., K. B. Jensen, et al. (2000). "Histochemically-reactive zinc in amyloid plaques, angiopathy, and degenerating neurons of Alzheimer's diseased brains." *Brain Res.* **852**(2): 274-8.

Sunde, M., L. C. Serpell, et al. (1997). "Common core structure of amyloid fibrils by synchrotron X-ray diffraction." *J. Mol. Biol.* **273**(3): 729-739.

Talafous, J., K. J. Marcinowski, et al. (1994). "Solution Structure of Residues-1-28 of the Amyloid Beta-Peptide." *Biochemistry* **33**(25): 7788-7796.

Tenidis, K., M. Waldner, et al. (2000). "Identification of a penta- and hexapeptide of islet amyloid polypeptide (IAPP) with amyloidogenic and cytotoxic properties." *J. Mol. Biol.* **295**(4): 1055-1071.

Thiyagarajan, P., T. S. Burkoth, et al. (2000). "pH dependent self assembly of beta-amyloid(10-35) and beta-amyloid(10-35)PEG3000." *J. Appl. Crystallogr.* **33**(1): 535-539.

Trewhella, J. (1997). "Insights into biomolecular function from small-angle scattering." *Curr. Opin. Struct. Biol.* **7**(5): 702-708.

Tycko, R. and Y. Ishii (2003). "Constraints on supramolecular structure in amyloid fibrils from two-dimensional solid-state NMR spectroscopy with uniform isotopic labeling." *J. Am. Chem. Soc.* **125**(22): 6606-6607.

Veselkov, A. G., V. V. Demidov, et al. (1996). "PNA as a rare genome-cutter." *Nature* **379**(6562): 214-214.

Wood, S. J., B. Maleeff, et al. (1996). "Physical, morphological and functional differences between pH 5.8 and 7.4 aggregates of the Alzheimer's amyloid peptide AP." *J. Mol. Biol.* **256**(5): 870-877.

Xu, Y. (2007) "Exploring the peptide nanotube formation from the self-assembly of the Aβ(13-21)K16A peptide in the presence of zinc ions." *Thesis, Emory University* 15-16.

Yang, D. S., J. McLaurin, et al. (2000). "Examining the zinc binding site of the amyloid-beta peptide." *Eur. J. Biochem.* **267**(22): 6692-8.

Yemini, M., M. Reches, et al. (2005). "Peptide nanotube-modified electrodes for enzyme-biosensor applications." *Anal. Chem.* **77**(16): 5155-5159.

Zhao, Z. Y., P. A. Banerjee, et al. (2005). "Simultaneous targeted immobilization of anti-human IgG-coated nanotubes and anti-mouse IgG-coated nanotubes on the complementary antigen-patterned surfaces via biological molecular recognition." *J. Am. Chem. Soc.* **127**(25): 8930-8931.